

INDUSTRIAL BRINE MINIMIZATION: DETERMINING THE PHYSICAL CHEMICAL PARAMETERS THAT AFFECT EVAPORATION RATES ON MULTI-COMPONENT HYPER-SALINE EFFLUENTS

Report to the
Water Research Commission

by

LF Petrik, OO Fatoba, MV Fey, NZN Ndlovu, EO Omoniyi, D Bent and J Nel
Environmental and Nano Sciences Group (ENS)
Chemistry Department, University of the Western Cape

WRC Report No 2100/1/15
ISBN 978-1-4312-0649-0

August 2015

Obtainable from

Water Research Commission
Private Bag X03
GEZINA, 0031

orders@wrc.org.za or download from www.wrc.org.za

DISCLAIMER

This report has been reviewed by the Water Research Commission (WRC) and approved for publication. Approval does not signify that the contents necessarily reflect the views and policies of the WRC, nor does mention of trade names or commercial products constitute endorsement or recommendation for use.

EXECUTIVE SUMMARY

Minimization of industrial waste water, through its reuse, or safe re-entry into the hydrological cycle, is a critical part of water management and integral in tackling water scarcity issues. Industrial brines are complex liquid mixtures of various salts with a composition that can vary dramatically depending on the intake water quality or water treatment process from which the final saline effluent derives. Currently, the typical method of brine disposal is the use of evaporation ponds to reduce the liquid volume and provide a manageable solid product. Predicting the evaporation rate of the pond is critical in effective management of the brine disposal holding area. However the meteorological models or empirical methods with evaporative pans which are used to predict evaporation from natural water bodies are generally considered being inappropriate for highly saline systems. Thus, this study investigated models that can be applied to predict evaporation rates in order to limit accidental release of saline effluents and prevent impacts on the receiving environment. This study investigated and ascertained the relative importance of critical chemical and physical parameters that could affect evaporation rates of industrial brines typically found within the Mpumalanga region of South Africa.

The study focused on understanding the desalination processes, identifying the type of brine generated in different sections of the desalination plant, and characterising and understanding the hyper saline water chemistry. The literature review indicated that it is salinity *per se* which has the most important effect on evaporation rate rather than the type of salt. This is because the effect of salt manifests itself primarily through control of vapour pressure which is a colligative property of solutions, implying that it depends on concentration rather than the nature of the dissolved species. Nevertheless there are situations in which the composition of the brine in its final stages can be expected to influence evaporation rate, simply because as the brine evolves through evaporative concentration, the less soluble species will precipitate leaving dissolved species which are typically the most hygroscopic or, as is the case with Ca and Mg chlorides for example, deliquescent. This phenomenon is well known in commercial salt production from sea water, where the residual bitterns, after fractional crystallization of gypsum ($\text{CaSO}_4 \cdot 2\text{H}_2\text{O}$) and halite (NaCl), consist largely of MgCl_2 which cannot be evaporated to dryness even in the driest of earth climates.

Analysis of the stage 3 reject brine collected from the Emalahleni RO plant retentate revealed that it is Na-SO_4 type water although it does contain significant concentrations of other major ions, namely Ca, Mg, K and Cl. Aq.QA software was used to classify the brine. ICP and IC analysis showed that seventy-one percent of the cation mole charge is accounted for by Na^+ , and the remainder by Ca^{2+} (15%) K^+ (9%) and Mg^{2+} (4%). In the case of anion charge, SO_4^{2-} accounts for 88% and Cl^- (10%) and HCO_3^{3-} (1%) for the remainder. The brine has a near-neutral pH. It was this analysis that guided the choice of salts for the small scale evaporation study designed to find out whether the type of salt has any effect on evaporation rate. The effect of salt type (single, binary and ternary solutions of Na_2SO_4 , NaCl, KCl, CaSO_4 , and MgSO_4) were studied. Considering the behaviour of different salts in solution in small scale laboratory experiments under controlled conditions, salts with alkali metals (monovalent metals) had a tendency to lower the evaporation rate while salts with alkali earth metals (divalent metals) had a tendency to increase the evaporation rate although the experimental design did not fully allow the simultaneous contribution of anion composition (especially sulphate vs chloride) to be assessed separately. There is no indication that brine compositional complexity *per se* is likely to substantially modify evaporation rate. The effect of some salts, especially Ca sulphate, on enhancing evaporation rates is likely to have been due to enhanced heat capture from the irradiation while suppression of evaporation rate when observed is consistent with the known behaviour of salt solutions with respect to their colligative properties. While the effect of salt is generally to reduce evaporation, the presence of salt also gives rise to greater heating of the solution by absorbing radiant energy. The experimental design did not account for the concentration of this sparingly soluble salt which could not match that (0.5M) of the other salts studied. The solution heating effect that was observed to result in a higher evaporation rate in the case of those solutions dominated by divalent as opposed to monovalent cations could have been confounding by an anion effect since the Ca- and Mg-dominated solutions were also dominated by sulfate

rather than chloride. In future studies inclusion of chlorides of Ca and Mg is recommended so that the deliquescence of these salts (essentially terminating the evaporation) could be observed. Despite these uncertainties, the overall effect of salts on evaporation rate was confirmed in both the small scale study as well as the subsequent pilot scale study to be essentially one of concentration, inhibiting evaporation as expected. Overall the effect of salts on evaporation rate is a function of the rate at which water will separate from a salt solution, which declines in proportion to the amount of water which has already been evaporated due to the increasing solution density. Since salts with lower solubility will crystallize over time when supersaturation for that salt is reached, the remaining aqueous solution composition and concentration is expected to change over time and the evaporation rate to fluctuate accordingly. However, the scale of the laboratory study did not allow for the empirical measurement of this fluctuation.

The effect of climatic conditions such as temperature, wind speed, humidity and irradiance on the rate of evaporation of brine was studied. In studying the factors affecting the evaporation rate, results confirmed that physical parameters namely humidity and temperature have a strong effect on the rate of the evaporation of water from the salt solution. During the pilot scale laboratory evaporation experiment using infrared lamp-heated Perspex tanks 0.5 m square and 0.5 m deep fitted with accessories for generating wind in which two systems, pure water or a solution of sodium chloride, were respectively exposed to infrared lamps, the effect of temperature on the rate of evaporation after a total of three 12-hour cycles was determined. In one tank 115 litres of a 0.5 M of NaCl was prepared using distilled water, and 125 litres of pure water was placed in a second tank. A total volume of 2.57 litres (2.06%) was evaporated from the pure water system while 2.48 litres (1.98%) was lost from the NaCl brine system under the same conditions. This result is again consistent with the theory of colligative properties in terms of which the vapour pressure is lowered in proportion to the concentration of the salt solution. The systems, when subjected to wind, showed an increase in the volume of water evaporated over time compared to the evaporation systems without the wind application. However, the input energy from the IR lamps of the evaporation system with wind was lower than that of the evaporation system without the wind. This led to a greater volume loss in comparison with the experiment without wind. However, when the extractor fans which removes the saturated air from the room was switched off, humidity played a major role in lowering the evaporation rates, as would be expected.

The wind had a greater impact when the water temperatures were higher than the ambient temperatures in terms of the water volume loss from the container. The initial role of the wind was to remove the saturated air where it enhances the process of changing water to vapour. With the reduction in the radiation the wind had a greater impact when the energy input was reduced by changing the IR bulbs. The wind speed was probably not effective enough to be regarded as the sole contributor to increase the evaporation rate by a larger margin.

Finally the depth of stratification in temperatures illustrated the energy dissipation, which demonstrated the delay in energy transfer from the water surface to the deepest part of the water. The dissipation of energy indicated that the surface level of the brine in the container absorbed a greater amount of energy than the substrata.

Comparison of the actual measurements of evaporation obtained for the Emalahleni RO retentate brine and the modelled brine evaporation for the same period was performed in the same pilot scale set-up. The daily average evaporation rate of the Emalahleni brine under natural convection was 5.33 mm/day. The Oroud (1999; 2000) model suggests a very similar figure over the same period. Under the forced convection, the model prediction was a bit lower than the actual recorded evaporation. The model also projects 11% increase in evaporation with wind being applied at 2 m/s every 12 hour cycle, a trend which was empirically observed.

The pilot scale study also involved making in duplicate a modified copy of the WAIV apparatus for brine evaporation which has been described in the literature, using infrared lamp-heated Perspex tanks 0.5 m square and 0.5 m deep fitted with accessories for generating wind, and intensified evaporation was achieved

on a fabric mesh exposed to brine irrigation and forced convection. This system can be used for testing novel materials that enhance evaporation by allowing the solution to spread by capillarity over a greater surface area.

Moreover the novel high surface area materials developed, namely composite nanofibres comprised of PAN loaded with Zeolite Y nanoparticulates were shown to significantly remove divalent cations from model brine solutions, allowing for brine simplification. The PAN TiO₂ nanofibres showed a high Na cation adsorption. It was observed that the Lagergren model fits suitably at the early stage of the adsorption for both nanofibers, but at the later stage of the adsorption process, the results deviated from the theory. Therefore, the model represents the initial stage where adsorption takes place rapidly but cannot be applied for the whole adsorption process.

This study has achieved its objective of setting up, investigating and describing different experimental methods and apparatus for the study of brine evaporation and evolution in a controlled laboratory environment which should provide a useful platform for future research in this increasingly important field of environmental science. This study has been concluded successfully in terms of construction and testing to demonstrate a sensitive response of evaporation to parameters such as salt concentration, wind and irradiance.

In future work with industrial brines the application of a brine evolution model is likely to be rewarding by describing the minerals that precipitate and explaining the final character of the brine. Seeking ways to concentrate and separate specific salts from local industrial brines through fractional crystallization as is widely practised in commercial salt production facilities may prove fruitful by having marketable products to offset some of the costs of brine disposal. Such products potentially include gypsum (with uses in agriculture), sodium sulphate (detergent additive), sodium chloride (common salt), Epsom salts (Mg sulphate for agricultural fertilizers) and liquid bitters (deliquescent MgCl₂, used for example, in dust suppression and as a fire retardant).

ACKNOWLEDGEMENTS

The project team wishes to thank the following people for their contributions to the project.

Reference Group	Organisation
Dr Valerie Naidoo	: Water Research Commission (Chairperson)
Prof Leslie Petrik	: University of the Western Cape (Project leader)
Ms Kerry Slatter-Christie	: Kalao Solutions
Mr Johan Steenkamp	: Eskom, Technology Division
Mr Meiring du Plessis	: ex Water Research Commission, Independent Consultant
Dr Lynette Baratta	: Sasol Technology, R&D
Ms Annalien Toerien	: Golder Associates Africa (Pty) Ltd
Mr Jeeten Nathoo	: Grahamtek NuWater
Ms Stephinah Mudau	: Chamber of Mines of SA

CONTENTS

EXECUTIVE SUMMARY	i
ACKNOWLEDGEMENTS	iv
CONTENTS	v
LIST OF FIGURES	viii
LIST OF TABLES	xii
ACRONYMS & ABBREVIATIONS	xiii
CHAPTER 1: BACKGROUND	1
1.1 INTRODUCTION	1
1.2 PROJECT AIMS	1
1.3 SCOPE AND LIMITATIONS	2
CHAPTER 2: LITERATURE REVIEW: THE NATURE, MANAGEMENT AND DISPOSAL OF BRINES GENERATED BY THE TREATMENT OF WASTEWATER	3
2.1 INTRODUCTION	3
2.2 THE TREATMENT OF WASTEWATER USING MEMBRANE TECHNOLOGIES.....	4
2.2.1 Electrodialysis (ED).....	5
2.2.2 Ultrafiltration (UF).....	7
2.2.3 Ion Exchange	7
2.2.4 Reverse Osmosis (RO).....	7
2.3 BRINES.....	8
2.3.1 Composition	9
2.3.2 Uses and impacts of brine	9
2.3.3 Disposal	10
2.3.3.1 Deep well injection.....	10
2.3.3.2 Discharge into surface water.....	11
2.3.3.3 Land application	11
2.3.3.4 Zero liquid discharge	12
2.3.3.5 Evaporation ponds.....	12
2.4 CHEMICAL AND PHYSICAL PRINCIPLES OF BRINE EVAPORATION PONDS	14
2.4.1 Environmental impacts of evaporation ponds.....	15
2.4.2 Pond water chemistry	15
2.4.3 Evaporation and the factors that affect it	16
2.4.3.1 Salinity	17
2.4.3.2 Meteorological parameters.....	17
Temperature	18
Humidity	18
Solar radiation	18
Wind	19
2.4.3.3 Calculating the rate of evaporation.....	21
CHAPTER 3: MATERIALS AND METHODS	23

3.1	INTRODUCTION	23
3.2	SAMPLE COLLECTION	23
3.3	CHARACTERIZATION OF EMALAHLENI BRINE	24
3.4	SYNTHETIC BRINES	25
3.5	WATER CONTENT DETERMINATION.....	25
3.6	EVAPORATION FROM SINGLE AND MIXED SALT SOLUTIONS.....	25
3.7	MEASUREMENT OF EVAPORATION UNDER CONTROLLED CONDITIONS	26
3.7.1	Evaporation study using distilled water (control experiment)	27
3.7.2	Evaporation study using water and NaCl solution	27
3.7.2.1	Scaffolding.....	28
3.7.2.2	Containers	28
3.7.2.3	Energy source	29
3.7.2.4	Pressure transducers	29
3.7.2.5	Temperature sensors	29
3.7.2.6	Humidity sensors	29
3.7.2.7	Data logger	29
3.7.3	Preparation of novel materials for enhanced brine evaporation.....	29
3.7.3.1	Electrospinning of PAN doped with TiO ₂ and zeolite	30
3.7.3.2	Adsorption experiments.....	30
3.7.3.3	Effect of contact time	31
3.7.4	Wind-aided experimental design.....	31
3.7.5	Irrigation system.....	33
CHAPTER 4: classification of Emalahleni brine AND EVALUATION OF A Small scale evaporation study		34
4.1	INTRODUCTION	34
4.2	CHARACTERIZATION AND CLASSIFICATION OF EMALAHLENI BRINE.....	34
4.2.1	Chemical composition.....	34
4.2.2	Classification of brine.....	36
4.2.3	Water content of salts	36
4.2.4	Water holding capacity of the salts	37
4.3	SMALL SCALE EVAPORATION STUDY	38
4.3.1	Effect of humidity and solution temperature on evaporation	38
4.3.2	Cumulative evaporation from different salt solutions.....	42
4.3.3	Material Balance	46
4.3.4	Energy Balance.....	50
4.3.5	Evaluation of heat transfer operation.....	54
CHAPTER 5: MAIN EVAPORATION STUDY (PILOT SCALE)		56
5.1	INTRODUCTION	56
5.2	MAIN EVAPORATION STUDY (PILOT SCALE).....	56
5.2.1	Hydrostatic pressure	56
5.2.2	Temperature and humidity	57
5.2.3	The energy output.....	59
5.2.4	Effect of physical parameters on evaporation of water.....	59
5.2.4.1	Effect of temperature and wind	59
5.2.4.2	Effect of humidity and wind.....	61
5.2.4.3	Effect of radiation.....	63
5.2.4.4	Discussion	72
5.2.5	Effect of climatic parameters on water and NaCl solution	73

5.2.5.1	Temperature of the NaCl solution and H ₂ O at different depths.....	73
5.2.5.2	Humidity and surface temperature of the NaCl solution and H ₂ O.....	75
5.2.5.3	Comparison of the evaporation rate of NaCl solution and distilled water	76
5.2.5.4	Effect of wind on the loss of water.....	77
5.3	EMPIRICAL AND THEORETICAL MODELLING OF INDUSTRIAL BRINE SYSTEMS	80
5.3.1	Model description.....	80
5.3.2	Activity Coefficient.....	81
5.3.3	Model selection	81
5.3.4	Brine analysis.....	82
5.3.5	Emalaheni brine comparison.....	83
5.3.6	Model validation	84
CHAPTER 6:	ADSORPTION OF Ca²⁺, Mg²⁺, K⁺ AND Na⁺ ON PAN+TiO₂ and PAN+ZEOLITE NANOFIBRES	93
6.1	INTRODUCTION	93
6.2	CHARACTERIZATION OF PAN-TiO ₂ AND PAN-ZEOLITE NANOFIBRES	93
6.2.1	Fourier Transform Infrared Spectrometry (FTIR).....	94
6.2.2	SEM images of raw PAN and PAN+TiO ₂	95
6.3	EFFECT OF CONTACT TIME ON ADSORPTION OF METALS.....	96
6.3.1	Effect of contact time on adsorption of calcium Ca ²⁺	97
6.3.2	Effect of contact time on adsorption of magnesium Mg ²⁺	97
6.3.3	Effect of contact time on adsorption of potassium K ⁺	98
6.3.4	Effect of contact time on adsorption of sodium Na ⁺	98
6.4	EFFECT OF CONCENTRATION ON ADSORPTION OF METALS	98
6.5	DETERMINATION OF RATE PARAMETERS.....	99
6.5.1	Pseudo-first order	99
6.5.2	Pseudo-second order.....	100
6.5.3	Adsorption equilibrium isotherm.....	101
6.5.4	Summary.....	102
CHAPTER 7:	CONCLUSIONS & RECOMMENDATIONS.....	103
7.1	CONCLUSIONS.....	103
7.2	RECOMMENDATIONS.....	105
REFERENCES		107
APPENDIX A.....		114

LIST OF FIGURES

Figure 2.1: Application of water by different sectors in South Africa (DWA, 2003).....	5
Figure 2.2: Electrodialysis (http://en.wikipedia.org/wiki/Electrodialysis).....	6
Figure 2.3: Osmosis and Reverse Osmosis (www.visionengineer.com/)	8
Figure 3.1: Schematic flow diagram of Emalahleni water reclamation plant with RO systems (Water Sewage & Effluent, 2006).....	24
Figure 3.2: Aerial view of Emalahleni water reclamation plant in Mpumalanga (Source: http://www.projectlink.co.za/portfolio-item/project-water-treatment-plant/)	24
Figure 3.3: Experimental set-up for brine evaporation in shallow basins mounted beneath infrared lamps with adjustable height.....	26
Figure 3.4: Schematic of experimental plant (Adapted from Schultheis et al., 2001)	26
Figure 3.5: A display of all the components from the experimental plant for the distilled water. A similar setup was used for the NaCl brine.	28
Figure 3.6: Schematic diagram for the electrospinning set up (a) Vertical set up and (b) Horizontal set up for electrospinning (Bhardwaj and Kundu, 2010).	30
Figure 3.7: Experimental setup with the Wind-Aided Intensified evaporation (WAIV) system (based on Gilron et al., 2003).....	32
Figure 3.8: The nets after experimental cycling. A crusted deposit developed near the orifice of the irrigation pipes	33
Figure 4.1: Piper diagram showing the % distribution of major cations and anions of Emalahleni and Tutuka brine water using the Aq.QA software	36
Figure 4.2: Humidity (A), Volume loss (B), and solution temperature (C) over time for single salt solutions .	39
Figure 4.3: Average humidity and the 3-hourly volume of water lost from solutions of A: single; B: binary and C: ternary salt mixtures.....	40
Figure 4.4: Average temperature and the volume of water lost from solutions of A: single; B: binary and C: ternary salt mixtures	41
Figure 4.5: Cumulative volume loss and average temperature with time in single salt solutions	43
Figure 4.6: Cumulative volume loss and average temperature with time in binary salt solutions.....	44
Figure 4.7: Cumulative volume loss and average temperature with time in ternary salt solutions	45
Figure 4.8: Input and output of the evaporation pond	46
Figure 4.9: Experimental and theoretical volume loss, A (CaSO_4), B (Na_2SO_4), C (MgSO_4), D (KCl), and E (NaCl) with respect to time	49
Figure 4.10: Different energies involved in the evaporation of water from the salt solution.....	50
Figure 4.11: Comparison of temperature and volume of water loss of CaSO_4 with respect to time (A = theoretical and B = experimental).....	53
Figure 4.12: Convection heat transfer from the heating lamp to the surface of salt solution	54
Figure 4.13: Variation of the heat that evaporated a volume of water from the salt solution at a given time .	55
Figure 5.1: A display of the experimental setup with all the components	56

Figure 5.2: The level of NaCl solution as a function of hydrostatic pressure (in bar) over time	57
Figure 5.3: The cycles of energy input which the sensors recorded in the larger pans	58
Figure 5.4: The change in humidity during the various cycles in the larger pans	58
Figure 5.5: The energy cycle of the larger pan system	59
Figure 5.6: The temperature variation at different depths of the container during the exposure to radiation energy from the IR bulbs over 48 h without wind	60
Figure 5.7: The temperature variation at different depths in the container with the wind factor using the same amount of heat source as above	60
Figure 5.8: The variation in the relative humidity above the water surface over a 48 hour period without wind	61
Figure 5.9: The relative humidity above the water surface with the wind factor over a 48 hour period compared to the relative humidity of the room	62
Figure 5.10: The variations of the radiation over a 48 hour time period with and without the wind assistance.	63
Figure 5.11: The evaporation rate is shown by the decrease in water level for the two experiments over the same time period	64
Figure 5.12: The temperature gradients after the height of the IR bulbs were increased from 100 mm to 200 mm from the water surface	64
Figure 5.13: The temperature gradient after the increased distance of the heating source with the added wind factor	65
Figure 5.14: The energy recorded on the surface of the water during the experiments with and without wind. The height between the lights and the water was 200 mm	66
Figure 5.15: The relative humidity of the air above the water after the height of the energy source was increase to 200 mm	66
Figure 5.16: The relative humidity of the air above the water surface when the wind was included in the experiment	67
Figure 5.17: The evaporation as determined by the change in water level of two experiments (with or without wind) over the same period (200 mm distance)	68
Figure 5.18: The temperature stratification in water during the reduction in radiation	69
Figure 5.19: The temperature stratification during the experiment with reduced radiation	69
Figure 5.20: The relative humidity during the reduced radiation	70
Figure 5.21: The relative humidity after the reduction in radiation input	70
Figure 5.22: The radiation over a 48 hour period without wind when the radiation was reduced from 250 Watts to 175 Watts	71
Figure 5.23: The experiments with and without the wind assistance with reduced radiation	71
Figure 5.24: The temperature of the NaCl brine at various depths over time	74
Figure 5.25: The temperature of the distilled water at various depths over time	74
Figure 5.26: The relative humidity and air temperature fluctuations of the NaCl	75
Figure 5.27: The relative humidity and air temperature variation of the distilled water container	75

Figure 5.28: The variation in the surface temperature and the changes in the volume of the NaCl brine solution; Lvl = level	76
Figure 5.29: The variation in the surface temperature and the changes in the volume of the distilled water .	76
Figure 5.30: The change in the volume levels of both the distilled water and the NaCl over time under a windy condition.	78
Figure 5.31: The temperatures at different depths of the NaCl brine with the wind blowing over the surface area at 2m/s.	78
Figure 5.32: The temperatures at various depths of the water with the wind blowing over the surface area at 2 m/s.	78
Figure 5.33: The evaporation of the water with the 2 m/s wind factor affecting changes in the surface temperature.	79
Figure 5.34: The evaporation of the NaCl brine with the 2 m/s wind factor affecting changes in the surface temperature.	79
Figure 5.35: The major ions of the Emalahleni brine which was analysed in 2013 using an Inductive Coupled Plasma with a mass spectrometer.	82
Figure 5.36: The analysis of Emalahleni brine based on the previous and the current study.	83
Figure 5.37: The change in brine levels over time of the Emalahleni brine under natural convection.	84
Figure 5.38: The change in temperature at specific depths during the Emalahleni brine experiments under natural convection.	85
Figure 5.39: The level change of the Emalahleni brine under forced convection	86
Figure 5.40: The graph indicates the temperature stratification of the Emalahleni brine during forced convection.	86
Figure 5.41: The mean monthly and annual A-pan equivalent potential evaporation annual evaporation of the relevant secondary catchment in the Olifants Catchment (Schulze et al., 1997).	87
Figure 5.42. The average minimum temperatures of the relevant secondary catchment of the Olifants Catchment over the last four years (Courtesy of SAWS 2013).....	88
Figure 5.43. The monthly average maximum temperatures of Emalahleni area over the last four years (Courtesy of SAWS 2013)	88
Figure 5.44. The monthly rainfall of the Emalahleni area over the last four years (Courtesy of the South African Weather Service, 2013).....	89
Figure 5.45. The temperature and the humidity of the Emalahleni area for 3 days (17 to 19 February 2009).	89
Figure 5.46. The temperature and humidity of the experimental results during the Emalahleni brine conducted in 2013.	90
Figure 5.47. The thermal energy distribution during the Emalahleni brine experiment.	91
Figure 6.1: FT-IR Spectrum of PAN	94
Figure 6.2: FT-IR Spectra of PAN and PAN+TiO ₂	94
Figure 6.3: FT-IR Spectra of PAN and PAN+Zeolite Y	95
Figure 6.4: SEM image of PAN nanofibre	95
Figure 6.5: SEM image of PAN+TiO ₂ nanofibre	96
Figure 6.6: Effect of contact time on adsorption of metal ions on PAN+TiO ₂ nanofibre	96

Figure 6.7: Effect of contact time on adsorption of metal ions on PAN+Zeolite nanofibre..... 97

Figure 6.8: Effect of concentration on the adsorption capacity of PAN+TiO₂ nanofibre 98

Figure 6.9: Effect of concentration on the adsorption capacity of PAN+Zeolite nanofiber..... 99

LIST OF TABLES

Table 2.1: Chemical constituents (ppm) in some South African power plant brines.....	9
Table 3.1: Parameters measured during the evaporation test.....	27
Table 4.1: pH and EC of the Emalahleni RO brine at different stages of development.....	34
Table 4.2: Chemical composition (concentration in mg/L except pH and EC (mS/cm)) of stage 3 reject brine from Emalahleni.....	35
Table 4.3: Major ions in Emalahleni brine calculated to include alkalinity as well as downward adjustment of sulphate and chloride values to balance cation charge.....	35
Table 4.4: Water loss of salts on drying at 100°C.....	37
Table 4.5: Water holding capacity of salts.....	38
Table 4.6: Different salts solutions used.....	47
Table 5.1: Volume losses for all the experiments over a 48 hour period.....	72
Table 5.2. The output file of the Emalahleni brine in PhreeqC.....	84
Table 5.3: Comparison of the actual measurements of the Emalahleni brine and the modelled brine evaporation for the same period.....	87
Table 6.1: Rate constants for first and second order adsorption on PAN+TiO ₂ and PAN+Zeolite.....	100
Table 6.2: Plot of Freundlich Isotherms vs Langmuir Isotherms.....	102

ACRONYMS & ABBREVIATIONS

AMD	Acid Mine Drainage (AMD)
DWAF	Department of Water Affairs and Forestry
EC	electrical conductivity
ED	Electrodialysis
IC	ion chromatography
ICP-OES	inductively-coupled plasma-optical emission spectroscopy
IR	Infra-red
IR	Infra-red
MF	Microfiltration
NF	Nanofiltration
OR	Reverse Osmosis
PAN	Poly acrylonitrile
RH	Relative humidity
SAWS	South African Weather Service
SMD	Sulphuric Mine Drainage
TDS	Total Dissolved Solid
UF	Ultrafiltration
ZLD	zero liquid discharge

CHAPTER 1: BACKGROUND

1.1 INTRODUCTION

Desalination is a well-established means of ensuring water supply in many countries and increasingly also used for the recovery of good quality water from waste water. Desalination generates reject brine which requires management and disposal. Challenges include the growing number and size of inland desalination plants, increased regulation of effluent discharge making disposal more difficult, and an increasing number of desalination plants in semi-arid regions where conventional disposal options are limited (Mickley, 2006). Brine disposal methods include deep well injection, land application, discharge into surface water bodies and evaporation ponds.

Brine disposal in evaporation ponds has been considered the most effective option due to ease of construction, low maintenance and minor operator attention (Mickley et al., 1993). These ponds work by concentrating the brine, causing precipitation of salt crystals which are periodically removed from the ponds. Fu et al. (2009) has described several problems with previous studies using pan evaporators such as pan size, orientation, material painting, incorrect placement, lack of preventative measure to prevent animals from drinking the water, improper use of baseline corrections during experimental runs, inadequate assessment of thermodynamics of the system, etc. In South Africa the use of evaporation ponds for commercial production of salt (sodium chloride) is widely favoured by climate and is carried out at a number of locations. However, much of the industrial brine production is located in less arid parts of the country, especially Gauteng and Mpumalanga provinces where securing effective evaporation is more challenging, requiring larger evaporation ponds and more awareness of how evaporation can be enhanced.

A recent Water Research Commission project examined the effect of salinity on evaporation of brine generated at Emalahleni from coal mine water treatment (Dama-Fakir and Toerien, 2009). The present study was commissioned in order to gain further insight into the factors affecting brine evaporation by developing and using a more controlled laboratory set-up to provide a platform for studies of South African brines in the future.

1.2 PROJECT AIMS

The following were the aims of the project:

1. Survey of the literature on evaporation rates from brines
2. Design and assembly of climate controlled enclosures for the study of evaporation processes of brines
3. Development of protocols for the measurement of evaporation rates from brines

4. Development of empirical models for determining evaporation processes of industrial brines under controlled laboratory conditions
5. Validation and calibration of the model developed using actual brine pans

The project deliverables were defined in terms of a series of programmed interim reports and this final report which will address the following list of tasks set at the start of the project:

- 1) Literature review
- 2) Characterization and classification of brine
- 3) Design and assembly of climate controlled enclosures
- 4) Industrial brine evaporation under controlled conditions
- 5) Empirical and theoretical modelling of industrial brine systems
- 6) Novel materials for enhanced brine evaporation

1.3 SCOPE AND LIMITATIONS

This study surveyed the literature on evaporation of brines and designed an assembly of climate controlled enclosures for the study of evaporation processes of brines at laboratory scale to ensure adequate measurement of all physical and chemical parameters influencing the evaporation. The study developed protocols for the measurement of evaporation rates from brines and investigated empirical models for determining evaporation processes of industrial brines under controlled laboratory conditions. The validation and calibration of the model developed using laboratory brine pans was undertaken but due to safety issues pertaining to Emalahleni during the project access to the actual evaporation pan was out of limits. Brines rich in Mg chloride (known as bitterns) and which are highly hygroscopic were not part of the study as Mg was a minor component of the Emalahleni brine. Most industrial brines sampled were predominantly sodium sulphate rich in character with very high sodium and sulphate levels.

CHAPTER 2: LITERATURE REVIEW: THE NATURE, MANAGEMENT AND DISPOSAL OF BRINES GENERATED BY THE TREATMENT OF WASTEWATER

2.1 INTRODUCTION

Currently South Africa is a highly mining intensive country. Associated with mining is a major increase in acid mine drainage (AMD) also termed sulphuric mine drainage, which has led to a negative impact on the environment and a threat to clean water supply. In recent years wastewater from power stations and mining in South Africa has generally been considered a lost resource due to the lost opportunity to treat it to a 'fit for purpose' quality. Sulphuric mine drainage (SMD) or AMD occurs as a result of natural oxidation of sulphide minerals that are contained in mining wastes at operational and closed mine sites. AMD may adversely impact the surface water and groundwater quality and land use. These impacts can be due to the low pH, high acidity and elevated concentrations of metals and sulphate content associated with SMD. Once it develops at a mine, control or treatment can be difficult and expensive. And if generation of SMD cannot be prevented, it must be collected and treated to remove all unwanted constituents. Composition of the sulphuric mine drainage may vary depending on the power plant or mine it originated from. A recent study (Gitari et al., 2005) reported the mine drainage produced at power stations in South Africa to have high concentrations of Fe, Mn, Al, and SO_4^{2-} and some trace concentrations of Co, Pb, Cr, Zn and Cu.

Most of the river systems such as the Olifants River are heavily polluted with saline water. To mitigate this impact, a few of the larger mining organizations and municipalities such as Emalahleni have invested in desalination plants. This process converted AMD into potable water, but accumulated hyper-saline (brine solution) at far greater rates than expected. This waste product is currently stored in ponds where further crystallization of the brine can take place. The use of solar energy to drive the process is cost effective. The current rate of this process needs to be increased to accommodate output brine volumes to be processed. The evaporation rate is a key element to increase the crystallization process. The climatic conditions in this respect govern all the relevant factors such as the radiation, wind element, temperature and humidity. It is often complex to simulate the natural elements that affect the behaviour of a solar brine pond in a specific geographical location in a controlled environment, to achieve optimal evaporation rates. With the geographical area known, the average evaporation can be calculated. For the area of Emalahleni, the annual potential evapotranspiration is 1513.7 mm (Shulze et al., 1997). An area subjected to the radiation, the wind, temperature, humidity in a controlled environment will help to comprehend the influence it has on the rate of evaporation and how close the parameters behave to reality.

2.2 THE TREATMENT OF WASTEWATER USING MEMBRANE TECHNOLOGIES

The increasing demand for potable water has led to the upgrading and expansion of municipal water and waste water treatment facilities across South Africa (Mema, 2009). This scarcity of fresh water has resulted in the use of mine water as a potential source of potable water. Several technologies have been introduced to purify the waste water. Recent advances in membrane technology used to convert acid mine drainage into potable water have led to an increase in the number of water treatment or reclamation plants.

Severe water shortages have led to a number of countries including South Africa, turning to desalination processes as a solution to getting good quality water. To meet the demand for domestic water use in the late 1960s several desalination plants were developed in various parts of the world. Despite its benefits, Lattemann and Hopner (2008) highlighted the challenges that remain over potential negative impacts of water desalination on the environment. They raised some of the key issues which include the high concentration of brines discharged to the marine environment, impacts caused by the feed water intake, emission of air pollutants and energy demand.

There are three basic categories of water purification technology used for desalination: membrane technologies, distillation processes (thermal technologies), and chemical approaches. Some water purification plants use a combination of these methods. Desalination membranes are being widely applied for treating brackish surface waters, ground waters, reclaimed waste water and seawater to create new water sources. Synthetic membranes are the most widely used in desalination and their use is growing at a rate of 5-10% annually (Krukowski 2001).

In South Africa the key factors driving the demand for water are the increase in the population, industrial growth and increased requirements to service the total population. Desalination plants, for purposes ranging from municipal water supply to industrial applications, are now in place in many countries. Many of these plants primarily utilize membrane technology and treat brackish water and seawater. In South Africa, there is diverse application of water by different sectors. Figure 2.1 shows the water use by different sectors in South Africa (DWAf, 2003).

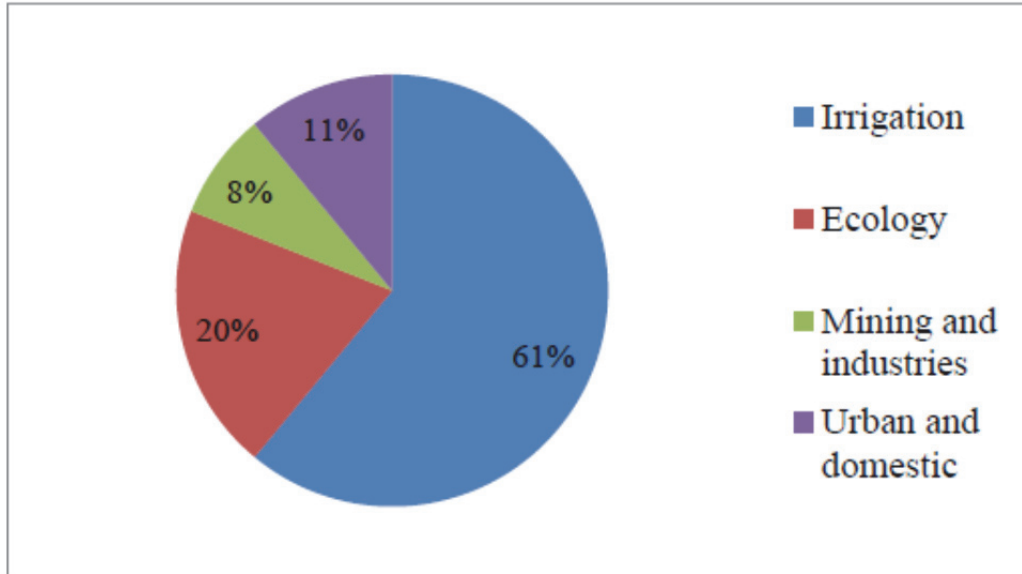
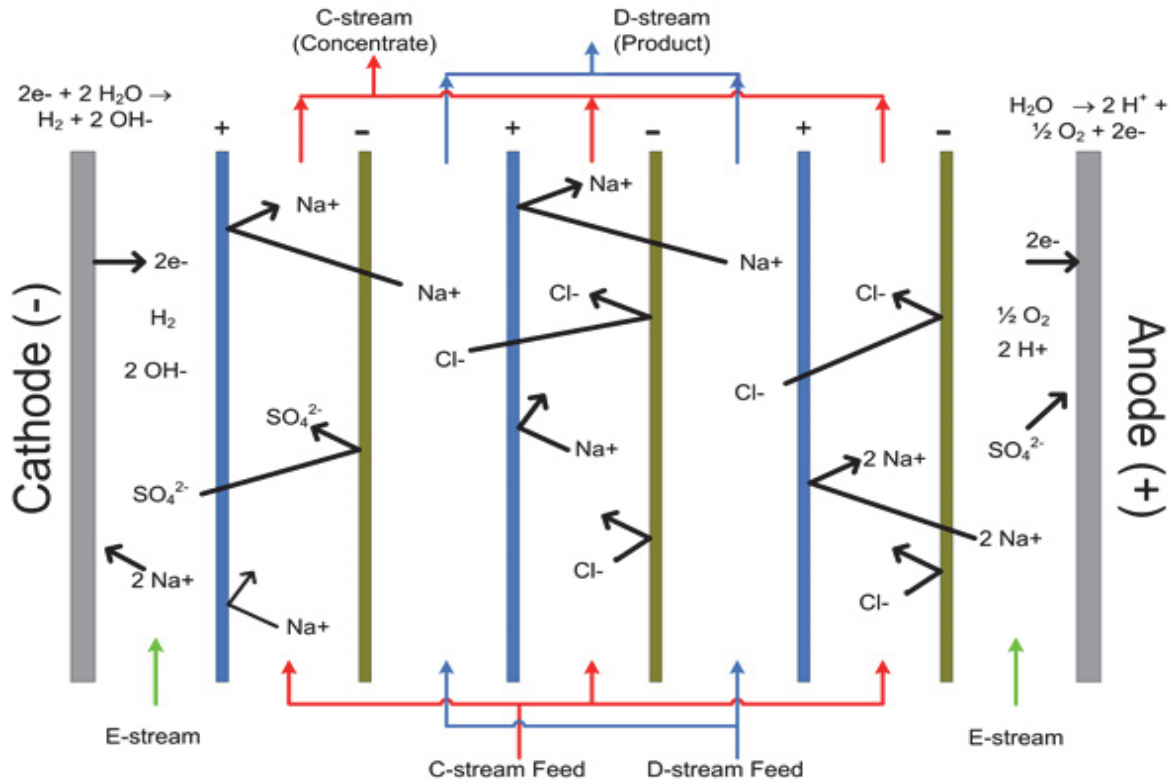


Figure 2.1: Application of water by different sectors in South Africa (DWAF, 2003)

Membranes are defined as thin films of porous material made of a wide variety of materials such as polymeric materials that include cellulose, acetate, and nylon, and nonpolymeric materials such as ceramics, metals and composites (Younos and Tulou, 2005). Membrane techniques are applied in water treatment technology wherever possible. Several membrane technologies are used for waste water treatment, which include electrodialysis (ED), reverse osmosis (OR), nanofiltration (NF), ultrafiltration (UF), and microfiltration (MF). Cabasso (1987) stated that the quality of the treated water produced is dependent on the pressure, the concentration of salts present in the feed water, and the salt permeation constant of the membranes. Membranes are said to be sensitive to a number of different factors. These include changes in pH, small concentrations of oxidized substances such as chlorine and chlorine oxides, a wide range of organic materials, and the presence of algae and bacteria (Otlis Semih and Otlis Serkan, 2004). Therefore due to these factors careful pre-treatment is required to prevent membrane contamination and fouling during treatment.

2.2.1 Electrodialysis (ED)

Electrodialysis (ED) is an electrochemical process in which ions migrate through ion-selective semipermeable membranes as a result of their attraction to two electrodes (Figure 2.2). The electric potential force is utilized to separate dissolved ions that are present in water. The separation of ions occurs in individual membrane units called cell pairs.



Courtesy EET Corporation
www.eetcorp.com

Figure 2.2: Electrodialysis (<http://en.wikipedia.org/wiki/Electrodialysis>)

Electrodialysis (ED) achieves salt removal from the feed water due to the anode that attracts the chloride ions and the cathode that attracts the sodium ions. During the process of ED a direct electrical current is established across the stack by electrodes positioned at both ends of the stack. This electric current “pulls” the ions through the membranes and concentrates them between each alternate pair of membranes. Partially desalted water is left between each adjacent set of membrane pairs. Scaling or fouling of the membranes is prevented in most ED units by operationally reversing the direction of the electrical current around the stacks at 15-30-min intervals. This reverses the flow of ions through the membranes so that the spaces collecting salty concentrate begin collecting less salty product water. Alternating valves in the water collection system automatically direct the flow in the appropriate direction. Typical freshwater recovery rates for ED (reversal) range from 80-90% of the feed water volume (Sonune and Ghater, 2004). A study conducted by Younos and Tulou (2005) revealed that an ED unit is able to remove from 50 to 94% of dissolved solids from a feed water with up to 12,000 mg/L total dissolved solid (TDS). The concentrated waste stream, electrode cleaning flows, and residuals from the pre-treatment process are a part of a typical waste stream flow that is disposed from the ED.

2.2.2 Ultrafiltration (UF)

For solutions of macromolecules or fine colloidal suspensions, ultrafiltration (UF) is the technique that is employed for simultaneous purification, concentration, and fractionation. Ultrafiltration can be applied in a wide variety of fields, from food and beverage industries to chemical industries. Today the most common use of UF technology worldwide is in the treatment of various water sources. The use of UF technology for municipal drinking water applications is a relatively recent development, and it is also common in many industrial applications. This process is operated with only residual disinfection in many surface water applications. Ultrafiltration and microfiltration are usually employed in conjunction with coagulants or adsorbents to provide greater removal of organic compounds (Mokhtar and Naoyuki, 2012; Uyak et al., 2014; Younos and Tulou, 2005).

2.2.3 Ion Exchange

The ion-exchange system is based on the interchange of ions between a solid phase and a liquid phase surrounding the solid. The technology is often used for water softening among other applications. In the ion-exchange process the undesirable ions in the feed water are exchanged for desirable ions as the water passes through granular chemicals, called ion-exchange resins. Resins can be made using naturally-occurring inorganic materials (such as zeolites) or synthetic materials. The higher the concentration of dissolved solids in the feed water, the more often the resins will need to be replaced or regenerated. The process removes sodium and chloride ions from feed water, thus producing potable fresh water. Ion exchange can be used in combination with reverse osmosis processes such as blending water treated by ion exchange with RO product water to increase water production (Tanaka and Ehara 2003).

2.2.4 Reverse Osmosis (RO)

Reverse osmosis (RO) along with nanofiltration (NF), ultrafiltration (UF) and microfiltration (MF) membranes are referred to as pressure driven membranes. Reverse osmosis (RO) systems are currently the fastest growing techniques in water desalination and are often selected for the treatment of acid or sulphuric mine drainage. This membrane technique is widely appreciated for its effectiveness in removing total dissolved solids (TDS) in concentrations of up to 45,000 mg/L (Younos and Tulou, 2005) and is being adopted increasingly in securing water supply for both industry and municipal use. Water that is treated by this method can range from ground water or sea water to brines and mine water. RO systems can vary from symmetric, asymmetric, to thin film composite membranes. This technique generates dynamic pressure to overcome the osmotic pressure of the salt solution that is generated, causing water-selective permeation from the saline side of a membrane to the fresh water side (Fig. 2.3). In RO systems, pre-treatment may consist of acidification, addition of anti-scalant chemicals, chlorination, and de-chlorination. All these processes generate wastes that are removed before the membrane process starts. A number of water treatment plants and power plants in South Africa use reverse osmosis for purifying waste water.

Salts streams are rejected from the RO membrane in order for the separation to be accomplished. Awerbuch and Weekes (1990) reported that reverse osmosis (RO) plants, in general, produce 25% of the total feed water flow as reject brine. For reverse osmosis in seawater desalination plants, the concentration of the concentrates is usually close to double that of the natural seawater (up to 65,000-85,000 mg/L).

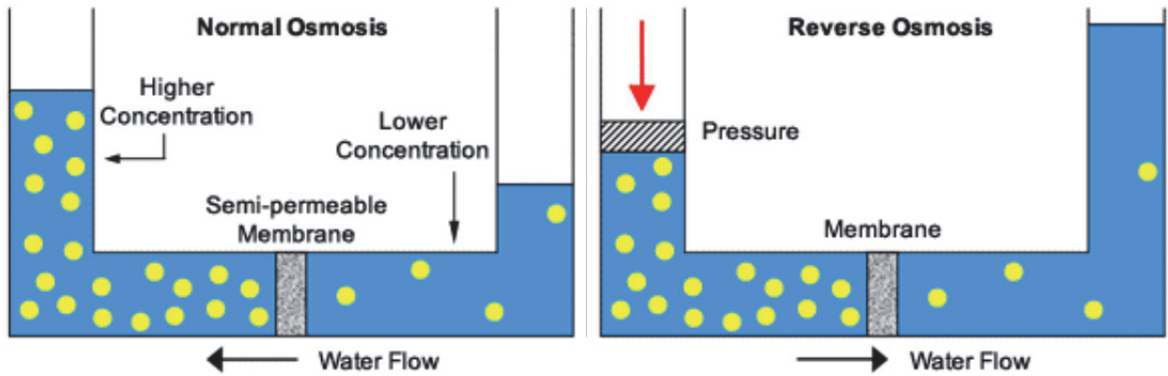


Figure 2.3: Osmosis and Reverse Osmosis (www.visionengineer.com/)

A reverse osmosis system at the Emalahleni plant in South Africa produces about 25,000 m³/d of potable water and about 150 m³/d of reject brine which is currently pumped into evaporation ponds (Himawan, 2003). Tanaka and Ehara (2003) reported that RO processes occur at ambient temperature and the only electrical energy required is for pumping the water to a high operating pressure varying from about 10 bars for brackish water to 50 bars for sea water. The quality of water produced depends on the pressure, the concentration of salts in the feed water and the salt permeation constant of the membranes.

2.3 BRINES

Saline water can result from many different sources. Some are natural sources and others are caused by human intervention. Natural brines contain a high concentration of dissolved constituents such as elements, molecules and ions. A study by Nyamingura (2009) described different ways for the formation of industrial brines to occur. Industrial brines have become one of the most problematic environmental pollutants in South Africa. The production of reject brine is an integral part of the operation of desalination plants. It is estimated that for every 1 m³ of desalinated water, an equivalent amount is generated as reject brine. Common contributors to the salinity of water are chlorides and sulphates of Na, Mg and Ca. Brines from industrial membrane treatment applications are generally considered to be more saline than sea water (35,000 mg/L TDS) and may contain up to 5 times the salt content of sea water. According to the World Health Organization the permissible limit of salinity in drinking water is 500 ppm and for special cases it could be up to 1000 ppm.

2.3.1 Composition

The composition of industrial brines is dependent upon several factors which include feed water quality, pre-treatment processes, the membrane employed, water recovery achieved and post-treatment that is applied (Du Plessis et al., 2006). Table 2.1 shows the composition of some of brines produced in water treatment circuits of South African power plants.

Table 2.1: Chemical constituents (ppm) in some South African power plant brines

Element	Tutuka Brine (Fatoba, 2011)	Lethabo Brine (Sonqishe, 2008)	Secunda Brine (Muriithi, 2009)
Al	0.045 ± 0.1	2.8	0.519
Ca	106.99 ± 12	112	616.56
K	106.2 ± 1	114.7	189.65
Mg	163.36 ± 1	198.4	22.31
Na	4804.88 ± 3	4719.1	1720.29
Si	13.11 ± 0.1	42.6	-
Cl	2424 ± 17	-	1110.87
SO ₄	8858 ± 86	-	3339.65
pH	7.75 ± 0.0	7.8	8.48
EC (mS/cm)	16.69 ± 0.5	15.83	-
TDS	5400 ± 283	-	-

2.3.2 Uses and impacts of brine

Industrial brine can be thought of as hyper-saline effluent that is potentially useful as raw material for the recovery of several salts. For brine disposal purposes, evaporation ponds reduce the volume and produce salt as part of the process. After the brine has evaporated to total dryness, the salts can be harvested and sold or disposed of approved waste disposal sites (Squire, 2000). However, for reuse the brine would need to be simplified to minimize the complexity of the salts. Saline effluents are industrially useful and may be used in agriculture, forestry, algae and mineral production. The traditional approach to deal with saline effluent has been to treat it as a waste disposal problem. However, a number of opportunities may arise after realizing that these effluents are a resource. The most common evaporate produced from the evaporation of brine is sodium chloride. Brines rich in Mg chloride after harvesting NaCl are known as bitterns which, on account of their hygroscopicity, may find valuable use as a dust suppressant and fire retardant. Other salts may also be generated through fractional crystallization as the brine dries. When disposing of reject brine serious precautions need to be taken to avoid impact on the environment.

2.3.3 Disposal

The major environmental concern related to desalination is the discharge of reject brine. Mickley et al. (1993) reported that brine disposal methods can significantly add to the cost of the desalination process. Thus, the method of disposal of the brine is one of the first matters to be investigated in determining the feasibility of a proposed desalination plant. In the US, this environmental concern is reflected in the national and state regulations where policies set up for the control of discharges have evolved into policies set up for the elimination of harmful pollutants to air, land and water. Regarding brine disposal, permission for any disposal method must be granted by the state. In the case of discharge to surface waters, demonstration of acceptable brine chemistry is required.

Although discharge into an open ocean is a common way that is usually practised to dispose of waste water, there are several harmful environmental effects caused by this direct discharge. This concentrated waste water has many properties, which badly affects the oceanic environment. It consists of highly concentrated salts and any un-reacted pre-treatment chemicals. Management of reject brine has become an increasingly difficult challenge due to many factors that include: growing number and size of desalination plants which limits disposal options, increased and stringent regulations of discharges that make disposal more difficult, increased public concern with environmental issues, and an increased number of desalination plants in semi-arid regions where conventional disposal options are limited (Mickley, 2006).

According to Economic and Social Commission for Western Asia (ESCWA, 1993), cost plays an important role in selection of the brine-disposal method. The disposal costs can range from 5 to 33 % of the total cost of desalination. The cost of disposal depends on reject brine characteristics, the level of treatment before disposal, means of disposal, volume of brine to be disposed and the nature of the receiving environment (Ahmed et al., 2001). Several techniques are reviewed below for handling reject brine. These include delivery into surface water resources or discharge to sewer, deep well injection into an aquifer, land application, and evaporation ponds, depending on the brine concentration (Younos, 2005, Ahmed et al., 2000, Mickley et al., 1993). Einav et al. (2003) reported that the choice between these brine disposal methods would depend on the practical conditions in the area, taking into consideration the environmental, engineering and economical aspects.

2.3.3.1 *Deep well injection*

Deep well injection is presently applied worldwide for disposal of industrial, municipal and liquid hazardous wastes (Saripalli et al., 2000). This method has also been employed for moving saline groundwater that must be relocated to protect fresh water aquifers. Prior to drilling any injection well, a careful assessment of geological conditions must be conducted in order to determine the depth and location of suitable porous aquifer reservoirs. Hence such wells should not be located in areas that are susceptible to earthquakes or regions with mineral resources. According to a study done by Skehan and Kwiatkowski (2000) there are several factors that have an impact on the reliability and

overall performance of an injection well. Due to the corrosive nature of the brine, many precautions must be added when designing the wells. Hence the costs associated with implementing these safety measures can make the deep well disposal option prohibitively expensive.

Saripalli et al. (2000) have surveyed literature on deep well injection of various aqueous waste streams in the United States. Research efforts by these investigators were focused on physical factors influencing well performance. Sabah et al. (2009) reported that one of the most important constraints on stable injectivity was the presence of total suspended solids (TSS) in the injection fluid. Frequent measurements of TSS are required to ensure steady well performance. Other factors include the selection of a suitable well site, costs that are involved in conditioning the reject brine, possibility of corrosion and subsequent leakage in the well casing, and the uncertainty of the well half-life.

2.3.3.2 Discharge into surface water

The continued discharge of saline water in South Africa has led to significant ground and surface water pollution and an increase in salinity levels in excess of regulatory limits (Department of Water Affairs and Forestry (DWAF), 2015). Discharging into surface water or to sewer dilutes the brine. Improper surface disposal has the potential for polluting the groundwater resources that are used as feed water for many of the reverse osmosis (RO) plants. The groundwater pollution is likely to result from high salinity and the presence of other detrimental chemicals in the reject brine. The resulting increase in the concentration of salts and minerals that is due to the disposal of brine into large bodies of water will be insignificant if the volume of the reject brine is not large relative to the volume of surface water (Ahmed et al., 2000). Many small RO plants dispose their reject brine in municipal sewerage systems. However, the increase in salinity may have some effects on the microorganisms of the system by reducing the amount of dissolved oxygen available (Mickley et al., 2006). Moreover, the disposed reject brine may overwhelm the existing capacity of the sewerage system. Mickley et al. (2006) further outlined the key factors that determine the costs of reject brine discharge to surface water. These include the costs to transport the brine from the desalination plant to the surface water discharge outfall, costs for outfall construction and operation, and the costs that are associated with monitoring the environmental effects of the brine discharge on the surface waters.

2.3.3.3 Land application

Land application used for the disposal of reject brine may include irrigation systems, percolating ponds and infiltration trenches. Irrigation systems can only be applicable where the resulting irrigation water will not harm crops or groundwater. The presence of high concentrations of exchangeable sodium or trace elements can render the reject brine unsuitable for irrigation purposes. Therefore, the quality of reject brine must satisfy crop and soil requirements (Ahmed et al., 2000). In their study, Mickley et al. (1993) provided a list of design criteria that are applicable to irrigation with reject brine: site selection, pre-application, treatment, land requirement, vegetation selection techniques, hydraulic

loading, and surface runoff control. It is essential to consider the long-term impacts of increasing salinization of agricultural soils.

2.3.3.4 *Zero liquid discharge*

The zero liquid discharge (ZLD) system includes the processes of pre-treatment and evaporation of the industrial effluent until the dissolved solids precipitate as crystals. These crystals are removed and dewatered. The water vapour from evaporation is condensed and returned to the process. The most important advantage of the ZLD method is that it reduces the discharge of brine to surface or groundwater (Mickley, 2006).

2.3.3.5 *Evaporation ponds*

Evaporation is the state of a liquid to transform into a vapour. Evaporation is an important factor in the hydrological cycle. It is a link between water on the surface of the earth and the atmosphere which operates continuously with no specific origin or ending. The rate of evaporation however varies around the world where many factors play an important role. Evaporation from a free water body is different to evaporation from a water body with vegetation. This makes evaporation estimates quite difficult in a natural environment (Brutsaert, 1982). The ambient temperature, humidity, density of the liquid and the energy input are major components which contribute towards the rate of the evaporation. In this study these contributing elements were tested in an environment, where some of the parameters were changed to resemble conditions in reality. Evaporation is a fundamental part of the hydrological cycle. The continuous transfer of water from one phase to another would not be possible without evaporation. This constant cycle of water from the surface of the earth to the atmosphere is a closed system. In terms of managing water resources it is very important to determine how much water evaporates into the atmosphere as the usable amount becomes less. With global water resources on the decline, it becomes more important to make accurate calculations regarding the use of the resources to ensure the safeguarding of resources for future generations. Evapotranspiration from the earth's surface in conjunction with precipitation governs the runoff which has a regulating effect on flooding although the infiltration rate can be a factor.

Evaporation is the process which transcends the water and the energy budget (Brutsaert, 1982). When a water body is subjected to energy it can transform into a different phase, from liquid to gas for example. The equation to demonstrate this is:

$$R_n = L_e E + H + G \quad (1)$$

R_n = specific flux of net incoming radiation.

L_e = latent heat of vaporization.

E = evaporation rate

G = heat flux into the earth.

With quite a large amount of energy being absorbed by the earth's surface, this energy drives various cycles like the hydrological cycle. Quite a large amount of this energy is converted into long-wave radiation. A part of the energy is used which is required to convert large amounts of water into vapour where it drives the atmosphere. The evaporation process along with other processes plays a vital role in weather patterns and climate processes. The latent heat and sensible heat flux is quite important in the consideration of energy plants on a micro scale as it may influence the global energy budget (Brutsaert, 1982).

Evaporation cannot be isolated with reference to other aspects and sensible heat cannot be singled out. Sensible heat is the process where energy is required to change the temperature without changing the phase of a particular object. This relationship can be expressed as;

$$B_o = H/L_e E \quad (2)$$

B_o = Bowen Ratio

H = Radiation flux

L_e = Latent heat of vaporization

E = Evaporation

The latent heat of evaporation refers to the amount of heat energy needed to convert a specific unit mass in liquid form into a vapour without any change in the temperature. The latent heat of evaporation for pure water is 2500 J g^{-1} at standard temperature and pressure (Monteith et al., 2008). The more volatile the substance is the less the energy is required to evaporate it.

The air near the surface of the earth is known as the boundary layer. Because of humidity, temperature and the wind, air at the boundary layer has shown a greater amount of change near the surface than at higher elevation (Brutsaert, 1982). The boundary layer at a water surface therefore has a far greater effect on the evaporation rate. Water vapour is being transported away from the surface layer by turbulent eddies which is a function of surface roughness and wind shear (Pal Arya, 1998).

The method of measuring evaporation has evolved over the years. In the early days, a tiled pit was one of the first methods to measure evaporation where water was refilled daily from the previous evaporation. The modern quantitative theories were developed during the nineteenth century by John Dalton and others. The Penman equation (1948) combined the energy balance and the mass transfer formulas for open water bodies and land saturated land surfaces (Pal Arya, 1998). Since then modification has been made to the formula. Today the Penman-Monteith method is widely used to estimate evapotranspiration.

Measuring evaporation with a number of variable factors influencing the evaporation rate is a challenging task. In a natural pond the density of the brine, ambient temperature, wind variation and fauna impact can influence the evaporation rate.

Evaporation ponds are ideal (Mickely, 2004):

- Under a suitable climate where the solar energy is sufficient (especially arid regions)
- Where the insulation system is adequate to contain the energy
- Where the volume and type of crystalline product suit the design of the pond.

The disposal of reject brine presents significant engineering, economic and environmental problems. The best option of disposal of brine solution from an environmental perspective is evaporation ponds, provided that the correct safety measures are taken in order to prevent leakage and correct disposal is performed. This disposal method is most effective for disposal from inland desalination plants, especially for dry, arid regions. Inland desalination plants are usually located in areas that are likely to have consistent dry weather, relatively high temperature and, consequently, high evaporation rates (Ahmed et al., 2000). The evaporation pond is often selected due to its several advantages which include easy construction, low maintenance and little operator attention (Mickley et al., 1993). This disposal method requires little mechanical equipment except for the pump that conveys the waste water to the pond (Ahmed et al., 2000). During the design of these evaporation ponds, two components are carefully considered which include the surface area and the depth. From the research that was done by Glater and Cohen (2003), freeboard, which is the excess capacity of the pond, is also one of the components that have to be considered during the design of these ponds. They noted that freeboard was difficult to estimate since it was dependent on the average rainfall and wind velocity in the pond area.

Evaporation ponds are fragile and should not be allowed to completely dry out as the liner system will become damaged. A study conducted by Ahmed et al. (2001) reported proper sizing of evaporation ponds is dependent on the accurate calculations of the evaporation rate. In this disposal method, the reject brine is discharged to ponds and evaporated to dryness for final disposal. The reject brine may require additional treatment before this option can be used depending upon the chemical makeup of the reject brine. Dama-Fakir and Toerien (2009) emphasized that dissolved salt results in a lower saturation vapour pressure and thus a lower evaporation rate. This adverse effect of increasing salinity on evaporation is well known in the solar salt industry and is taken into account in the design of ponds.

2.4 CHEMICAL AND PHYSICAL PRINCIPLES OF BRINE EVAPORATION PONDS

Apart from the few areas where salt mining is possible, nearly all forms of salt production require evaporation of water to concentrate brine and ultimately produce salt crystals (Akridge, 2008). The use of evaporation ponds for brine disposal has increased greatly in recent decades. During the evaporation process ponds work by concentrating the brine, eventually causing precipitation of salt

crystals as the solubility limit is reached. The most common water that is introduced into evaporation ponds for producing salt is sea water. In South Africa a number of salt production companies make use of evaporation ponds along with crystallization ponds for the production of commercial salts along the coast. Evaporation ponds also offer an opportunity to develop resource recovery measures such as aquaculture, brine shrimp, beta-carotene production, salt harvesting, recovery of bitterns, and linking to solar ponds for electricity generation (Ahmed et al., 2000). Common salt or sodium chloride (NaCl) in South Africa is recovered from seawater and from natural, inland brines. South Africa has 16 operating salt companies, of varying size. It is unlikely that highly contaminated industrial brine could be economically used for NaCl recovery.

2.4.1 Environmental impacts of evaporation ponds

The design of the evaporation ponds is done by accurate calculations of evaporation rate. The rate at which an evaporation pond can transfer this water governs the size of the pond. For an evaporation pond to be a viable disposal alternative for membrane concentrates, it must be able to accept concentrate at all times and under all conditions so as not to restrict operation of the desalination plant (Ahmed et al., 2000). The constraints of evaporation ponds are: availability of sufficient land, and lining with impervious liners of clay or synthetic membranes such as PVC or Hypalon. There is potential for contaminating underlying potable water aquifers through seepage from poorly constructed evaporation ponds (Squire, 2000). The saline water, if containing high dissolved gas levels (leading to cavitation in pipes) or iron sludge (due to the presence of iron bacteria), can cause rapid deterioration of conveying pipes and pumps (Ahmed et al., 2000).

Salt removal from evaporation ponds is necessary in order to maintain evaporation efficiency. In some cases, the evaporite minerals that form in the ponds constitute hazardous wastes. Some of the incorporated toxic elements found in these evaporite minerals include Se, B, As and Mo.

2.4.2 Pond water chemistry

Evaporation ponds are constructed to receive and hold saline water until water is evaporated out. During evaporation the air above the evaporation ponds becomes humid and chemical constituents progressively concentrate. Numerous chemical, physical and biological reactions take place in the pond during the evaporation of brine water. Kokya and Kokya (2006) attributed progressively lower evaporation rates to decreased chemical potential of the water during evaporation and hence correspondingly lower saturation vapour pressures. Brine waters are mostly rich in sulphate and chloride salts of Na, Mg, K and Ca. Upon dissolution of these salts in water, dissociation of constituent cations (Na^+ , Mg^{+2} , K^+ , Ca^{+2} ,) and anions (Cl^- , SO_4^{2-} , NO_3^- , HCO_3^-) takes place (Mao, 1999). The hydration of these cations and anions in solution contributes to the reduced chemical potential of the water.

The association of ions is one very important aspect when trying to understand many of the chemical properties of brine water. Solubility can be defined as the limiting amount of solute that can dissolve in a solvent under a given set of physical conditions. The resulting dissolution of salts in water affects the physical and the chemical properties of water (Mao, 1999). Certain combinations of ions can lead to compounds which have low solubility. Once the solubility is exceeded the compounds precipitate from solution as solids.

During mineral precipitation from a brine solution, the less abundant ion of the mineral pair of ions will become drastically depleted compared to the other (Hardie and Eugster, 1970). Precipitation of solids takes place as the result of changes in ionic composition, pressure, temperature and pH of the brine water (Merdhah and Yassin, 2008). A decrease in pressure or an increase in temperature of a brine results in reduced solubility of the salts that are present.

Nearly all forms of salt production require the process of evaporation of water in order to concentrate brine and ultimately produce salt crystals. The amount of salt that is produced after the evaporation process can be determined using the formula:

$$m_s - m_w(1.52 \times 10^{-2} S^2 + 9.50 \times 10^{-3} S) \quad (3)$$

Where m_s represent the mass (kg) of salt crystallized, m_w is the mass (kg) of the water evaporated, and S is the initial salt concentration of the brine in wt% (Akridge, 2008).

The crystallization path or sequence of minerals produced from evaporation of brine is the other aspect that has been studied (Nie et al., 2009, Shadidzader-Bonn, 2008). Nie et al. (2009) investigated the behaviour of elements such as Li, B, K and other trace elements in brine isothermal evaporation at 25°C using Zabuye salt lake brine. The mineral zabuyelite (Li_2CO_3) precipitated in the early stage of evaporation due to the fact that it was this mineral which was supersaturated in the brine. At an intermediate stage of evaporation, potassium was precipitated as aphthitalia ($3\text{K}_2\text{SO}_4 \cdot \text{Na}_2\text{SO}_4$) and in the last stage potassium was precipitated as sylvite (KCl). Boron was concentrated in the early and intermediate stages and then precipitated as borax ($\text{Na}_2\text{B}_4\text{O}_7 \cdot 10\text{H}_2\text{O}$) in the late stage. Schultheis et al. (2001) reminds us that in a quinary brine system of oceanic salts, the following crystallization sequence occurs: halite, carnallite, leonhardtite, bischofite ($\text{MgCl}_2 \cdot 6\text{H}_2\text{O}$).

2.4.3 Evaporation and the factors that affect it

The rate of evaporation is defined as the amount of water evaporated per unit surface area per unit time. It can be expressed as the mass or volume of liquid water evaporated per unit area which equates to a depth (in mm or m) of liquid water evaporated per unit time. The concentration of the brine (specifically its salinity) and the meteorological environment to which it is exposed are the chief determinants of evaporation rate (Dama-Fakir and Toerien, 2009).

2.4.3.1 *Salinity*

Any addition of solute to the solvent causes changes in colligative properties of the solution which include freezing point, boiling point, vapour pressure and osmotic pressure. The effect of salinity is both to reduce evaporation and to increase the energy returned to the atmosphere by other physical processes, so that under equilibrium conditions, a saline solution reaches a temperature higher than that of pure water (Harbeck, 1955). In the study conducted by Ahmed et al. (2000), it was stated that salinity of water influences the rate of evaporation. As the salinity increases, evaporation of water decreases. This is due to the reduction in the water vapour pressure at the water surface (Al-Shammiri, 2002). From Raoult's Law, it is stated that the partial pressure of a solute in a solution is equal to the vapour pressure of solvent times the mole fraction of the solute in solution. The law dictates that vapour pressure lowering is proportional to the mole fraction of water in the solution and inversely proportional to the water activity.

In his study of the effect of salinity upon evaporation from pans and shallow lakes, Oround (1995) explained how saline water responded differently to the meteorological conditions. These were some of the factors that he highlighted in his study:

- The latent heat that is released during evaporation is smaller over saline water than over fresh water due to the effect of salinity in reducing saturation vapour pressure. This results in different modifications of atmospheric moisture within an air mass over a saline water body compared to that of fresh water.
- Atmospheric stability over a saline water body also differs from that over a fresh water body due to the distinct temperature differentials between each water body and the contiguous atmosphere. Under identical meteorological conditions, it is expected that turbulent transport within the atmospheric surface layer over a saline water body is likely to be more developed than its counterpart over a fresh water body, although a higher evaporation rate over the fresh water body would slightly increase atmospheric buoyancy over it.
- Both volumetric heat capacity and latent heat of vaporization for saline water bodies differ from those of fresh water, with the departure becoming more pronounced as salinity increases.

There is evidence that evaporation rates under specific climatic conditions depend more on the density of the brine than on the types of salts present (Turk, 1970; Harbeck, 1955). Their study further emphasized that variation in total salinity and the density are more important in controlling evaporation than is chemical composition.

2.4.3.2 *Meteorological parameters*

Even though evaporation ponds have been considered the most effective method for brine disposal several factors can limit the rate of evaporation. For example, operation is greatly hampered during

cold winters. The main climatic parameters that affect the rate of evaporation are temperature, humidity, radiation and wind.

Temperature

There is a direct relationship between the ambient temperature, water temperature and the evaporation rate. With an increase in the surface temperature, the water temperature increases and the evaporation rate can be influenced (Wahlin et al., 2009). Temperature is a primary driver of the evaporation process. Oroud (1999) indicated that irradiated salt water shows a higher temperature in comparison with fresh water. Mickley (1993) concluded that while an increase in temperature of saline water tends to increase evaporation, the water is less efficient in converting radiant energy into latent heat due to the exchange of sensible heat and long-wave radiation with the atmosphere. The net result is that, with the same input of energy, the evaporation rate of saline water is lower than that of fresh water. Ahmed et al. (2000) suggested one of the practical ways of enhancing the rate of evaporation is to introduce dyes into the brine which will cause an increase in the temperature. They further indicated that the use of a naphthol green dye at a concentration of around 2 ppm will increase the evaporation by 13%. In some instances, algae are also employed to accelerate the rates of evaporation of brine water. The experimental setup should be conducted where the ambient temperature should have a minimum effect on the evaporation rate with most of the energy input directly supplied by the equipment.

Humidity

The humidity is also referred to as the ratio of partial vapour pressure of water in the air and the saturated vapour pressure in the air at a given temperature (Monteith et al., 2008). The partial vapour pressure is a function of temperature and wind. With an increase in temperature the humidity decreases indefinitely. The evaporation rate is a function of humidity (Hisatake et al., 1993). With an increase in humidity the evaporation rate decreases and vice versa. The humidity is measured using a hygrometer and can be regulated using a humidistat. Humidity has a large influence on the rate of brine evaporation. Due to high levels of saturation that are reached at high levels of humidity, low rates of brine evaporation result. Leaney and Christen (2003) stated that some dissolved salts such as sodium chloride tend to stop the process of evaporation when humidity is above 70%. For some salts evaporation ceases at lower levels of humidity. Hence they concluded that the dissolved salt composition has an effect on the level of humidity at which evaporation will cease.

Solar radiation

The radiation from the sun known as solar flux, reaches the outer atmosphere at around 1368 W/m² (Pal Arya, 1998). The amount of solar radiation received by a surface area is known as irradiance and is expressed in W/m². The solar radiation at the surface of the earth is lower than the amount received

by the outer atmosphere (Brutseart, 1982). From a spatial perspective the radiation intensity from a point source can be expressed (equation 4) as;

$$I = d4/dw \tag{4}$$

I=Intensity of the radiation

d4 =Change in flux emitted from the source

dw =Change in solid angle

The heat flux penetrating the water can be determined by measuring the water temperatures at various depths of the water. At the surface the radiation can be measured using a pyranometer (Brutseart, 1982). A number of sensors are placed at various depths of the water to observe the thermal stratification of the water. The depth of the solar pond along with the surface area is highly significant in crystallized salt production rate. The radiated energy from the sun can dissipate in deeper waters and consequentially influence the thermal stratification of the pond. A shallow pond might have the ability to increase the evaporation rate and crystalize salts at a faster rate. This however might have an adverse effect on the production of the salts in the longer term if the produced salt is not removed. Salt production in a shallow pond with a large enough surface area can reflect the radiated energy back into the atmosphere (Coleman, 2000). Evaporation ponds are usually selected for brine disposal due to their effectiveness in capturing solar energy – a property of salinity gradient solar ponds. In solar ponds, the energy is received by the pond as direct radiation from the sun and indirectly from the atmosphere. Part of this energy is reflected, part absorbed, and the rest is transmitted to the pond bottom. Solar radiation emanating from the sun provides the heat that is required for the process of evaporation to occur. Enough energy is required to convert the water from a liquid phase into a vapour phase. Several studies have indicated that the process of evaporation is greatest on hot, windy, and dry days and is greatly reduced when air is cool and humid. Paneharatnam (1972) proposed that some heat is lost during sunlight hours by conduction into the ground, but all of this heat is regained at night when the brine and soil surface become colder than the soil sub-layer. Heat transfer also takes place between the brine and surrounding air by conduction and convection. This may represent a gain or loss depending on whether the air or the brine is at a higher temperature. The difference between the energy gain and loss is accounted for by changes in the brine temperature and by evaporation of water.

Wind

Wind speed is one important aspect ignored by most literature reporting trends in pan evaporation and theoretical explanations. Any reductions in wind speed could contribute to the observed declines in pan evaporation (Fu et al., 2009). Wind is required to displace humid air otherwise the air above the pond will become saturated with water vapour and evaporation will cease. One of the main purposes of the wind energy is to remove the saturated air above the water solution during evaporation. The wind has a major influence in maintaining the atmospheric moisture gradient to allow consistent

evaporation of the water solution. With the saturated air above the brine ponds constantly removed this will favour a high evaporation rate if the other conditions are suitable.

The impact from wind blowing over a pond is highly dependent on many variable factors. The wind speed, flow direction and wave breaking of the water, play a significant role in the rate of evaporation (Duan et al., 2009). A shear stress is developed when wind comes into contact with the surface of a water body which results in a surface roughness which consist of three segments. The surface roughness is proportional to the viscous layer during the initial shear velocity (O'Conner, 1983). The second segment, the shear velocity, is squared to the same proportion of the viscous layer. In the third segment the shear force breaks through the viscous layer and remains constant.

Within the boundary of the air-water interface the air flow and the stream flow can reduce the turbulence of the water resulting in a viscous layer between the water and air (Duan et al., 2009). Turbulence, which is generated in a stagnant pond, is mainly wind driven and promotes gas transfer through diffusion. The viscous layer strength is highly dependent on impurities and temperature of the water. An increase in impurities will increase the strength of the viscous layer. With an increase of the water temperature the strength of the viscous layer decreases and vice versa. For a liquid to evaporate successfully, it requires enough energy to overcome the cohesive forces between the molecules generated by the viscous layer.

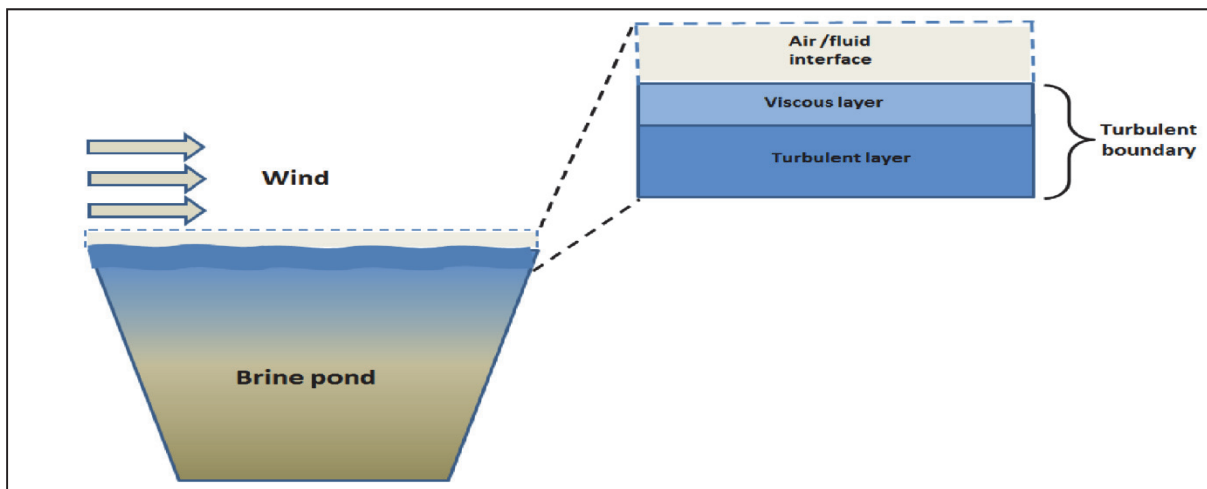


Figure 2.4 The wind interaction with a fluid surface (adapted from Duan et al., 2009)

Various experiments have been conducted concerning the evaporation rate with restricted parameters in a wind tunnel (Duan et al., 2009). The standard Class A pan with water was exposed to different wind velocities along with different water depths. The evaporation was measured using a water level sensor with a resolution of 0.097 mm and the net radiation was 10W/m^2 . With an increase in wind velocity, the evaporation rate increased at higher water levels (Chia-Ren., 2010). Extreme high wind velocities caused the water to be physically removed from the Class-A pan. This relates to the entire water loss shared between evaporation and spillage. At lower water levels of the Class-A pan, the

results were fairly different. Initially a steady increase in the evaporation rate occurred with an increase in wind velocity until the evaporation rate remained constant even at much higher wind speeds (in excess of $7\text{m}\cdot\text{s}^{-1}$ for a 10 minute duration) (Figure 2.5). Based on the experiment, the side wall acted as a shield for the lower water level against the high velocity winds (Chia-Ren., 2010). With experiments conducted outside a wind tunnel, variations in wind speed is of significance to trends in pan evaporation (Ryner, 2007).

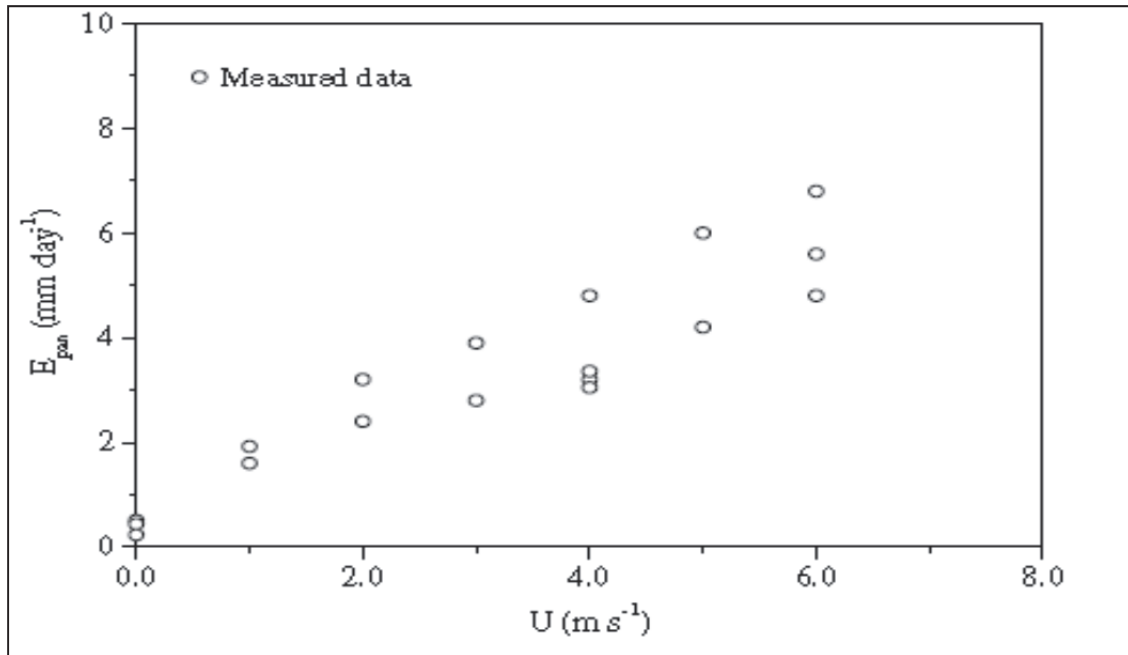


Figure 2.5: The results for pan evaporation for various wind speeds and different depths (from Chia-Ren., 2010).

2.4.3.3 Calculating the rate of evaporation

Much effort has been made to understand the different methods that are used to calculate the rate of evaporation. The evaporation rate from salt water depends mostly on saturated vapour pressure above its surface (Kokya and Kokya, 2008). In order to establish a correlation that describes the water surface and the evaporation process, methods that can measure the evaporation rate accurately are needed. Several methods that provide reasonable results for the rate of evaporation have been developed (Al-Sammiri, 2001). These methods include measurements of humidity change in the air stream, weight change of the water pan, water level change, moisture absorption by an absorbent material, and heat and mass balance. The process of evaporation applies to different types of water including sea water, shallow lakes and effluents occupying evaporation ponds (Oround, 1995; Calder and Neal 1984; Kokya and Kokya 2008).

A standard evaporation pan (class A pan) is widely used to measure pan evaporation rates (Ahmed et al., 2000). The use of these pans is to directly measure evaporation in the field. They provide a simple, integrated measurement of complex interactions between wind speed, temperature, solar

radiation and humidity. Sunken tank evaporimeters were formerly used by the Australian Bureau of Meteorology for measuring pan evaporation. These tanks were not of a standard size and were not made of consistent materials, and as a result data were reported to be difficult to use for climate characterisation. In the study conducted by Fu et al. (2009), pan evaporation measurements were described. The steps involved are: (1) the pan is installed in the field; (2) the pan is filled with a known quantity of water (the surface area of the pan is known and the water depth is measured); (3) the water is allowed to evaporate over a certain period of time during which rainfall is also measured; (4) a second water depth measurement is made; (5) the amount of evaporation per unit time (the difference between the two measured water depths, plus precipitation amount during the same period if any) is then calculated (Brouwer and Heibloem, 1986) as:

$$E_{\text{Pan}} = P + (n_1 - n_2) \quad (5)$$

where E_{Pan} is the pan evaporation (mm), P is precipitation (mm), and n_1 and n_2 are initial and final water levels (mm) measured in the pan.

Expected evaporation can also be calculated from climate data and the salt content of the water. The most widely used equation for evaporation from a water surface is that of Penman (1948) which has subsequently been modified quite extensively for different applications. The modification by Calder and Neal (1984) is quite widely employed for accommodating the effect of salinity on evaporation by computing the salt concentration-dependent activity of water which is a determinant of vapour pressure, while that of Shuttleworth (1993) simplifies and adapts the Penman equation for calculation using SI units so that the key determinants of evaporation, namely temperature, net irradiance, wind speed and vapour pressure deficit (humidity) can be employed in the calculation more directly.

Suffice it to say that the prediction of evaporation rate and therefore the design of a brine evaporation facility will ultimately be limited by the availability of detailed long-term weather data for the site which would permit the water balance to be calculated not only for median circumstances but also for extreme events with their associated risk. Calculations of this kind are routinely performed in applications such as watershed hydrology and management, crop insurance and solar salt production.

CHAPTER 3: MATERIALS AND METHODS

3.1 INTRODUCTION

This chapter describes the Emalahleni brine sample and the experimental protocols used in this study

3.2 SAMPLE COLLECTION

The Emalahleni water reclamation plant situated in Middleburg in the Mpumalanga province was used as the sampling site to obtain the brine used in this study. Sampling of brines and permeate was done at the Emalahleni plant on 16th May 2011.

The Emalahleni plant recovers on average about 99.5% of the water that is treated with the rest being disposed of as brine in the evaporation pond. The plant receives its feed water from 4 different collieries, namely Kleinkopje, Greenside, South Witbank and Navigation. The water is blended to manage pH and sulfate concentration. Normally, the pH of the combined mine water is about 4.5 and this water can be stored in the intake ponds for up to two days. Figure 3.1 is a schematic flow diagram of the plant operation. The combined mine water with a pH of about 4.5 is pumped directly into neutralization reactors and then passed at high pressure through permeable RO membranes that produce clean water and a by-product known as reject brine. This brine, after several stages of treatment is pumped into the evaporation ponds. The RO permeate is transported to the Emalahleni municipality. As the brine passes from one RO stage to another it becomes more concentrated. Figure 3.2 shows the three intake ponds as well as the large evaporation pond. The reject brine that is taken from the Reverse Osmosis (RO) of stage 3 is pumped directly into the large evaporation pond.

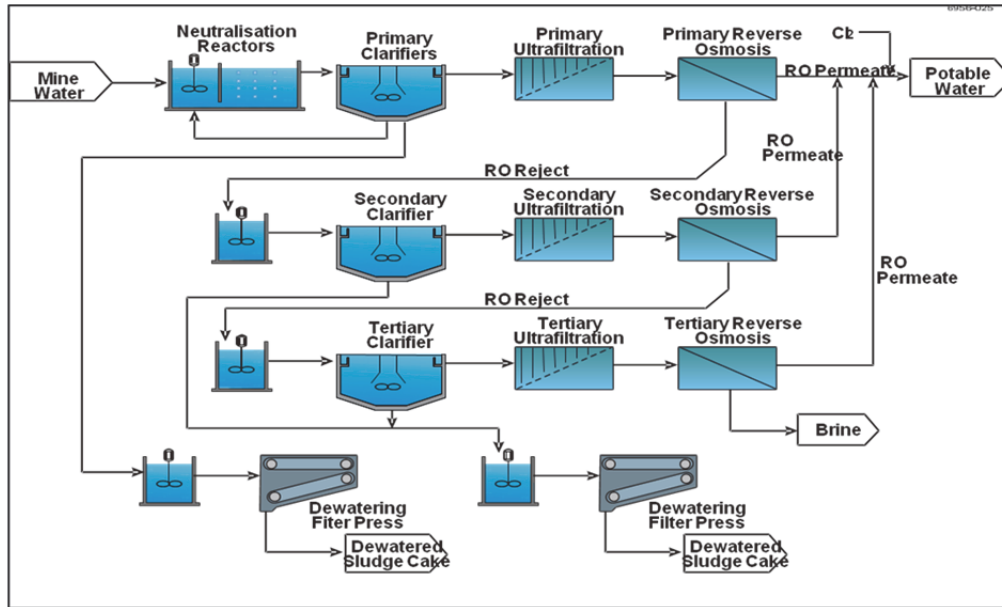


Figure 3.1: Schematic flow diagram of Emalahleni water reclamation plant with RO systems (Water Sewage & Effluent, 2006)



Figure 3.2: Aerial view of Emalahleni water reclamation plant in Mpumalanga (Source: <http://www.projectlink.co.za/portfolio-item/project-water-treatment-plant/>)

3.3 CHARACTERIZATION OF EMALAHLENI BRINE

The pH and electrical conductivity (EC) of the brines were measured on site. Samples were filtered through a 0.45 μm millipore filter. Filtered samples were divided into two portions; one portion was used for anion analysis and the other portion was acidified with concentrated nitric acid for cation analysis. Acidification of the sample was done in order to stabilize metal concentration and prevent

loss through precipitation. The samples for cation and anion analyses were kept in a refrigerator at 4°C until analysed by ion chromatography (IC) for anions using a suppressed system (Dionex) with carbonate-bicarbonate mobile phase and inductively-coupled plasma-optical emission spectroscopy (ICP-OES) was used for metal determinations.

The brine was classified using Aq.QA software in terms of the relative abundance of cations and anions.

3.4 SYNTHETIC BRINES

Simulated brine was studied alongside the raw Emalahleni brine in order to assess the effect of different salts on the rate of evaporation. The brine solutions were simulated based on the chemical analysis of the original brine waters collected from the plant. Simulation was conducted using the following salts, alone or in combination: sodium sulphate, sodium chloride, calcium sulphate, magnesium sulphate and potassium chloride.

3.5 WATER CONTENT DETERMINATION

The water holding capacity of different salts when subjected to the same temperature was investigated as a basis for anticipating dependence of evaporation rate on the composition of mixed salt solutions. Dehydration was conducted in an oven at 100°C using 5 g of each salt in a crucible, and recording the mass every 2 h until a constant mass was obtained.

3.6 EVAPORATION FROM SINGLE AND MIXED SALT SOLUTIONS

A 0.5 M solution was prepared of each of the five salts mentioned in section 3.4. In the case of CaSO_4 which has a solubility in water of about 2.5 g/L, dissolution was incomplete and when preparing mixtures with other salts the suspension was stirred thoroughly before separating a measured volume for combination. Binary mixtures of salts were prepared by combining solutions of NaCl and either CaSO_4 (suspension), Na_2SO_4 , MgSO_4 or KCl, at a molar ratio of 1:2. Ternary mixtures were prepared consisting of NaCl/ Na_2SO_4 /KCl, MgSO_4 / Na_2SO_4 /KCl, Na_2SO_4 / CaSO_4 /NaCl or MgSO_4 /NaCl/ CaSO_4 all in molar proportions of 1:1:1. Deionized water was used as a control.

The rate of evaporation was initially investigated using a series of 3-L evaporation pans (shallow Pyrex glass basins) mounted at a fixed height beneath 175 W infrared heating lamps as shown in Figure 3.3. Temperature above and within the solution, electrical conductivity (EC) as an index of total dissolved solids (TDS), and air humidity were measured using the same sensors as those described below in section 3.7.2. Water loss was determined gravimetrically. Measurements were repeated at intervals of 3 h for 45 hours. Wind speed was not recorded but a gentle convection and exchange of air in the room was periodically affected by activating the air conditioning system.



Figure 3.3: Experimental set-up for brine evaporation in shallow basins mounted beneath infrared lamps with adjustable height

3.7 MEASUREMENT OF EVAPORATION UNDER CONTROLLED CONDITIONS

Having studied evaporation from shallow basins as affected by different salts, the main focus of experimentation switched to the construction of a pair of deep tanks fitted with accessories which allowed the interaction of factors such as wind speed, temperature, humidity and salt content of the brine to be studied and compared under controlled conditions. This set-up is based on a system described by Schultheis et al. (2001) for the simulation of solar-driven brine evaporation and salt crystallization, as depicted in Figure 3.4.

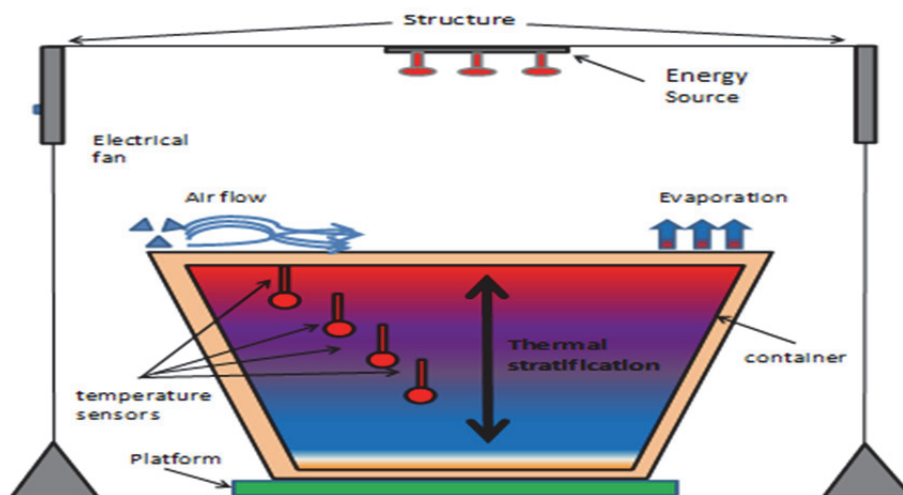


Figure 3.4: Schematic of experimental plant (Adapted from Schultheis et al., 2001)

3.7.1 Evaporation study using distilled water (control experiment)

There are various parameters in an artificial evaporation plant which need to be recorded and controlled to reflect the condition of a natural pond. A list of measured parameters is shown in Table 3.1.

Table 3.1: Parameters measured during the evaporation test

Parameters	Units	Logging periods
Ambient temperature	^o C	Continuous
Water thermal stratification	^o C	Continuous
Humidity of the room	%	Hourly
Humidity 10 mm above	%	Continuous
Evaporation	Mm	Hourly per cycle (24 hrs)
Wind	m/s	Once per cycle

The experimental arrangement allows the relative importance to be assessed of humidity, temperature, radiation and wind in influencing the rate of evaporation. The main objective is to determine water loss to the atmosphere under controlled conditions. The rate of evaporation was compared in two experiments, with and without wind. Several adjustments were made to the wind exposer, height of the heating source and intensity of radiation source. The ambient temperature and humidity were not altered during the experiments and measurement indicated minor variation relative to one another.

The data were analysed by means of time series plots. The continuously logged data from the data logger and manually logged data were combined. The water loss over a specific interval was recorded on an hourly basis although there were periods where no data was recorded. At the start of the experiment the water temperature was close to room temperature. The accuracy of this method was subject to the coefficient of expansion of the water and the container during the experiments. Both of these factors were neglected in calculations. The measurement from the specific measuring point itself had an error of 12%.

3.7.2 Evaporation study using water and NaCl solution

The experimental evaporation tanks consisted of 0.5 m deep container constructed of Perspex. The two 125-L tanks were charged with 115 L water, either alone or with NaCl dissolved to give a 0.5 M solution. Each tank was fitted with an identical array of sensors and lamps. The experiment had 12 hour cycles simulating day and night. The containers were well insulated to minimize the impact of the external ambient conditions. The main energy input into the system was derived from the energy source, namely the infrared lamps (Figure 3.5). Each container was deep enough to account for thermal stratification of the brine. The surface area was large enough to absorb most of the radiated

energy emitted from the energy source above the container. The structure of the framework was made of galvanised steel to resist corrosion.

To simulate energy input a number of infrared lights and heaters were required. Four infrared lights with an energy output of 250 Watts each were mounted above the containers.

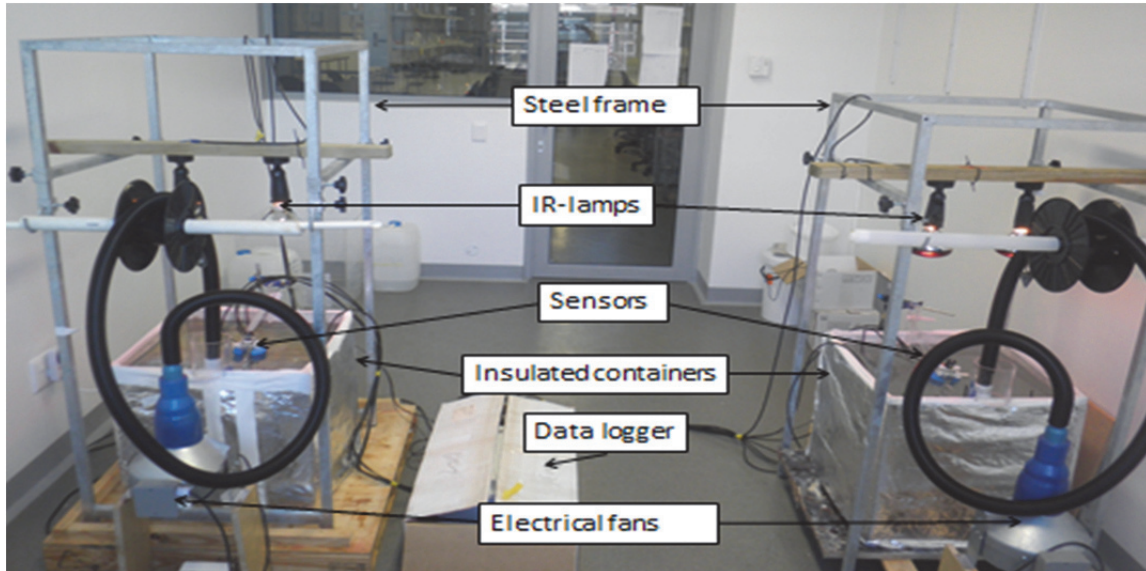


Figure 3.5: A display of all the components from the experimental plant for the distilled water. A similar setup was used for the NaCl brine.

3.7.2.1 Scaffolding

The structure surrounding the experimental plant was to support the equipment suspended above the water containers with minimal impact on the various processes. The structure had the strength to allow adjustments to be made to the system throughout the experiments. It was coated with a non-corrosive material to prevent rust.

3.7.2.2 Containers

The containers' size and specifications were optimised for experimental duration and the evaporation rate. The water was held in a Perspex container which was folded and sealed into a 0.25 m² square area and had a wall thickness of 5 mm. The container was well insulated using a fibre blanket. This ensured the majority of the energy input for the water to only be derived from the energy source above the containers. The containers had to be deep enough to account for thermal stratification of the water. The surface area had to be large enough to absorb most of the radiated energy emitted from the energy source above the container.

3.7.2.3 *Energy source*

The average energy from the sun is about 1368 W/m^2 before it enters the atmosphere (Pal Arya, 1998). A further reduction in the energy due to scattering occurs before it reaches the earth surface. Two infrared lights with an energy output of about 250 W each were suspended above the containers to simulate a hot summer day maximum temperature and two 175 W lamps were used to simulate a cooler day's maximum temperature.

3.7.2.4 *Pressure transducers*

The pressure transducers recorded the change in volume of the brine and water during the experiments. These were placed at the bottom of each container.

3.7.2.5 *Temperature sensors*

The temperature sensors recorded the heat energy transfer in the water and mapped the thermal stratification that develops with depth. To maintain the correct sensing depth, the temperature sensors were mounted on a float which was free to fluctuate with any changes in the water level.

3.7.2.6 *Humidity sensors*

The humidity was measured 10 cm above the container continuously. The data was recorded on the data logger. The humidity of the room was recorded manually at random intervals and these readings were taken in the centre of the room in which the experiments were carried out.

3.7.2.7 *Data logger*

The data logger CR 1000 was obtained from Campbell Scientific ®. All sensors relayed the information to the data logger simultaneously. The recording interval for the data was every hour. Data were retrieved from the logger using a laptop.

3.7.3 **Preparation of novel materials for enhanced brine evaporation**

Zeolite Y was used as adsorbent to be incorporated into the electrospun PAN nanofibres, and was a commercial zeolite obtained from Südchemie AG. It was finely ground and mixed with PAN with the aid of a magnetic stirrer and was stirred for 3 days until it was evenly mixed with the PAN+DMF solution. Nanoparticulate TiO_2 was sourced from Aldrich and was also evenly mixed with PAN+DMF solution, to form TiO_2/PAN nanofibres.

3.7.3.1 Electrospinning of PAN doped with TiO_2 and zeolite

The PAN powders were dissolved in DMF at 8 wt% and doped with TiO_2 , or zeolite Y, respectively at a 3 wt% concentration under constant stirring at room temperature for 24 hours to make the electrospinning sol solution spin evenly. These prepared solutions were loaded separately in 10 mL plastic syringes with metal needles. The electrospinning parameters were determined based on the information in the literature. The applied voltage, distance from the needle tip to the collector and the flow rate were fixed at 20 kV, 15 cm and 0.2 mL/hr respectively. The droplet was ejected out of the needle under the applied high voltage and accelerated towards the collector in the external electrostatic field and therefore collected on the aluminium foil surface as a nanofibrous mat. The solution surface tension was overcome by the electrical force at the surface of the drop, and therefore resulted in the stretching and elongation of the polymer solution into nanofibers.

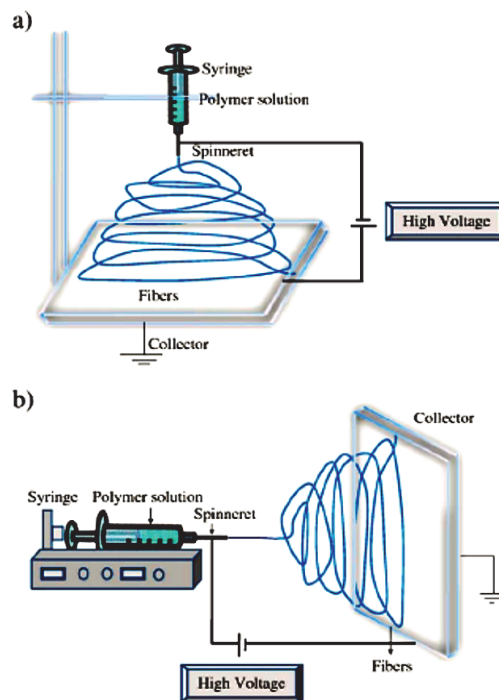


Figure 3.6: Schematic diagram for the electrospinning set up (a) Vertical set up and (b) Horizontal set up for electrospinning (Bhardwaj and Kundu, 2010).

3.7.3.2 Adsorption experiments

Adsorption experiments were conducted with model salt solutions using the electrospun nanofibres containing either the zeolite Y or TiO_2 particulates. The salt solution was prepared by weighing the appropriate mass of each salt and making it up to 1000 mL, i.e. making 1000 ppm of the mixture. The chemicals used were calcium chloride dihydrate, potassium nitrate, magnesium nitrate hexahydrate and sodium chloride. The preparation of the adsorbate was carried out by preparing stock solution containing 1000 mg/L of Ca, K, Mg and Na respectively. 3.67 g of $CaCl_2 \cdot 2H_2O$, 10.55 g of

Mg(NO₃)₂·6H₂O, 2.54 g of NaCl and 2.59 g of KNO₃ in 1000 mL of deionized water. Working concentrations in the range of 100-500 mg/L were prepared by serial dilution of each respective salt.

The adsorption experiments were carried out in 100 mL plastic bottles at 298 K. Dried PAN+TiO₂ and PAN+zeolite nanofibre mats of the same surface area were immersed in 25 mL aqueous metal solutions for different time duration as specified, and the mats were subsequently removed from the bottles at 1, 2, 3, 4, 5, 6, 7, 8 h. The remaining metal solutions were appropriately diluted for measurement. The concentration of the metal ions in solutions was measured by inductively-coupled plasma optical emission spectrometry (ICP-OES). Kinetics and adsorption isotherm were determined. The adsorption amounts were calculated as follows:

$$Q = \frac{v(c_i - c_f)}{w} \quad (6)$$

where Q = the amount of solute adsorbed from the solution (mg/g); V = Volume of the adsorbate; C_i = the concentration before adsorption; C_f = the concentration after adsorption; and W = the weight in gram of the adsorbent.

3.7.3.3 Effect of contact time

Contact time is an important parameter because it is a factor that determines the adsorption kinetics of an adsorbate at a given concentration of the adsorbate. The effect of contact time on uptake of calcium, magnesium, potassium and sodium metal ions by PAN+TiO₂ and PAN+Zeolite nanofibers was investigated for 8 hours. The kinetic studies were carried out for different initial concentrations 100, 200, 300, 400 and 500 mg/L for Ca²⁺, Mg²⁺, Na⁺ and K⁺ ions on PAN+TiO₂ and PAN+Zeolite nanofibers at 298 K.

3.7.4 Wind-aided experimental design

Incorporation of wind in experimental setups has been done successfully in the form of WAIV (wind aided intensified evaporation) as described by Gilron et al. (2003) and Macedonio et al. (2011). These principles were adopted for the current study. The main purpose of the electrical fan was to provide wind energy to remove the saturated air above the containers during evaporation. The key feature for the inclusion of the fan was to demonstrate the increase in the evaporation rate when subjected to air currents. To achieve equal distribution of air currents over the surface area of the container, the air currents were funnelled through a slotted pipe mounted on the side of the containers. The wind speed was constant throughout the experiments at 2 m.s⁻¹. The wind speed was checked by using an anemometer near the ventilated areas of the cylinder.

A grid with nets was constructed and made to float above the brine surface to enhance evaporation via Wind-Aided Intensified eVaporation (WAIV). This was achieved by attaching a floatable material

underneath the grid. The material used for the grid was a 6 mm thick clear acrylic plastic glass. The grid was strategically placed so as to expose the thick nets to the orifices of the polyvinyl chloride (PVC) pipe. This positioning of the grids exposed the nets directly to the wind and allowed the maximum wind force to pass through. According to Macedonio et al. (2011), the orientation of the nets parallel to the wind direction can be highly effective. In the case of the present experiment, the parallel orientation of the nets helped with removal of the saturated air in the area behind the nets.

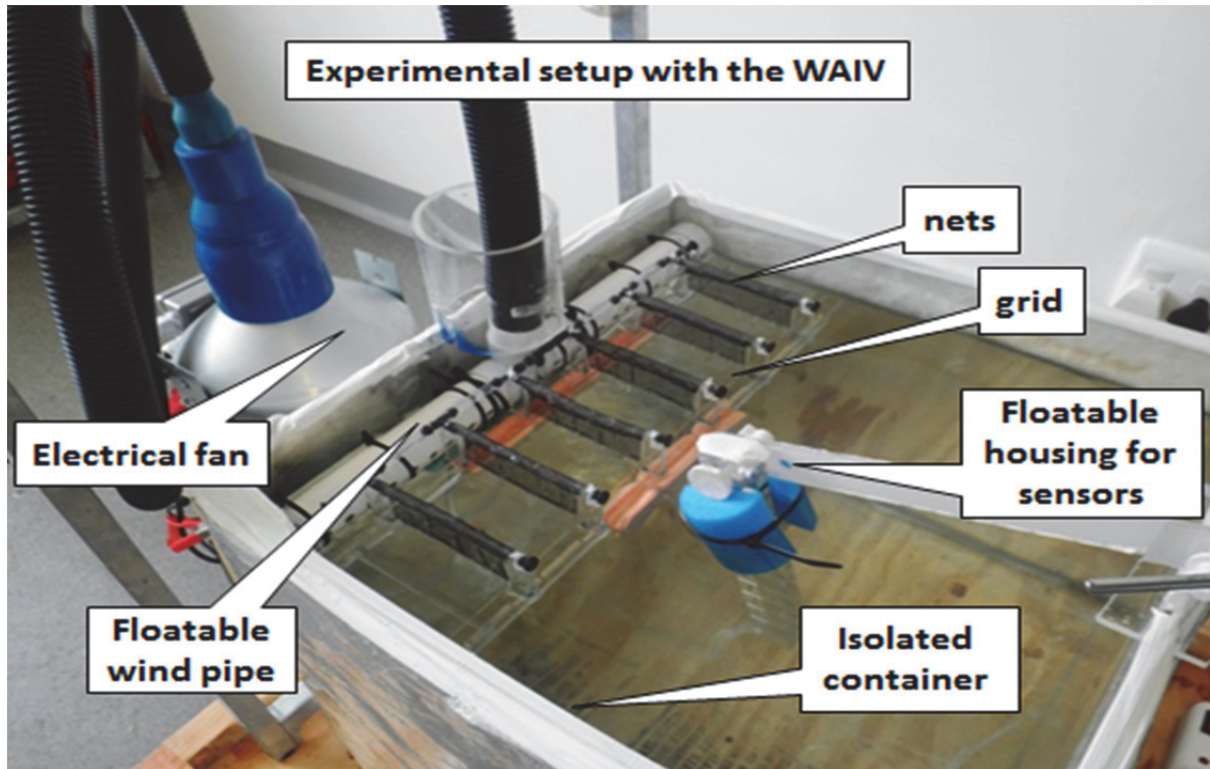


Figure 3.7: Experimental setup with the Wind-Aided Intensified evaporation (WAIV) system (based on Gilron et al., 2003).

The design of the grid addition was done so as to have a minimal impact on the surface area of the container when exposed to the infrared lighting (Figure 3.7). The grid consisted of a 450x125 mm frame. There were 6 nets suspended across the grid each with a dimension of 96x40 mm. The net composition is a fibre strand with a PVC coating. The fibre makes the net very flexible while the PVC coating makes it durable and resistant against deterioration by corrosive substances. The netting mesh size is approximately 1.5 mm square and the nets were suspended by the irrigation pipes on top (Figure 3.7) and tied with a thin fishing reel line at the bottom of the frame. The squares of the nets served to make it less susceptible to clogging (Gilron et al., 2003) and improved the absorption of IR radiation because of the black colour. A material with larger pores has a higher capacity to attract foreign material and may result in clogging. The nets were evenly spaced to ensure both sides of the nets were exposed to an equal amount of wind currents. The nets were seamed together on the one end of the 96 mm to create a holding position for the pipe which irrigated brine onto the nets to pass through.

3.7.5 Irrigation system

A whale pump with a 60 W output was used to pump the brine from the container and disperse it over the nets. The pump is a 12 V, 5 A, DC device which needs a constant power rate to maintain the flow rate of the irrigation over the experimental period. The inlet of the whale pump was approximately 50 mm in diameter with a pipe diameter of 10 mm. A coupling was connected to the 10 mm pipe for a further reduction to accommodate a 5 mm pipe. The 5 mm pipes were fed through the sewed section of the nets. The piping was connected with couplings to create one complete network. The transparent 5 mm diameter pipe was used to irrigate the entire grid system which delivered a flow rate of about 34 mL/s. The pump was fitted under the PVC pipe which provided the air currents over the surface of the brine container. This, however, ensured that the brine was subjected to minimal temperature and wind current interference. However, the ambient temperature plays a significant role in the temperature of the brine (Wahlin et al., 2009). A 14 A battery charger was connected to the same timing device as the IR lighting and the electrical fan (Figure 3.8). The experiment continued without the other parameters on a 72 hour, 12 hour day and night cycle. It is anticipated that in future, once larger scale novel nanofibres can be produced, that these would replace or augment the nets applied in the WAIV experiments to enhance the evaporation and simplify the brine solution simultaneously.

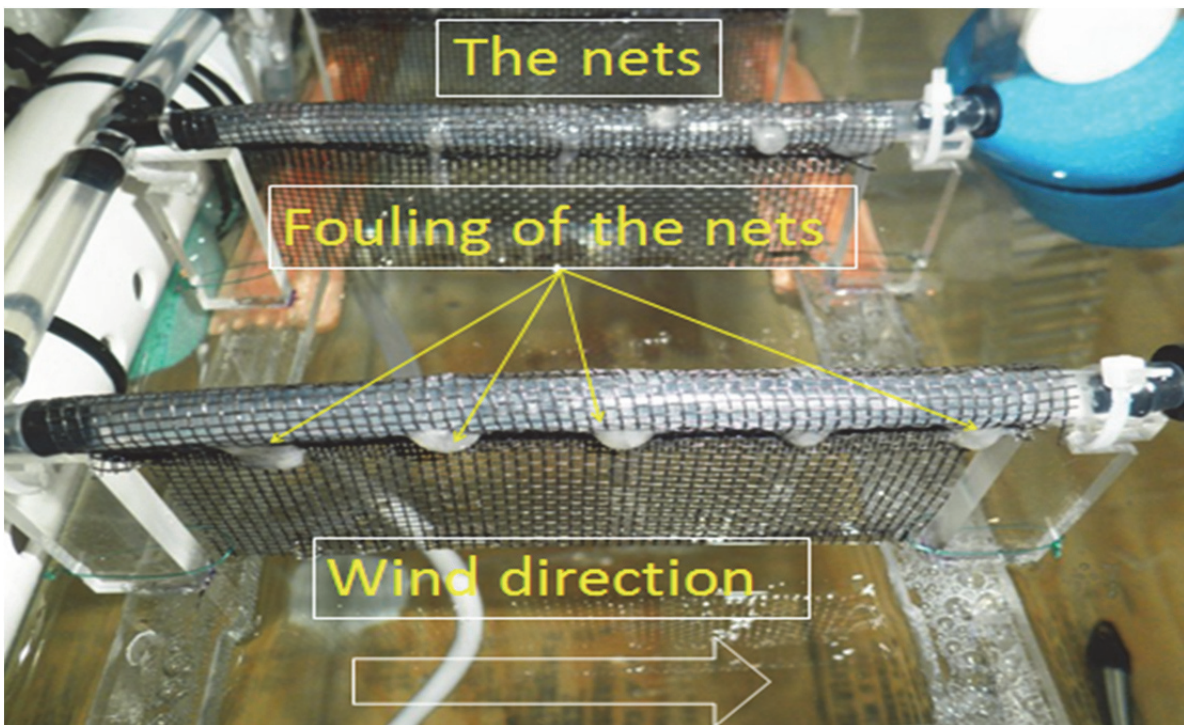


Figure 3.8: The nets after experimental cycling. A crusted deposit developed near the orifice of the irrigation pipes

CHAPTER 4: CLASSIFICATION OF EMALAHLENI BRINE AND EVALUATION OF A SMALL SCALE EVAPORATION STUDY

4.1 INTRODUCTION

This chapter presents and discusses the results of the chemical composition of Emalahleni brine. The results of the experiments carried out to study the effect of chemical composition of brine on the rate of evaporation are also presented and discussed in this chapter.

4.2 CHARACTERIZATION AND CLASSIFICATION OF EMALAHLENI BRINE

4.2.1 Chemical composition

The pH and EC of the brines measured on site during field sampling are presented in Table 4.1.

Table 4.1: pH and EC of the eMalahleni RO brine at different stages of development

Brine	pH	EC (mS/cm)
Leaving stage 1	6.69	7.36
Leaving stage 2	6.97	10.5
Leaving stage 3	7.67	21.7

The raw brine from the various leaving stages at the RO plant was analysed to determine chemical composition using IC for major anions and ICP for remaining elements. Table 4.2 shows the chemical composition of the eMalahleni stage 3 reject brine while Table 4.3 presents the equivalent concentrations of major ions after additional determination of alkalinity (by titration to pH 4.5 with HCl) and the likely adjustment needed in anion values for charge balance. The pH of the eMalahleni stage 3 brine was 7.67 which is nearly neutral and the EC was 21.7 mS/cm which represents a hypersaline condition. The strong salinity is attributable mainly (more than two thirds) to sodium sulphate, with other major ions (Ca, K, Mg and Cl) being present in much smaller concentrations. A range of minor elements including P and Si were present but some, notably Zn, Mn, As and Pb were not determined.

Table 4.2: Chemical composition (concentration in mg/L except pH and EC (mS/cm)) of stage 3 reject brine from Emalahleni.

Major elements (mg/L)		Minor elements (mg/L)	
Ba	0.15±0.01	Al	0.07
Ca	610.2±10.47	As	ND
K	758.75±2.05	Ba	0.15
Na	3355±25.46	Cr	0.02
Si	1.54±0.03	Zn	ND
Mg	111.85±0.07	Se	0.06
SO ₄	12847.54	Fe	0.07
Cl	1072.78	Mo	0.01
pH	7.67	Mn	ND
EC	21.7 mS/cm	P	1.19±0.01
		Pb	ND

ND= Not determined

Table 4.3 gives the major ions in Emalahleni brine that were calculated to include alkalinity and with downward adjustment of sulphate and chloride values to balance cation charge.

Table 4.3: Major ions in Emalahleni brine calculated to include alkalinity as well as downward adjustment of sulphate and chloride values to balance cation charge

Constituent	Actual		Adjusted*	
	mg/L	mmolc/L		%
Ca	610	31	31	15
K	759	19	19	9
Na	3355	146	146	71
Mg	112	9	9	4
SO ₄	12847	268	181	88
Cl	1073	31	21	10
Alkalinity	325	3	3	1
Sum cations		205	205	100
Sum anions		298	205	100

Nitrate does not appear in the table while phosphate concentration is effectively trace (1 ppm) compared with sulphate and chloride. With a sulphate concentration as high as this it would have been impossible to detect nitrate accurately by ion chromatography. The trace elements detected included Al, Ba, Cr, Se, Fe, Mo. Trace elements such as Mn, Zn and As were not detected in the brine solution during the analysis. Seventy-one percent of the cation mole charge is accounted for by Na⁺, and the remainder by Ca²⁺ (15%) K⁺ (9%) and Mg²⁺ (4%). In the case of anion charge, SO₄²⁻ accounts for 88% and Cl⁻ (10%) and HCO₃⁻ (1%) for the remainder. The brine has a near-neutral pH.

4.2.2 Classification of brine

The piper diagram in Figure 4.1 depicts water types at different stages in the Emalahleni plant and Tutuka brine for comparison.

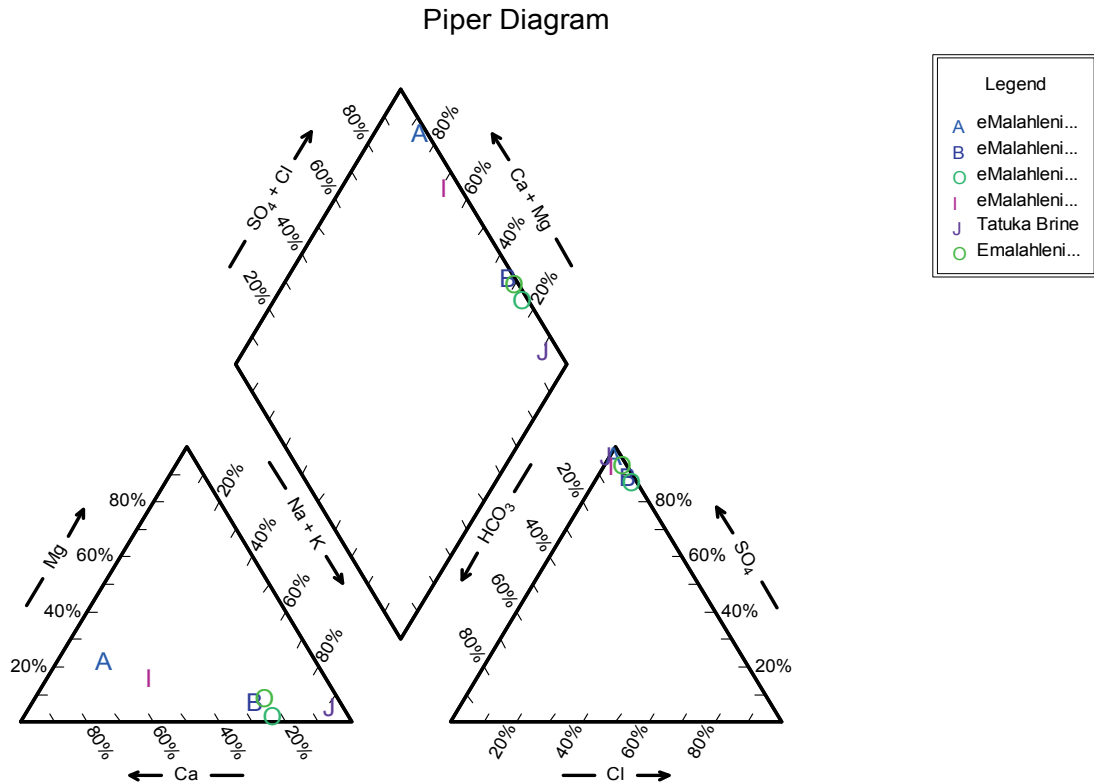


Figure 4.1: Piper diagram showing the % distribution of major cations and anions of Emalahleni and Tutuka brine water using the Aq.QA software

The brines all have sodium as the dominant cation and sulfate as the dominant anion. Figures set out in the Appendix 1 present Stiff diagrams of the Emalahleni brine at different stages of development.

4.2.3 Water content of salts

The weight loss on drying of the salts used in preparing synthetic brine solutions varied widely (Table 4.4). In some cases the water is likely to be hydration water (e.g. NaCl) whereas in others (especially CaSO₄ and MgSO₄) it is more likely to be structural water of crystallization. Gypsum (CaSO₄.2H₂O) for example will convert to the hemihydrate form well below 100°C. Consequently the apparent degree of hydration of the salts suggested by the weight loss on drying cannot be used as a basis for anticipating the relative effects of different salts on evaporation of water from salt solutions.

Table 4.4: Water loss of salts on drying at 100°C

Salt	Water (%)
MgSO ₄	16.0
KCl	9.2
Na ₂ SO ₄	0.8
CaSO ₄	16.2
NaCl	17.6

The water content of the different salts ranged from 0.8 to 17.6 %. Most solid chemical compounds possess large amounts of water adsorbed on the surface of the crystals, with some other solid compounds containing smaller amounts of water that is chemically bound in the crystal. The temperature of 100°C is a reasonable temperature to remove adsorbed water from the salt's surface. The results showing the water content of the salts suggest that it is necessary to dry salts prior to use in order to determine the exact amount to be used in experiments to make up the required molar concentrations.

From the results presented in Table 4.4, it was observed that NaCl (17.6 %) contained the highest percentage water content followed by MgSO₄, which indicates that these salts could hold more water than the other salts such as Na₂SO₄ which showed the lowest percentage water content of 0.8 %. The different water content of these as-received salts gives an indication of the water holding capacity of different salts. Some of the water is in fact water of crystallization. For example CaSO₄ and MgSO₄, if AR grade, are likely to have the moles of waters specified on the label. CaSO₄·2H₂O (gypsum) dehydrates to the hemihydrate, bassanite (CaSO₄·0.5H₂O) and eventually anhydrite (CaSO₄), with the conversion beginning around 85 °C which is well below the oven temperature used. The speed and completeness of dehydration depends also on relative humidity. Thus using oven drying as the basis for weighing accurate molar amounts of salts can be erroneous depending on the type of salts (especially Ca and Mg).

4.2.4 Water holding capacity of the salts

Table 4.5 shows the water uptake by the dried salts when exposed to saturated conditions. The salts had been dried in a desiccator for 24h and were then humidified.

Table 4.5: Water holding capacity of salts

Salt	Dry mass (g)	Humidified mass (g)	Water uptake (%)
MgSO ₄	4.20	5.86	39.5
KCl	4.54	5.16	13.6
Na ₂ SO ₄	4.96	4.99	0.60
CaSO ₄	4.19	4.54	8.40
NaCl	4.12	5.32	29.1

Sodium sulphate was the least hygroscopic of the salts while magnesium sulphate was the most hygroscopic, with sodium chloride also showing a large weight gain on humidification. These results suggest that magnesium salt solutions will evaporate less easily than solutions of Ca, Na and K salts, and that chloride salts can be expected in general to retain water more strongly than sulphate salts and thus their solutions will evaporate less readily. Two salts that were not tested but which are known to be deliquescent and would be relevant when studying salt mixtures are MgCl₂ and CaCl₂. Their exceptional hygroscopicity is likely to impose itself on salt mixtures to which Mg or Ca may have been added as a sulphate but Na or K may have been added as a chloride.

4.3 SMALL SCALE EVAPORATION STUDY

4.3.1 Effect of humidity and solution temperature on evaporation

Figure 4.2 shows the change with time of humidity above the evaporation dish (A), volume loss (B), and the temperature inside the evaporation dish (C) during evaporation from solutions of single salts. The humidity decreased to around 35% as temperature inside the dish rose to about 33°C following which volume loss stabilised at about 80 mL per 3-hour measuring interval. There was no clear difference between deionised water (control) and the salt solutions with the possible exception of CaSO₄ which appeared to lose consistently slightly more water than the other solutions although the difference was not significant. In the initial stages the humidity above NaCl decreased more gradually than above the other solutions while the temperature increased to a slightly higher level over both NaCl and CaSO₄ solutions. The absence of any consistent difference between the solutions may be due to the opposing effects of salt concentration (and increasing density) reducing vapour pressure and of dissolved salts increasing the absorption of heat from the radiation source.

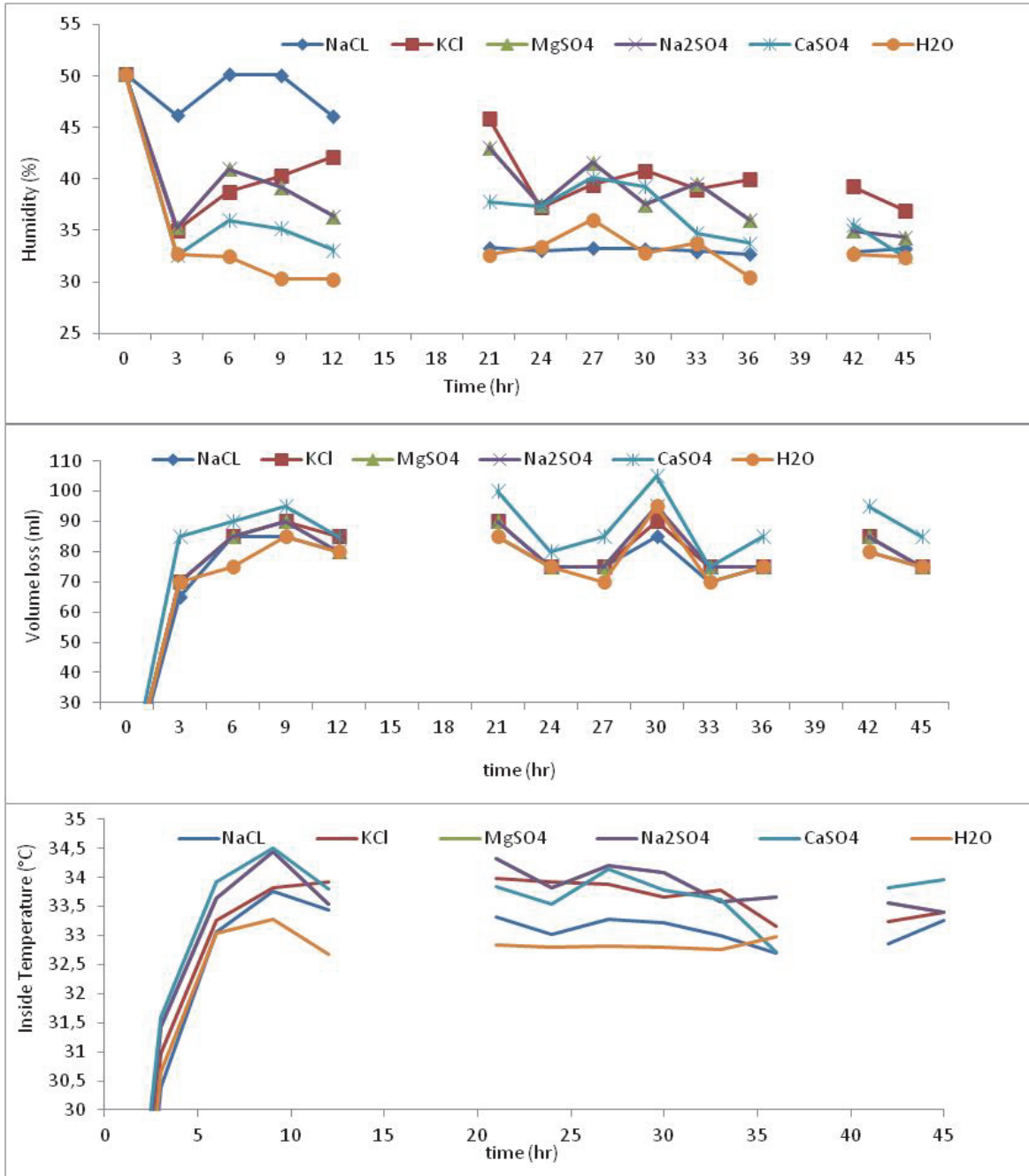


Figure 4.2: Humidity (A), Volume loss (B), and solution temperature (C) over time for single salt solutions

An attempt has been made in Figures 4.3 and 4.4 below to present the 3-hourly volume loss data for all three types (single, double and triple) of salt solution in relation to average humidity and temperature, respectively, over a 78-hour period of measurement. Although the average humidity declined steadily with time to a value around 33% (Figure 4.3 A and B) in the experiments with single and binary salt solutions, it declined negligibly in the ternary salt experiment (Figure 4.3C) and the cause of this is possibly the fact that the air conditioning of the laboratory was not amenable to sufficient control to create an identical atmosphere for each experiment. By contrast the average temperature profiles for the three experiments were very similar (Figures 4.4A-C), suggesting that

external climate may have had something to do with the sustained higher humidity of the ternary salt experiment.

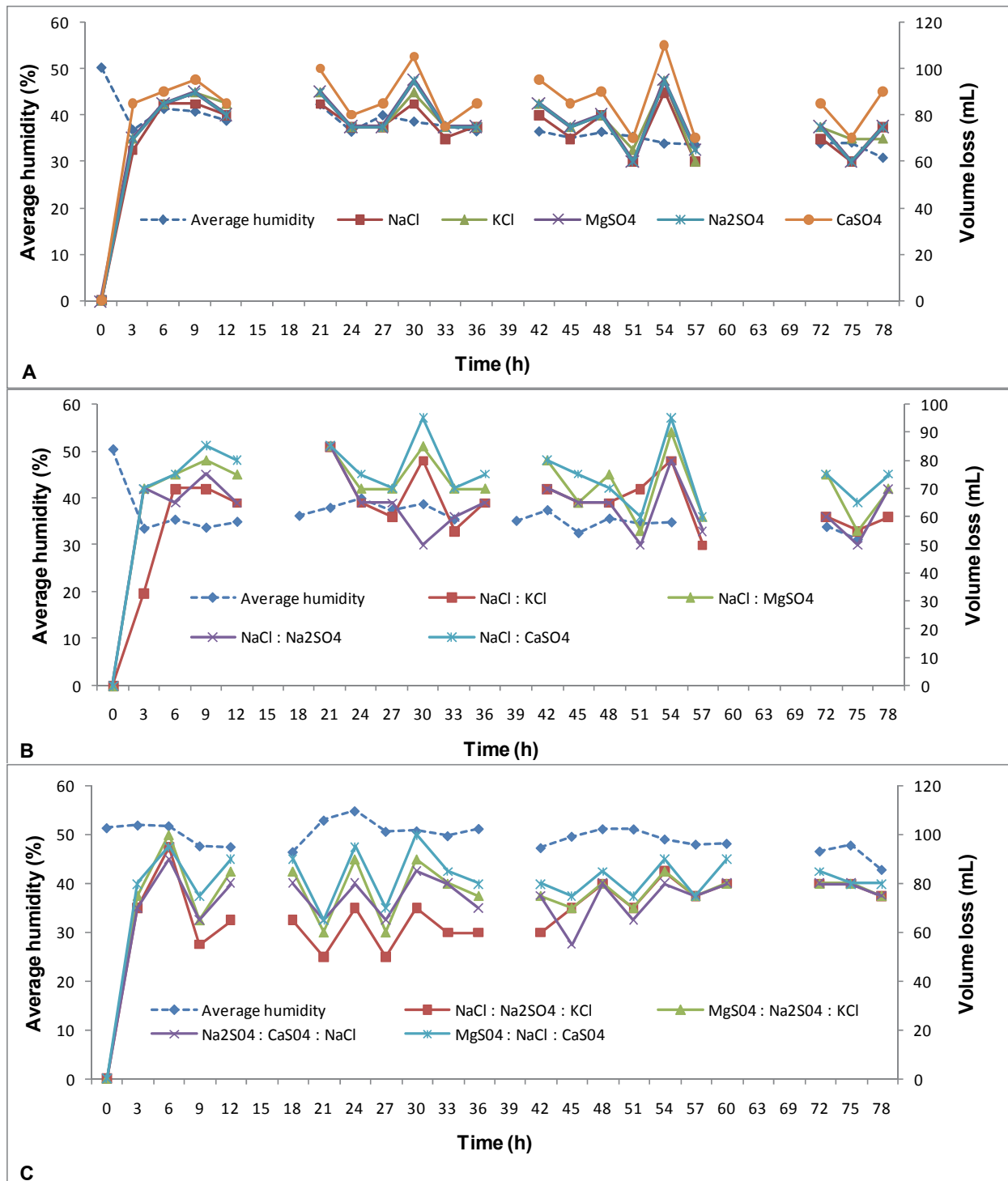


Figure 4.3: Average humidity and the 3-hourly volume of water lost from solutions of A: single; B: binary and C: ternary salt mixtures

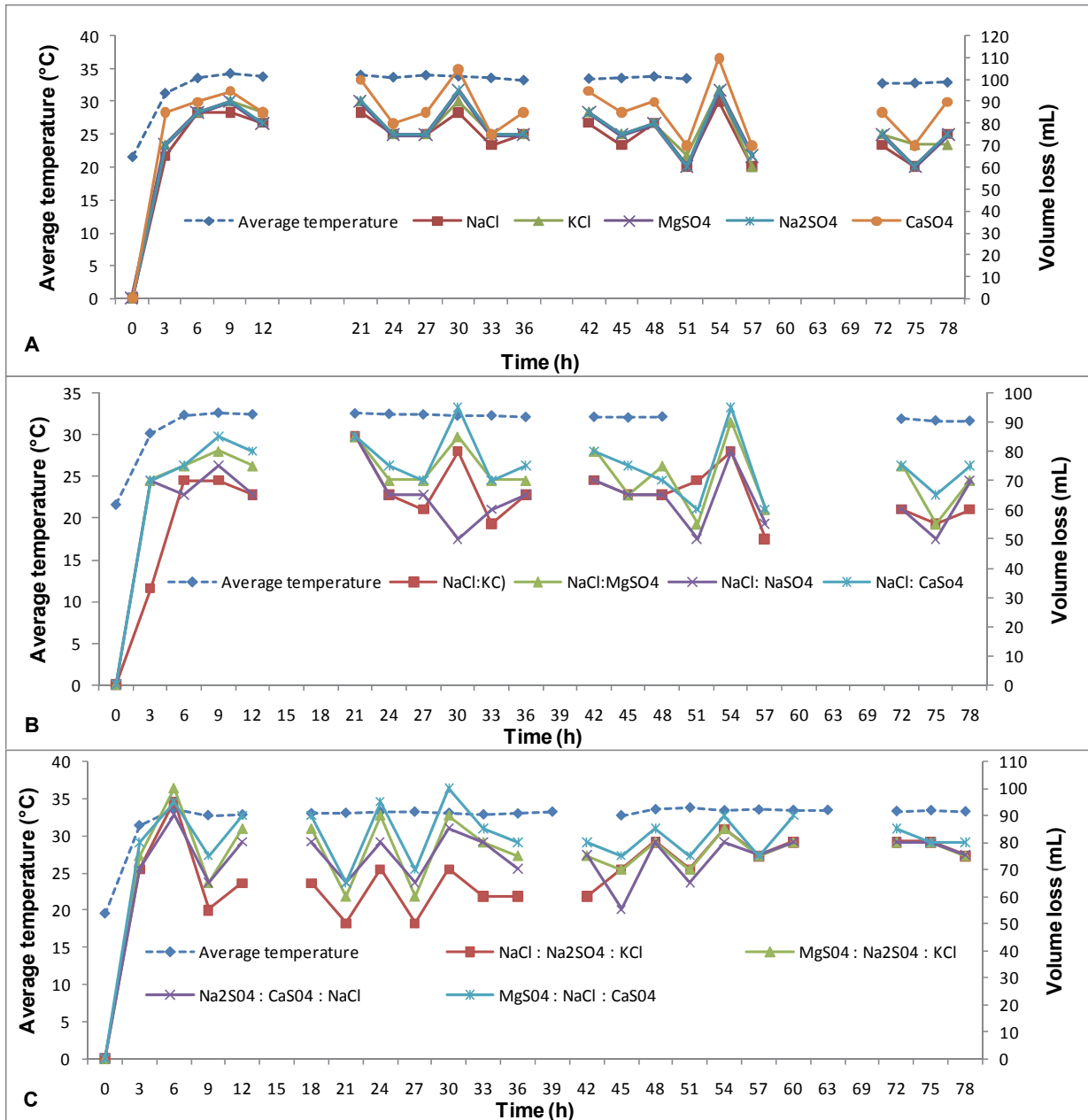


Figure 4.4: Average temperature and the volume of water lost from solutions of A: single; B: binary and C: ternary salt mixtures

The three experiments in Figs. 4.3 and 4.4 were revealing in that there appeared to be a consistent tendency for salt solutions with Ca and Mg in the mixture to evaporate more water than solutions containing only Na or K salts. Instead of concluding, however, that this is a general effect of monovalent cations being more water retentive than divalent ions, it should be recalled that the Ca and Mg salts used were sulphates only and that the monovalent salts were added as chlorides or sulphates. All salt mixtures containing Ca or Mg would therefore have had a higher sulphate concentration than those dominated by Na and K salts. Hence the difference, albeit a small one and not amenable to a test for statistical significance, could be due to a greater heat absorption from the radiant energy source by solutions with higher sulphate (and in this case lower chloride) concentrations. Since these are clear, colourless solutions it could be speculated that the effect would not be so much that of albedo as one involving the vibrational energy induced by the interaction of infrared radiation with the dissolved ions.

4.3.2 Cumulative evaporation from different salt solutions

Figures 4.5 4.6 and 4.7 show the evaporation data for single, binary and ternary salt solutions, respectively, plotted cumulatively against time in relation to temperature. In the single salt experiment (Fig. 4.5) calcium sulphate was the only salt solution which showed a tendency to evaporate more rapidly than either pure water or the other salt solutions. As mentioned earlier this is possibly due to sulphate absorbing heat from an IR source more effectively than chloride (the CaSO_4 median temperature was 33.8°C as opposed to between 33.2 and 33.6°C for the other solutions) and/or the limited tendency of CaSO_4 to dissociate and thus reduce the vapour pressure of water compared with the other salts. It is noteworthy that none of the other salt solutions showed cumulative evaporation significantly different from that of pure water which suggests that the opposing vapour pressure and energy absorption effects of these dissolved salts mutually cancel out. Interpretation of the mixed salt solution data (Figs. 4.6 and 4.7) can be made along similar lines, with sulphate dominated solutions showing a greater tendency to evaporate than those having a high chloride content although in these experiments some salt mixtures (notably those with Na, K and Cl which would be expected to have a higher degree of dissociation) appeared to exhibit the classic colligative property of vapour pressure reduction and hence a lower evaporation rate than that of pure water.

The idea that complex brines may evaporate differently from simple ones is therefore not supported by the data in this study, since comparisons between single, binary and ternary brines indicate inconsistent effects and in general the differences in the rate of evaporation are probably not large enough to be statistically significant and to the extent that there are real differences these are likely to be small in comparison with the effects that changes in temperature, humidity and wind speed will have in practice.

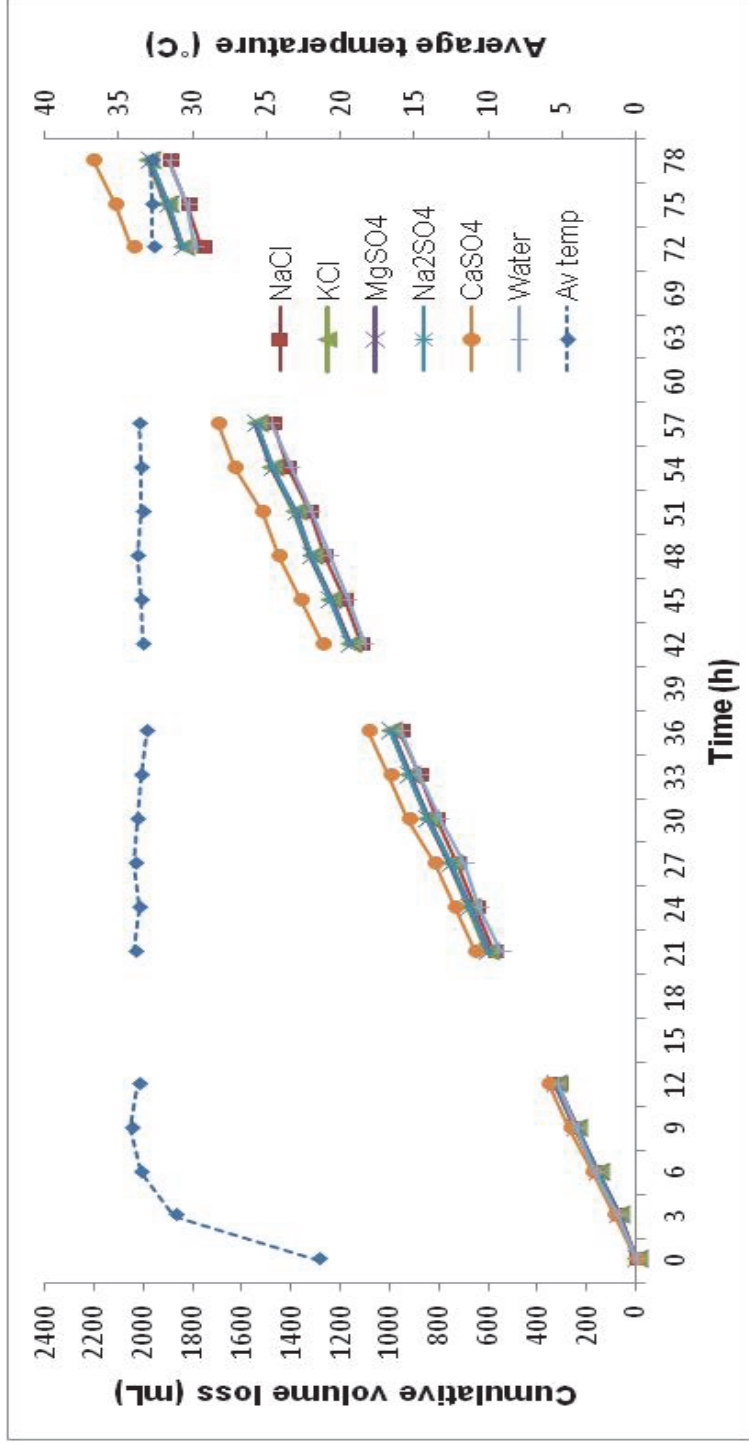


Figure 4.5: Cumulative volume loss and average temperature with time in single salt solutions

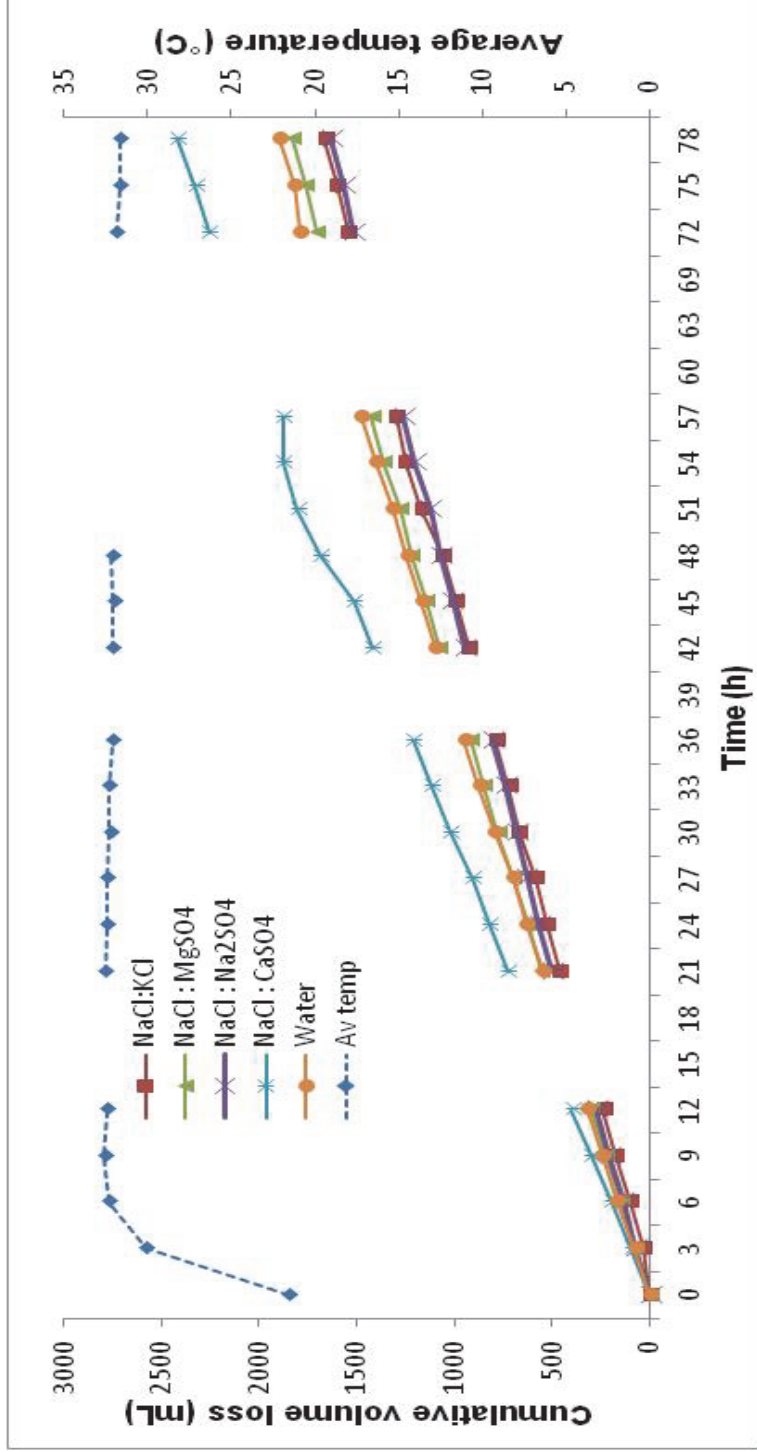


Figure 4.6: Cumulative volume loss and average temperature with time in binary salt solutions

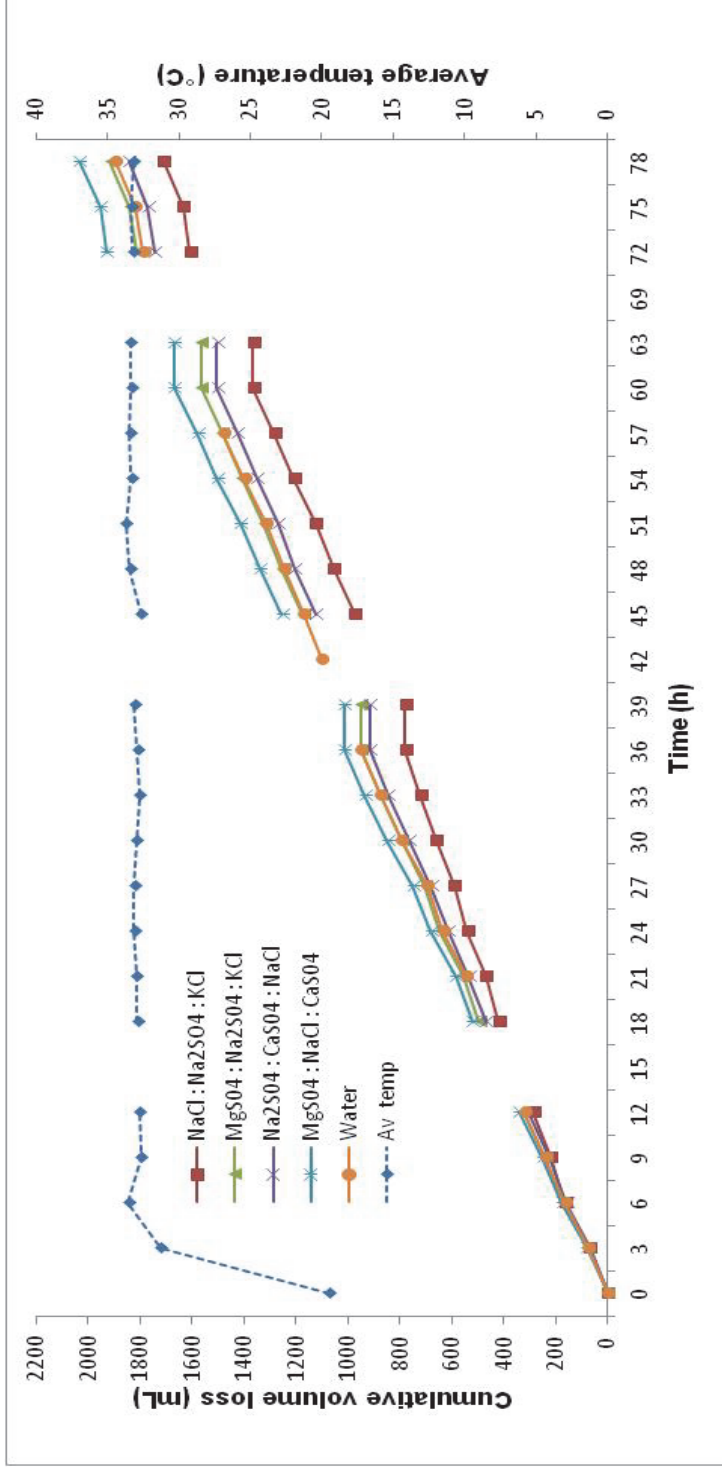


Figure 4.7: Cumulative volume loss and average temperature with time in ternary salt solutions

4.3.3 Material Balance

The material balance calculations are essential in process design, they are used in determining the quantities of raw materials required and products produced. In this report, the material balance was done to determine the amount of water evaporated and consumed. The objectives of calculating material balances are to improve efficiency, maintain production, reduce environmental discharge and maintain control of the processes in the plant; it allows understanding of what is occurring in a processing plant. The concentrations of the solutions were determined using the equation 7;

$$C_t = \frac{n}{V} \quad (7)$$

Where C_t is the concentration of the solution (mol/L), n is the number of moles of the solution (mol), and V is the volume of solution (L).

Figure 4.8 shows an evaporation pond block flow diagram.

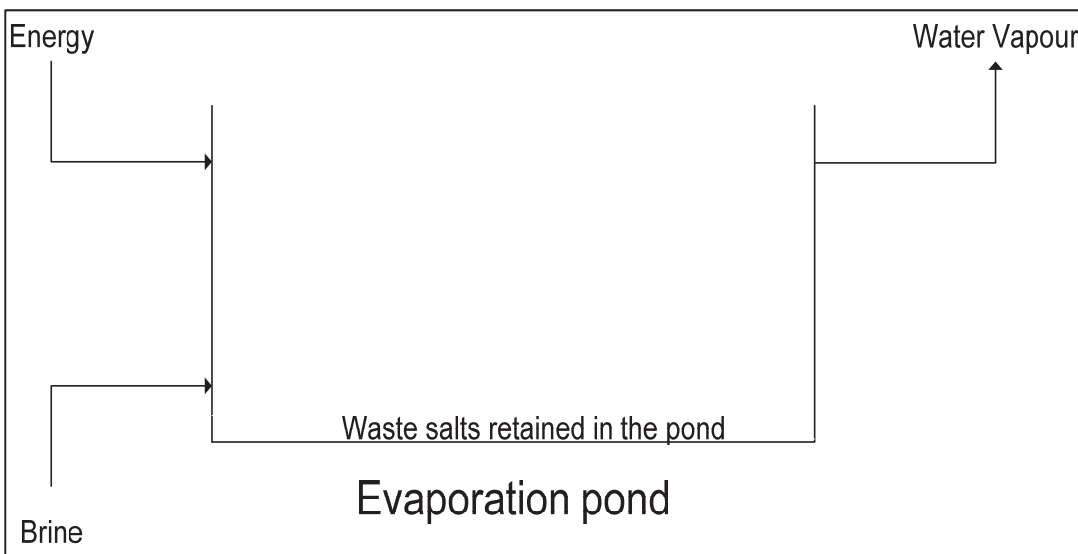


Figure 4.8: Input and output of the evaporation pond

Material balance calculations were done for single, double and triple salts. The compositions of the salt solutions prepared are presented in Table 4.6.

Table 4.6: Different salts solutions used

Single salt	Double salt	Triple salt
NaCl	NaCl/CaSO ₄ (1:2)	NaCl/Na ₂ SO ₄ /KCl (1:1:1)
MgSO ₄	NaCl/Na ₂ SO ₄ (1:2)	MgSO ₄ /Na ₂ SO ₄ /KCl (1:1:1)
Na ₂ SO ₄	NaCl/MgSO ₄ (1:2)	Na ₂ SO ₄ /CaSO ₄ /NaCl (1:1:1)
KCl	NaCl/KCl (1:2)	MgSO ₄ /NaCl/CaSO ₄ (1:1:1)
CaSO ₄		

The results for the single salts are presented in this report, because the trends of single, double and triple salts are similar.

The general conservation equation for any process system can be written as:

(Change in the total mass within the system)/time = (Total mass entering the system)/time – (Total mass leaving the system)/time

Assumptions:

- No flowing streams
- Assume only water evaporates
- Density is constant

$$\frac{dM}{dt} = \sum_{INLETS} \dot{M}_I - \sum_{OUTLETS} \dot{M}_O \quad (8)$$

Because there are no flowing streams, only the vapour is considered for the material balance.

The equation will therefore be:

$$\frac{dM}{dt} = \rho V_t \quad (9)$$

Where V_t is the volumetric flow rate of water vapour evaporated at a given time (L/h), ρ is the density of water evaporating (kg/L) and M is the mass of water evaporating (kg).

$$\rho = \frac{m}{v} \longrightarrow m = \rho v$$

$$\frac{d\rho v}{dt} = \rho v_t$$

$$v \frac{d\rho}{dt} + \rho \frac{dv}{dt} = \rho v_t$$

Derivative of a constant = 0

$$\frac{vd\rho}{dt} = 0$$

Therefore:

$$\frac{\rho dv}{dt} = \rho V_t$$

Therefore

$$\frac{dv}{dt} = V_t$$

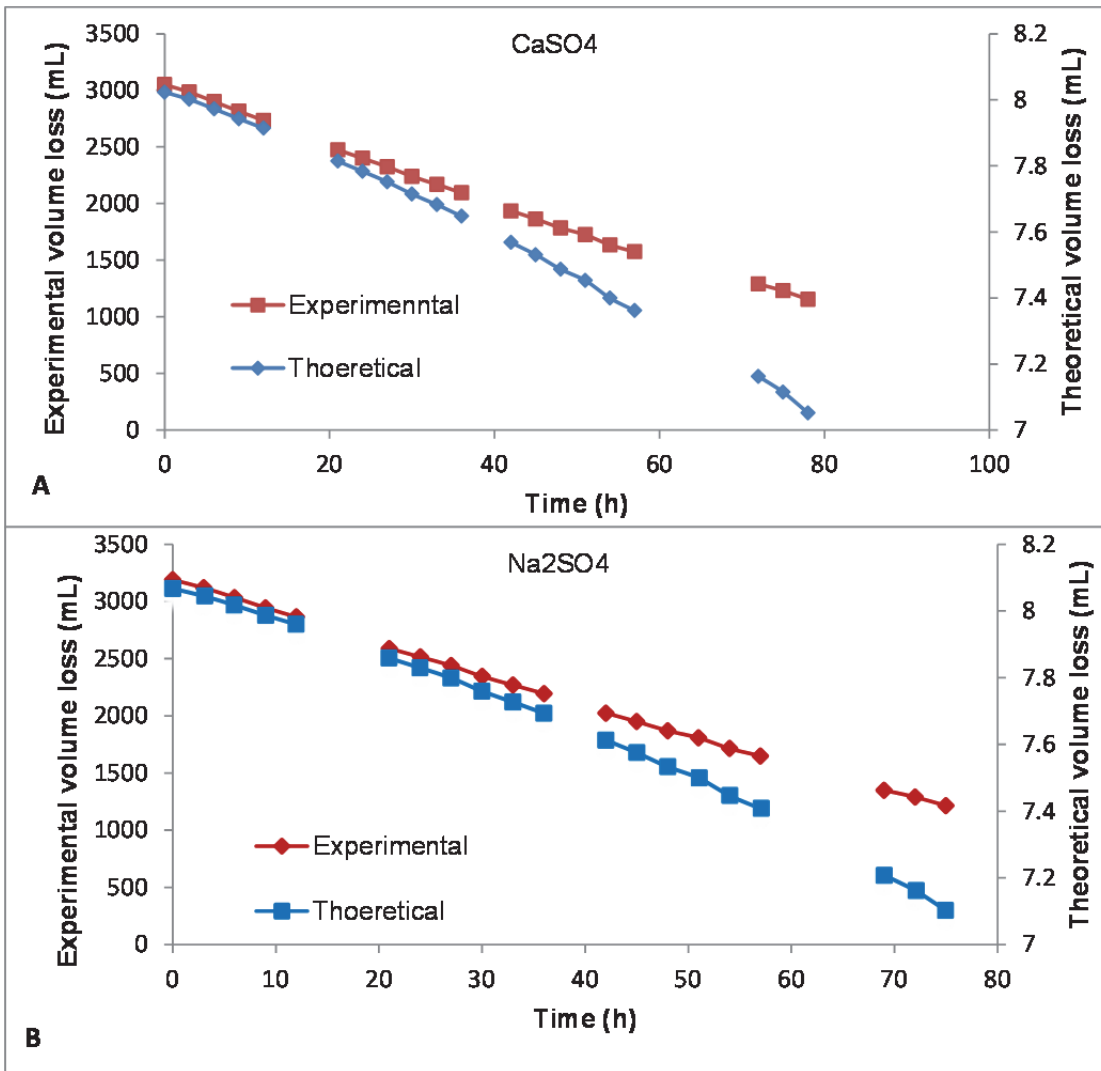
$$\frac{dv}{V_t} = dt$$

$$\int \frac{dv}{V_t} = \int dt$$

$$\ln V = t + C$$

(10)

Equation 10 gives the theoretical volume of water loss at a given time. Figure 4.9 compares the experimental and theoretical volume of water loss trends with respect to time.



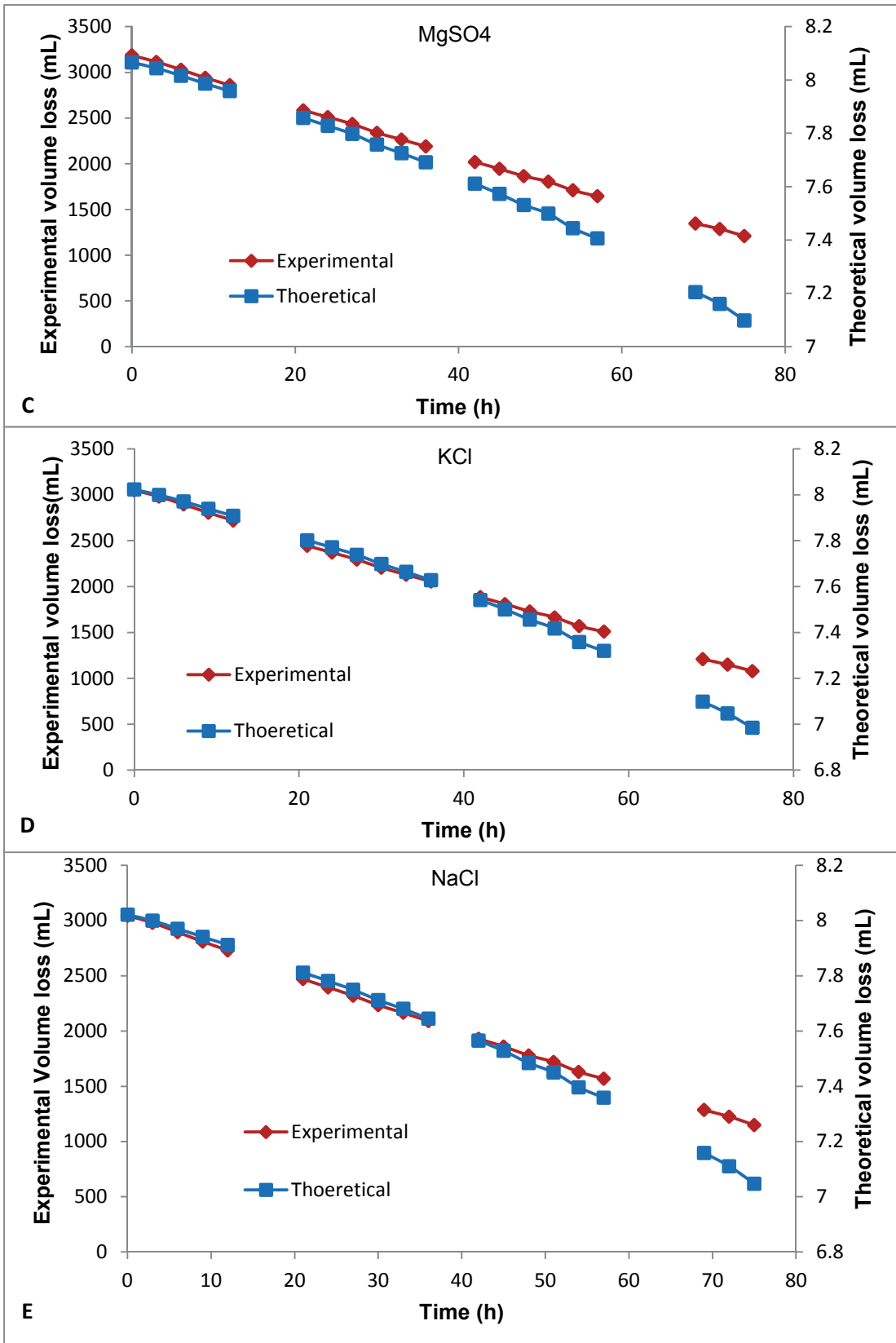


Figure 4.9: Experimental and theoretical volume loss, A (CaSO₄), B (Na₂SO₄), C (MgSO₄), D (KCl), and E (NaCl) with respect to time

Figure 4.9 shows the trend of theoretical and experimental volume loss of water for single salts as a function of time. The experimental volume loss resulted from the actual mass values obtained from the experiment, whereas the theoretical volume loss trend was obtained from Equation 10. It could be seen that the slope of

the experimental volume loss trend was higher than that of the theoretical volume loss trend. The theoretical trend showed how water should ideally be lost from the evaporation pan while the experimental trend showed a deviation from the ideal conditions. The experimental and theoretical trends were plotted to show the deviation between the two. Observing the trends for the theoretical and experimental graphs for each single salt solution, it could be noted that the theoretical rate of evaporation is faster than that of the experimental one. This deviation could be induced by experimental inaccuracies. The reason for the difference could be the fact that the conditions in the laboratory were not ideal and there were many parameters such as temperature and humidity, which could not be controlled. The difference in the trends could also be as a result of the differences due to solute effects and associated changes in chemical potentials as water mole fraction decreases and density increased, which the developed theoretical model did not adequately account for.

4.3.4 Energy Balance

The energy balance is done for the isolated system simulated in the laboratory composed of the lamp as source of energy and the evaporation pan containing salt solutions. An open system is a system which continuously interacts with its environment; interaction can be in the form of energy or material transfer into or out of the system boundary. A system is open if mass crosses the system boundary. For such a system, work must be done on the fluid mass to push it into the system and work is done by the fluid mass exiting the system. For this report an energy balance calculation was carried out on the evaporation pan, and Figure 4.10 shows the different energies involved in the brine evaporation process.

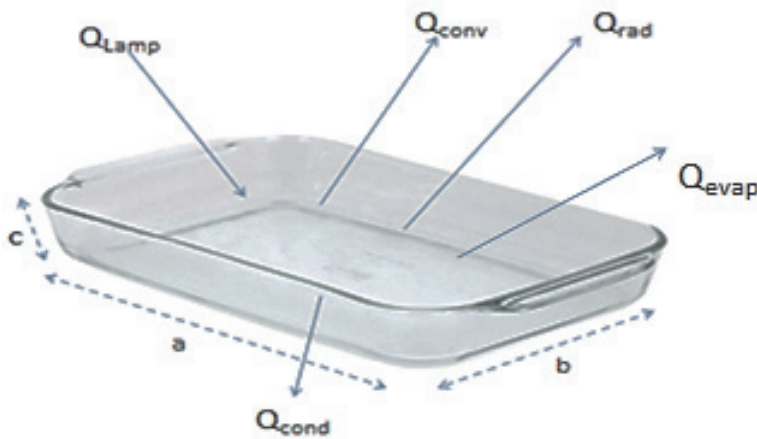


Figure 4.10: Different energies involved in the evaporation of water from the salt solution

$$Q_{Lamp} = \text{Energy from the lamp } (\dot{Q}_{Lamp} = 175 \text{ w}),$$

$$Q_{conv} = \text{Energy going out of the system by convection } (Q_{conv} = hA_1(T - T_{sur})),$$

$$Q_{rad} = \text{Energy going out of the system by radiation } (Q_{rad} = \epsilon\sigma A_1(T^4 - T_{sur}^4)),$$

$$Q_{cond} = \text{Energy going out of the system by conduction through the wall of the dish}$$

$$\left(Q_{cond} = KA_2 \frac{(T - T_{sur})}{L} \right),$$

(11)

$$Q_{evap} = \text{latent energy of vaporisation} = 2260 \times 10^3 \text{ J/Kg}$$

h = convection heat transfer coefficient (W/m²K),

T = temperature of water,

T_{sur} = temperature of surroundings,

ϵ = emissivity,

σ = Stefan-Boltzmann constant= 5.67×10^{-8} W/m².K⁴,

K = thermal conductivity (W/m.K) =0.058 W/m.K at 300 K,

A = water surface= $a.b$ (m²)

Assumptions:

- All the energy (Q_{Lamp}) is transferred to the salt solution,
- $Q_{cond}=0$,
- $Velocity=0$,
- $T_{sur}=25^{\circ}C=298$ K,
- $\epsilon=0.8$,
- $A=1$ m²

Conservation of energy:

$$E_{cumulative} = E_{in} - E_{out} \tag{12}$$

$$\dot{E}_{cumulative} = \frac{dq}{dt} = \frac{d}{dt}(mcT) = \frac{d}{dt}(\rho VcT) \tag{13}$$

$$\dot{E}_{in} = \dot{Q}_{Lamp} = 175(W) \tag{14}$$

$$\dot{E}_{out} = \dot{m} Q_{evap} + \dot{Q}_{conv} + \dot{Q}_{rad} + \dot{Q}_{cond} \tag{15}$$

$$\dot{E}_{out} = \rho \dot{V} Q_{evap} + hA(T - T_{sur}) + \epsilon\sigma A(T^4 - T_{sur}^4)$$

Substituting equations (13), (14) and (15) in (12)

$$\frac{d}{dt}(\rho VcT) = \dot{Q}_{Lamp} - \rho \dot{V} Q_{evap} - hA(T - T_{sur}) - \epsilon\sigma A(T^4 - T_{sur}^4)$$

$$\frac{dT}{dt} = \frac{\dot{Q}_{Lamp} - \rho \dot{V} Q_{evap} - hA(T - T_{sur}) - \epsilon\sigma A(T^4 - T_{sur}^4)}{\rho VcT} \tag{16}$$

A steady state condition would be reached when $\frac{dT}{dt} = 0$; the temperature is then determined by an algebraic equation of the form:

$$\dot{Q}_{Lamp} = \rho \dot{V} Q_{evap} - hA(T - T_{sur}) - \epsilon\sigma A(T^4 - T_{sur}^4) \tag{17}$$

The Australian Standard on solar heating for swimming pools (Australian Standard 3634-1989) recommended the following wind coefficient values (O'Reilly, 2009):

$$h = 3.1 + 4.1v$$

With v =velocity, $v=0$ then $h=3.1$ W/m²K

$$175 = V * 2260 * 10^3 + 3.1(T - 298) + (0.8)(5.67 * 10^{-8})(T^4 - 298^4)$$

Make V the subject of the formula

$$2260 \times 10^3 V = 175 - 3.1(T - 298) - 4.54 * 10^{-8}(T^4 - 298^4)$$

$$V = \frac{175 - 3.1(T - 298) - 4.54 * 10^{-8}(T^4 - 298^4)}{2260 * 10^3}$$

$$V = \frac{1456.9 - 3.1T - 4.54 * 10^{-8} T^4}{2260 * 10^3} \tag{18}$$

From Equation 18, the theoretical volume of water lost could be determined using the recorded temperatures, assuming that no energy coming from the heating lamp was lost. Figure 4.16 compares the theoretical and experimental temperature and volume of water loss of CaSO₄ with respect to time. Figures that give the trend of recorded temperature (K) and theoretical volume loss (m³) for NaCl, MgSO₄, KCl and Na₂SO₄ are included in the appendix A.

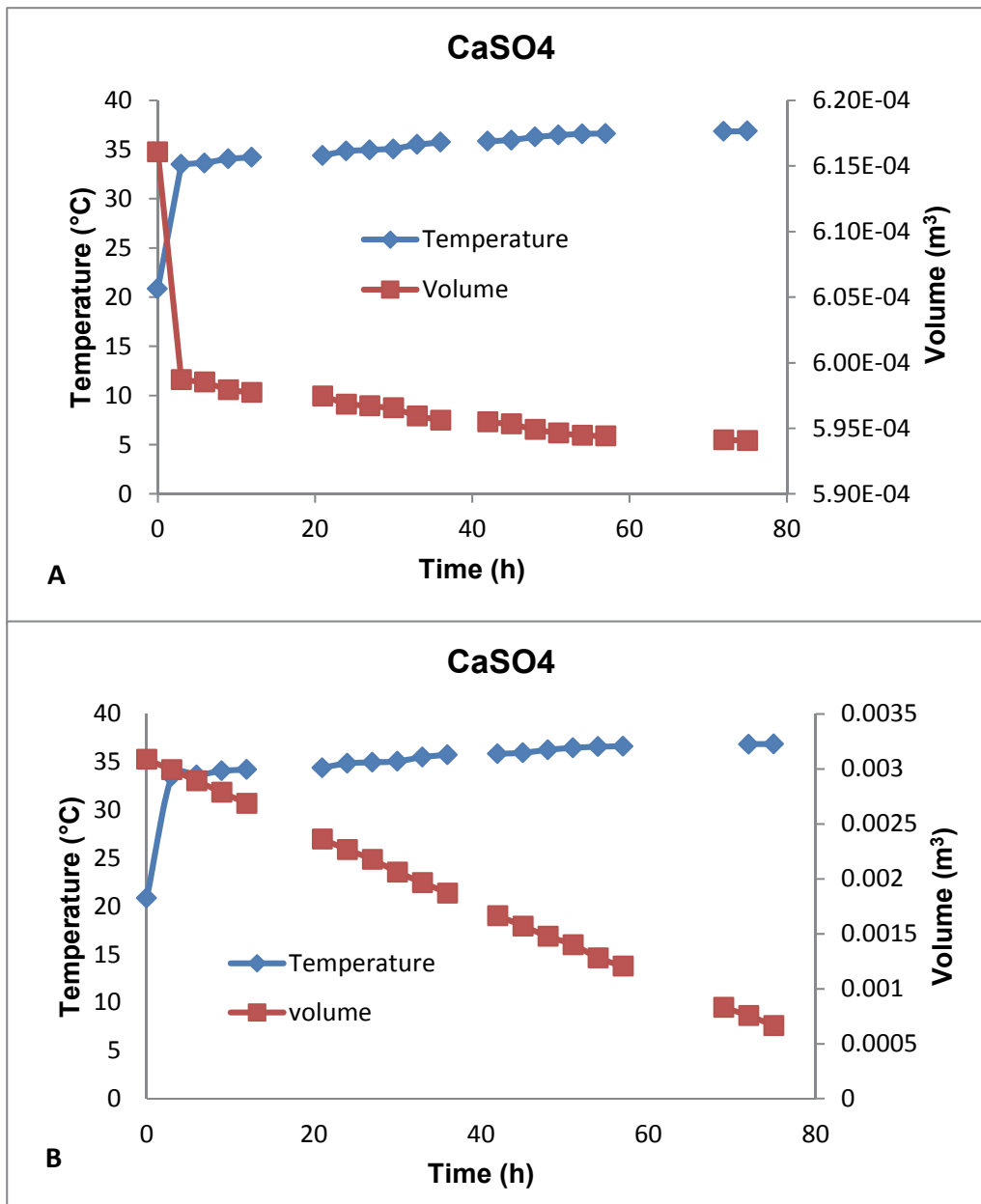


Figure 4.11: Comparison of temperature and volume of water loss of CaSO₄ with respect to time (A = theoretical and B = experimental)

Figure 4.11 shows comparisons between theoretical (A) and experimental (B) volume loss of water with respect to time. The temperature for A and B was the temperature recorded during the experiment and used to calculate the theoretical volume loss from equation 10. In Figure 4.11 (B), the volume comes from the experiment. Figure 4.11 showed how the theoretical and experimental water were lost from the salt solution at constant temperature. It could be seen that the theoretical volume loss was relatively constant while the experimental volume decreased with constant temperature. When calculating the theoretical volume loss of water many assumptions were made, which might have led to a slight decrease in the predicted volume of water lost. For the experimental conditions, the volume of water lost decreased gradually at a constant temperature; this could be caused by the fact that the parameters such as humidity and room temperature were not constant or because the brine becomes increasingly concentrated and denser over time. The volume of water evaporated at a given temperature and time can be easily determined.

4.3.5 Evaluation of heat transfer operation

Heat transfer is thermal energy in transit due to a spatial temperature difference. There is a temperature difference in a medium or between media that heat transfer must occur, which can be a solid or a fluid. The term conduction is used when the heat transfer occurs across the medium and convection is used when the heat transfer occurs between a surface and a moving fluid when they are at different temperatures. The third form of heat transfer is called radiation in which the energy that is emitted in the form of electromagnetic waves (Incropera et al., 2006). This section presents only the convection and radiation heat transfers that occur between the heating lamp and the surface of the salt solution fluid in motion and a bounding surface. Figure 4.12 presents the convection heat transfer from the heating lamp to the surface of the salt solution.

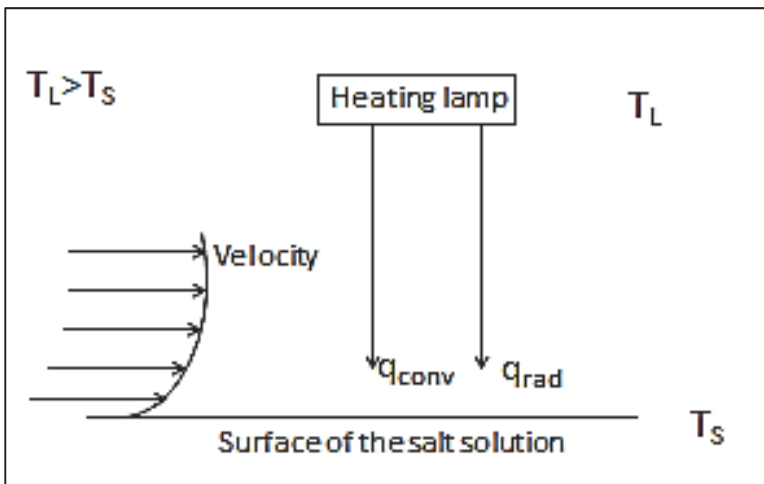


Figure 4.12: Convection heat transfer from the heating lamp to the surface of salt solution

$q = \text{heat} = J$

$T_L = \text{temperature of heating lamp (K)}$,

$T_S = \text{temperature of surface of the solution (K)}$,

$\sigma = \text{Stefan-Boltzmann constant} = 5.67 \times 10^{-8} \text{ W/m}^2 \cdot \text{K}^4$,

$A = 1 \text{ m}^2$

$\epsilon = \text{emissivity} = 0.8$,

$h = 3.1 + 4.1v$

With $v = \text{velocity}$, $v = 0$ then $h = 3.1 \text{ W/m}^2 \text{K}$

Assumptions:

- The heat is transferred from the heating lamp to the surface of the salt solution by convection and radiation,
- No heat is lost,
- Velocity = 0 (m/sec),
- $A = 1 \text{ m}^2$,

$Q = q_{\text{conv}} + q_{\text{rad}}$

$q_{\text{conv}} = hA(T_L - T_S)$ and $q_{\text{rad}} = \sigma \epsilon A(T_L^4 - T_S^4)$

$$q = hA(T_L - T_S) + \sigma \epsilon A(T_L^4 - T_S^4)$$

$$q = 3.1 \cdot 1 \cdot (375 - T_S) + 0.8 \cdot 5.67 \cdot 10^{-8} \cdot 1 \cdot (375^4 - T_S^4) \quad (19)$$

From equation 19, the heat that was transferred from the heating lamp to the surface of salt solution was determined and Figure 4.13 shows the variation of the heat that evaporated a volume of water from the salt solution at a given time.

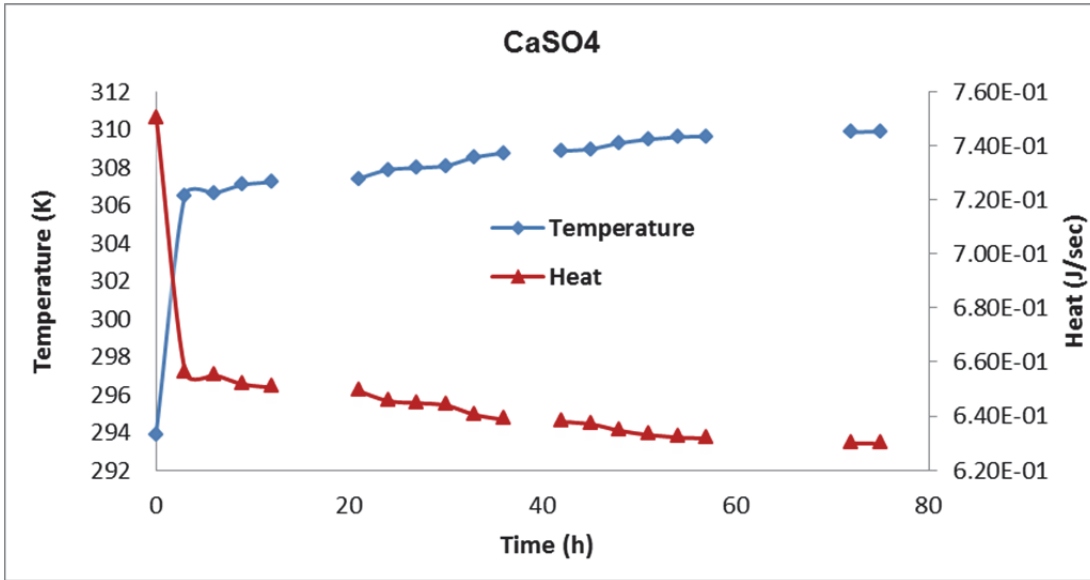


Figure 4.13: Variation of the heat that evaporated a volume of water from the salt solution at a given time

Figure 4.13 shows a similar trend to Figure 4.11 (A) where the volume of water loss was relatively constant at constant temperature. This can be explained by the fact that in ideal conditions, the heat that transferred from the lamp to the water surface was constant; therefore the volume of water evaporated was also constant. The heat given by the heating lamp is 175 J/sec which is about a 1000 larger than the heat given in Figure 4.13. This could be explained by the fact that the temperature of the heating lamp, which was 375 K, was recorded by putting the thermometer just below the lamp without touching it for 5 minutes. Then the exact temperature of the lamp was not recorded and this could be the reason why the values of the heat in Figure 4.13 are much less than 175 J/sec.

CHAPTER 5: MAIN EVAPORATION STUDY (PILOT SCALE)

5.1 INTRODUCTION

This chapter presents and discusses the results of the pilot scale experiments carried out to determine the effect of physical parameters on the rate of evaporation.

5.2 MAIN EVAPORATION STUDY (PILOT SCALE)

The following results were obtained during the experiments (Figure 5.1). All the experiments were conducted over a 48 hour period and the initial temperature of the water was similar to the ambient temperature. The temperature of the liquid (water) had a tendency to be uniform after it was subjected to the heating source in a 48 hour period.

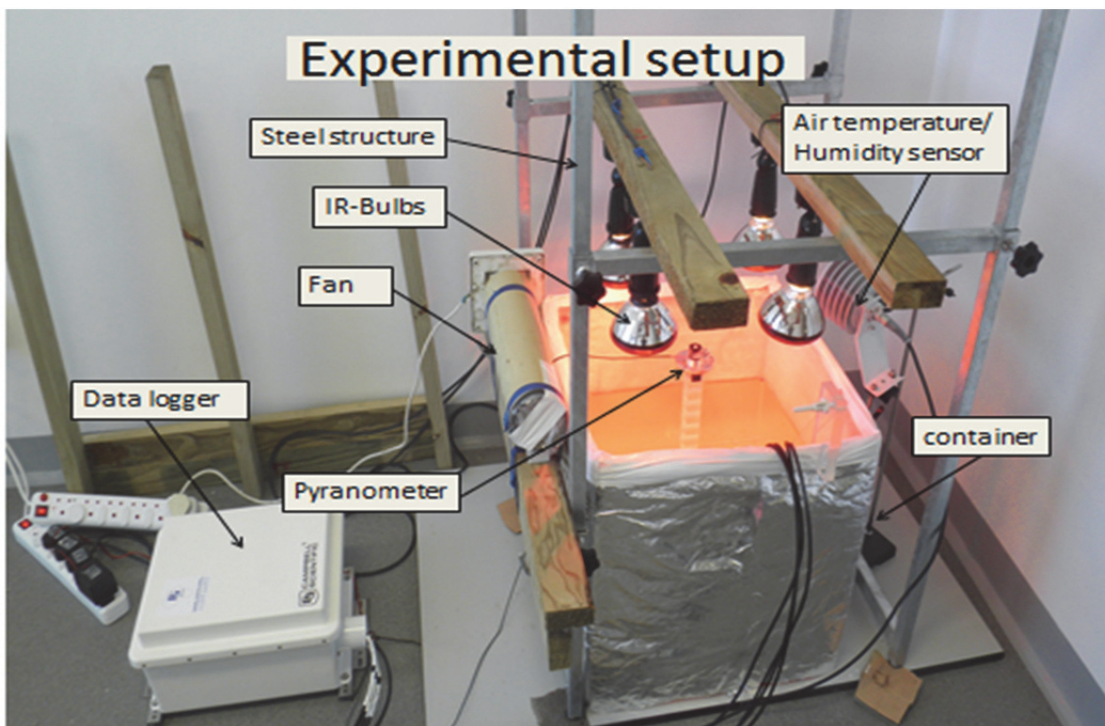


Figure 5.1: A display of the experimental setup with all the components

5.2.1 Hydrostatic pressure

In the larger scale experiments conducted (section 3.7); the evaporation rate was calculated with a Solinst ® Levelogger device or known as a “diver” over an elapse time period. The device was placed at the bottom of the container. The hydrostatic sensor recorded the temperature and the pressure exerted by the volume of the brine. The pressure can be converted into volume if the total volume is known prior to the recordings from the hydrostatic sensor. Although the hydrostatic sensor recorded a decrease in pressure during the experiment, the atmospheric pressure was not incorporated in the calculation. The level of brine and hydrostatic pressure (in bar) over time is presented in Figure 5.2.

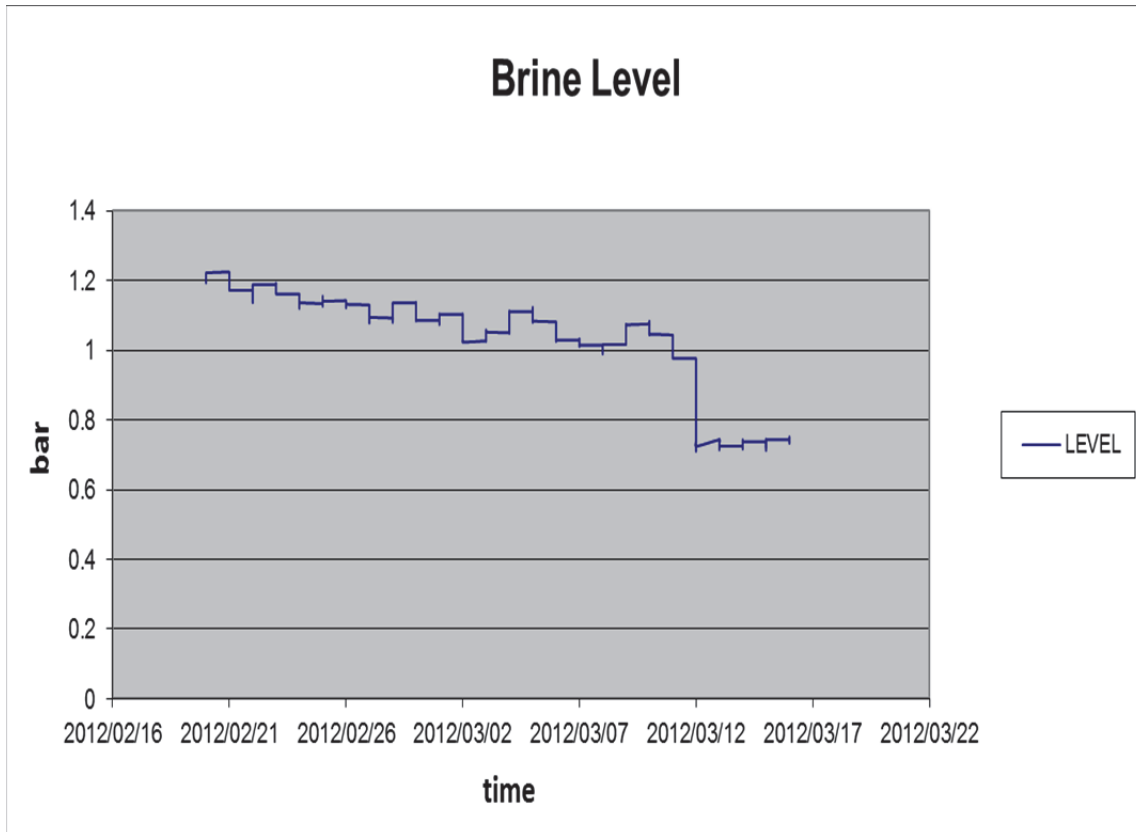


Figure 5.2: The level of NaCl solution as a function of hydrostatic pressure (in bar) over time

In Figure 5.2 there are a number of slight increases in hydrostatic pressure during the experiment. This could be the result of a change in atmospheric pressure while the brine was evaporated. The level sensor showed that the level of water was affected by the hydrostatic pressure.

5.2.2 Temperature and humidity

The temperature sensors in the larger scale ponds clearly showed significant temperature stratification within the tank during the IR radiation period (Figure 5.3). The (Temp1) which was situated 25 mm from the water surface indicated the highest temperature reading. The maximum daily temperature slowly increased from below 35°C to nearly 38°C. This is the direct result of the water level dropping below the first sensor as the water starts to evaporate. This pattern was visible with the other sensors but at a lower increase. The second sensor (Temp 2) had identical peaks as the first sensor but slightly smaller with a small delay in temperature response due to IR radiation. The response of the third sensor (Temp 3) shown in the graph had dramatically changed in shape as the energy started to dissipate at a depth of 150 mm below the surface. The last sensor which was located at a depth of 250 mm remained almost at a constant temperature (Temp 4) during the test period. A slight wave movement was observed with an extended time delay compared to the first sensor. Furthermore, the air temperature showed a cycle of about 5°C daily fluctuation although there was evidence of an increase of air temperature which synergised with the other sensors. The air temperature was more irregular than the temperature recorded by the sensors in the pond at varying depths. The controlled room temperature to some extent corresponded with cyclical change in temperature from the brine artificial lighting system.

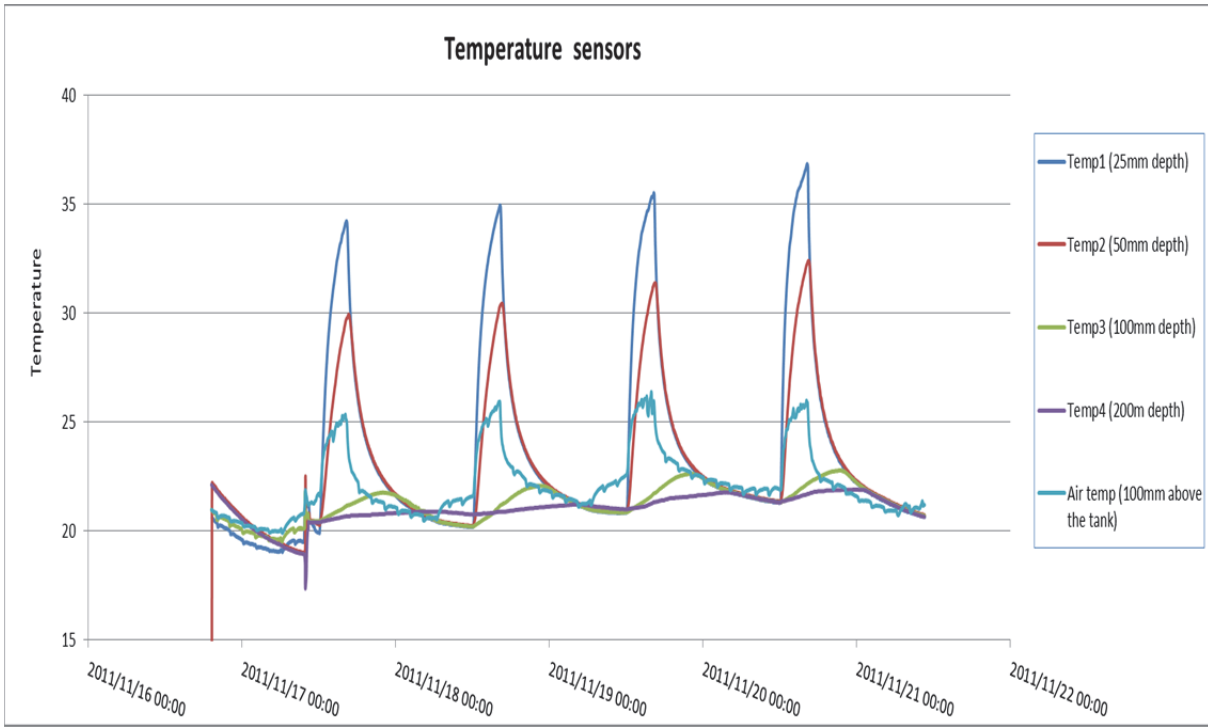


Figure 5.3: The cycles of energy input which the sensors recorded in the larger pans.

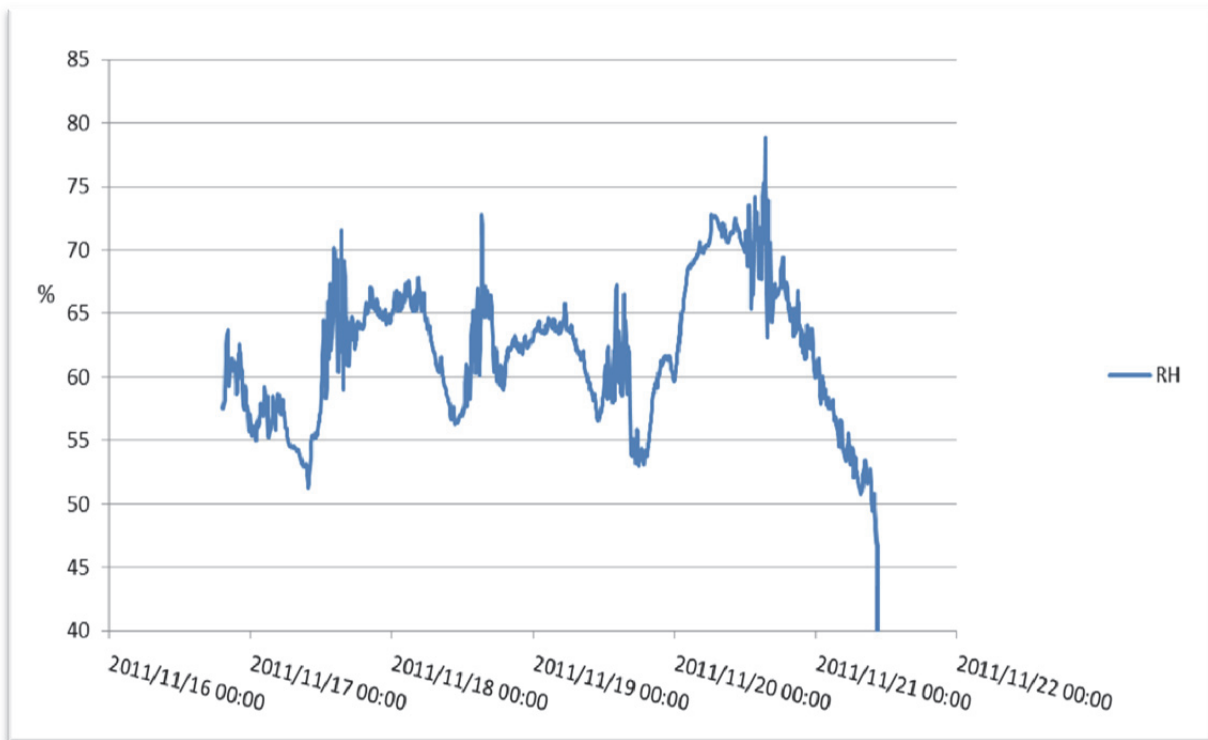


Figure 5.4: The change in humidity during the various cycles in the larger pans.

In Figure 5.4 the relative humidity is presented over the time of 4 days. The humidity range was large, ranging between 55-80 %. This however represents a segment of the weather pattern at the study site. The distance between the sensor and the brine water surface played a significant role in the humidity results. The sensor's close proximity to the brine surface level could be within the saturated area above the brine tank.

The reading might not have reflected the entire experimental area as such but only the portion around the brine tank. This is a major component in the evaporation rate especially with the limited wind factor.

5.2.3 The energy output

The energy output from the bulbs used to irradiate the larger pans was close to 500 Watts over the quarter metre square tank. The silicon cell of the pyranometer was able to detect other light sources which had minimal or no impact on the experiment. The baseline of the graph shown in Figure 5.5 appeared to be on zero but indicated minimal elevation which reflected the external light sources. The cyclical high peaks of 450 Watts indicated the time period when the energy source was activated for a four hour cycle. Although an extra set of bulbs of 500 Watts was added, the pyranometer continued to record the output as 500 Watts. The position of the pyranometer was located in the middle of the 1000 Watts lamps and only recorded half of each set of the IR bulbs. The combined output of a 1000 Watts would influence the rate of evaporation.

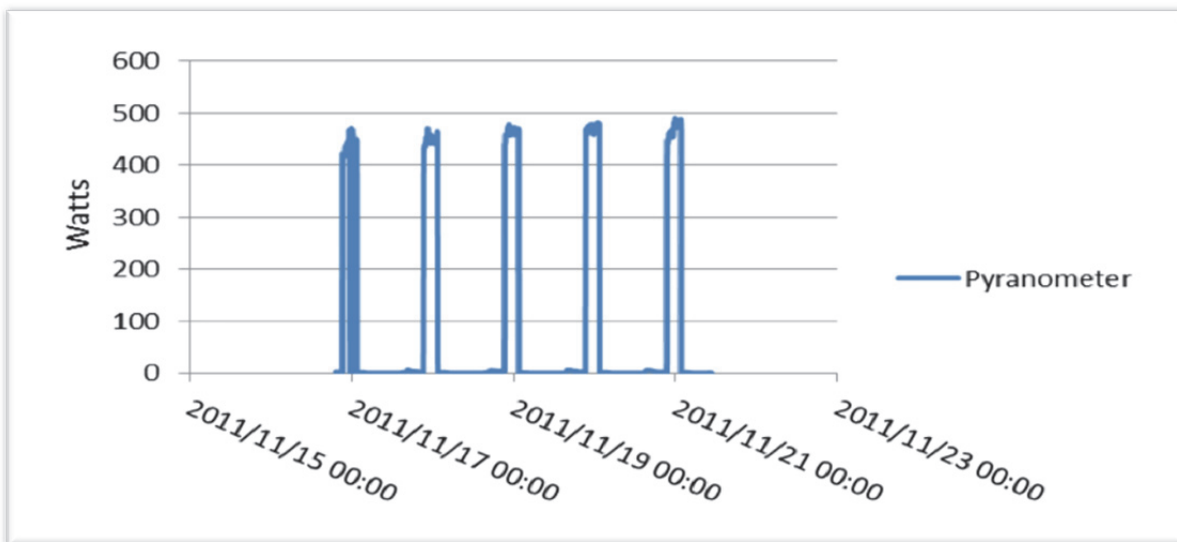


Figure 5.5: The energy cycle of the larger pan system.

5.2.4 Effect of physical parameters on evaporation of water

The effect of physical parameters (temperature, wind, humidity and radiation) on the rate of evaporation was carried out in distilled water. All the experiments were conducted over a 48 hour period and the initial temperature of the water was similar to the ambient temperature. The temperature of the liquid (water) had a tendency to be uniform after it was subjected to the heating source over a 48 hour period.

5.2.4.1 Effect of temperature and wind

The results shown in Figures 5.6 and 5.7 were obtained when the water surface was exposed to (250 Watts x2) at 100 mm distance from the IR bulbs without and with wind factor.

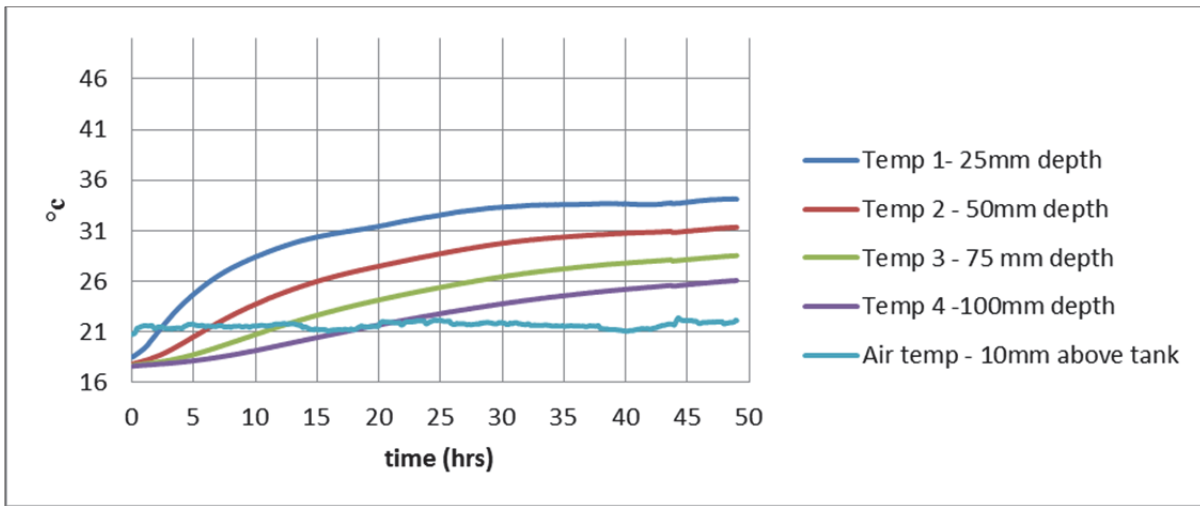


Figure 5.6: The temperature variation at different depths of the container during the exposure to radiation energy from the IR bulbs over 48 h without wind

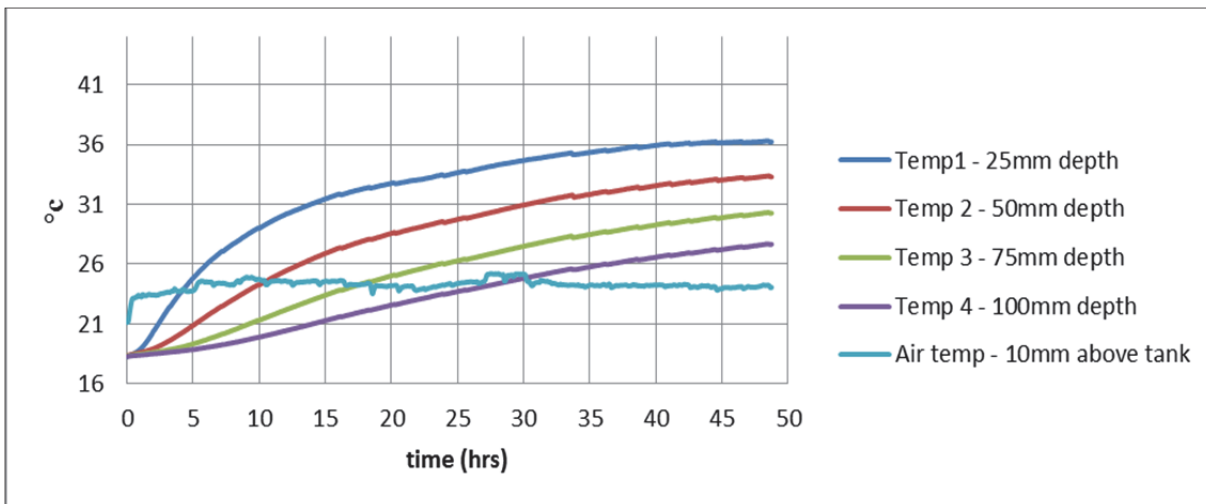


Figure 5.7: The temperature variation at different depths in the container with the wind factor using the same amount of heat source as above

From the result shown in Figure 5.6, the sensors portray temperature stratification in the container. The surface of the liquid was warmer than the lower part of the container. The first sensor (Temp1) which was situated 25 mm down from the water surface indicated the highest temperature reading. The temperature steadily increased from below 18.5°C to nearly 34°C over the course of 48 hr. This was as a result of the water absorbing the energy from the IR bulbs through radiation. This trend was visible with the other sensors but at lower maximum temperatures. The temperature of the second sensor (Temp 2) started at a slightly lower value and followed a similar trend to Temp 1. A delay was noted in the rise of the temperature of (Temp 2), which was due to the delay in energy penetrating the water depth over a longer time period. It took the first sensor more than 6 hours to reach 26°C while in the case of the second sensor (Temp 2) it took approximately 15 hours. This delay was filtered down to the other sensors. Temp 3 sensor took close to 27 hours and Temp 4 sensor close to 48 hours to reach 26°C. The third sensor (Temp 3) recorded a temperature of approximately 10°C lower in relation to the first sensor (Temp 1) as the heat transfer started to diminish at a depth of 75 mm below the water surface. The sensor located at a depth of 100 mm portrayed a pattern very similar to the curve for the third sensor (Temp 3). Furthermore the air temperature above the

container had minor variations which might be attributed to fluctuations in the ambient temperature and the heating of the IR bulbs.

The results presented in Figure 5.7 which represent the experiment with a fan to generate a light breeze, showed a very similar pattern compared to the graph without the wind. The average peak temperatures achieved over 48 h were generally higher than the experiment without the wind influence. The air temperature above the container was approximately two degrees higher in the case where the wind was applied than the temperature at the same height in the experiment without wind. This difference impacted the maximum temperatures of all the other temperature sensors at the specific depths respectively. This is ascribed to the constant removal by the wind of the boundary layer, which would have had an insulating effect in the case where no wind was applied. It is also possible that the floating system of the probes could have shifted and decreased the distance between the sensors and the surface of the water.

5.2.4.2 *Effect of humidity and wind*

The variation in the relative humidity above the water surface without wind as well as with the wind factor over a 48 hour period compared to the relative humidity of the room is shown in Figures 5.8 and 5.9

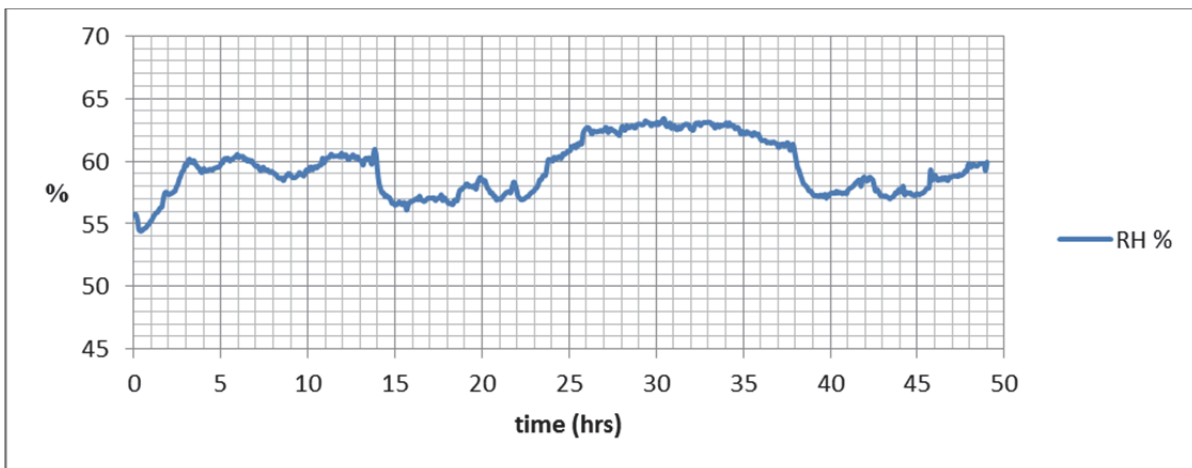


Figure 5.8: The variation in the relative humidity above the water surface over a 48 hour period without wind

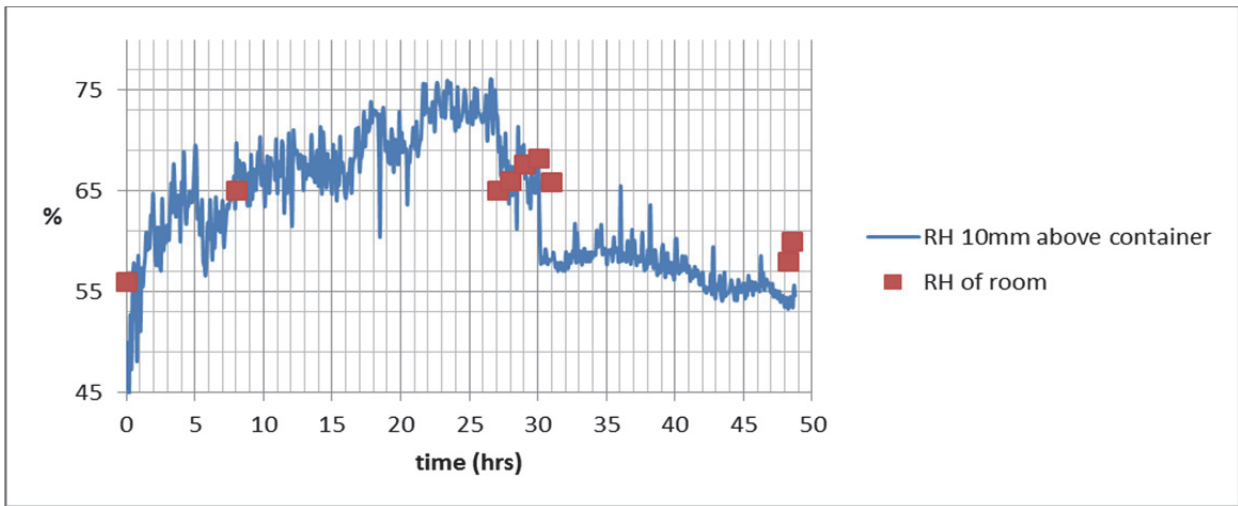


Figure 5.9: The relative humidity above the water surface with the wind factor over a 48 hour period compared to the relative humidity of the room

The humidity of the room during the experiment was not constant. The feed from air conditioning was set at 60%, but fluctuated. The experiment itself had an effect on the humidity of the room. When water in the container without wind started to evaporate, the humidity showed a random pattern (Figure 5.8). The humidity varied between 55-63%. The humidity values initially increased during the first period (5 hours) and then remained relatively stable for about 10 hours. In contrast to the RH (Figure 5.8), the water temperature at the surface was still rising (Figure 5.6). This highlighted the relationship between temperature and humidity without a wind factor. With a decrease in the humidity the temperature decreased. After 23 hours the humidity increased to 60 and 65% for approximately 10 hours duration. After 40 hours the water temperature had stabilized but the humidity then decreased and remained stable for about one and a half hours and increased again until the end of the experiment, even when temperatures were stable. The variable cycle in the humidity can be the result of the lamps used as heating source heating up a column of air directly under the lights which was discharged though turbulent motion (Pal Arya, 1998). This process of constant replacement of the air which had a conveyer belt effect is a possible answer for this observation. The frequency was the direct fluctuations of the ambient temperature as cooler air was replaced more quickly. The temperature graph in Figure 5.7 (which incorporates the wind factor) did not relate to that of Figure 5.9 regarding humidity. The added wind factor had disrupted the air columns which can be illustrated by the smaller variation in the distinctive pattern of Figure 5.10 below. The humidity increased from the start of the experiment with a rise in temperature of the water which occurred for about 25 hours and decreased rapidly for about 1 hour. The humidity remained within a 60-65% range. The water level decrease could have potentially affected this result. If the water level was below a certain point, then the wind had very little effect as the side wall of the container acted as a shield for the water. Another scenario was the higher room temperature which had the same variation pattern as the humidity reading above the container. These experiments showed the difficulty of attaining absolute control over each applied parameter even in well controlled environments.

5.2.4.3 Effect of radiation

Figure 5.10 shows the radiation output generated from the 2 IR bulbs (250 watts x2) that was recorded by a pyranometer (silicon cell). The pyranometer was mounted on the floating device which housed the temperature probes. The initial total output of 450 Watts from the bulbs shown in Figure 5.10 represents the combined 500 Watts output of the IR bulbs. The linear decrease of the radiated energy was directly proportional to the decrease of the water level, which symbolizes the inverse square law (Monteith and Unsworth, 2008). The smaller variations in the curve were the result of the radiation flux which acts as frequency. Both the curves had a linear decline as shown in Figure 5.10 with relatively high variations. In particular, the experiment with the wind effect (red curve) had shown a rapid decrease around the 7 hour period.

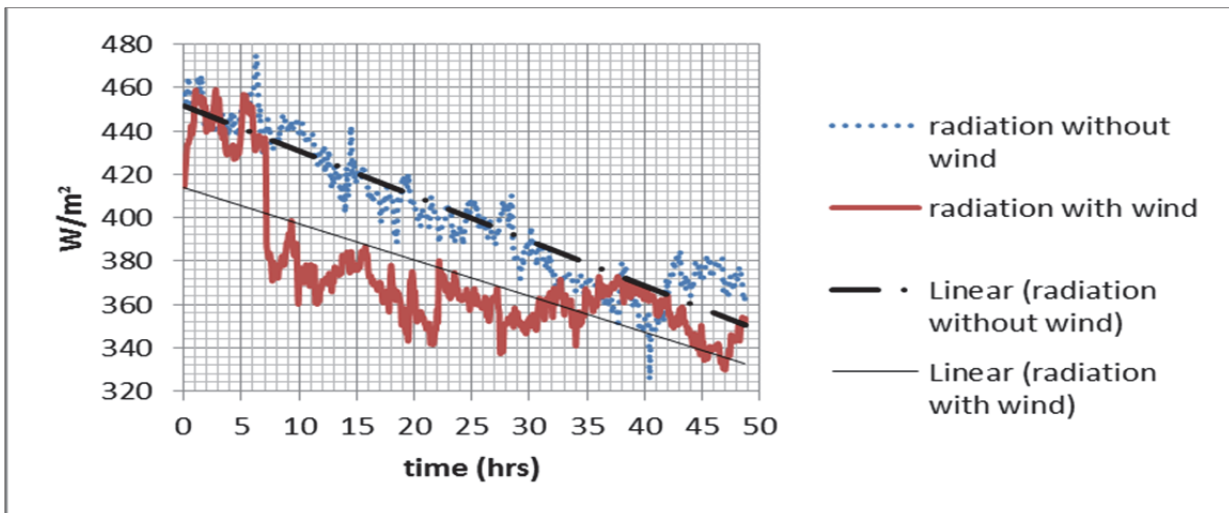


Figure 5.10: The variations of the radiation over a 48 hour time period with and without the wind assistance.

The data of the experiment started at different times over the same time duration. After 5 hours, data obtained for both experiments (without or with wind) indicated the same water level decrease. The temperature at this stage had a major impact where it affected the saturated air. From the 10 hour mark onwards there was a clear separation between the two curves as the evaporation rate in the case of the experiment conducted with the constant wind accelerated faster than the case without the addition of wind. This was confirmed in Figure 5.9 where the humidity continued to rise above 70%. In contrast, the humidity graph (Figure 5.8) indicated cycles where RH remained relatively stable. The saturated air from the faster evaporation rate (red scatter dots in Figure 5.11) was constantly being removed by the wind while the slower evaporation rate (blue curve) was as a result of the accumulation of the saturated air above the container (boundary layer). Furthermore this trend continued where the two rates remained practically parallel in relation to each other. The radiation for both experiments was reduced as the distance between the lights and the water level increased. The energy required to transfer the water molecules from the liquid gas phase was constantly reduced over the specific time period. Approximately 10.42 litres of water was added to return the water level to the origin point in the experiment with the constant wind factor. The experiment excluding the constant wind managed to evaporate only 9.84 litres of water over the same period.

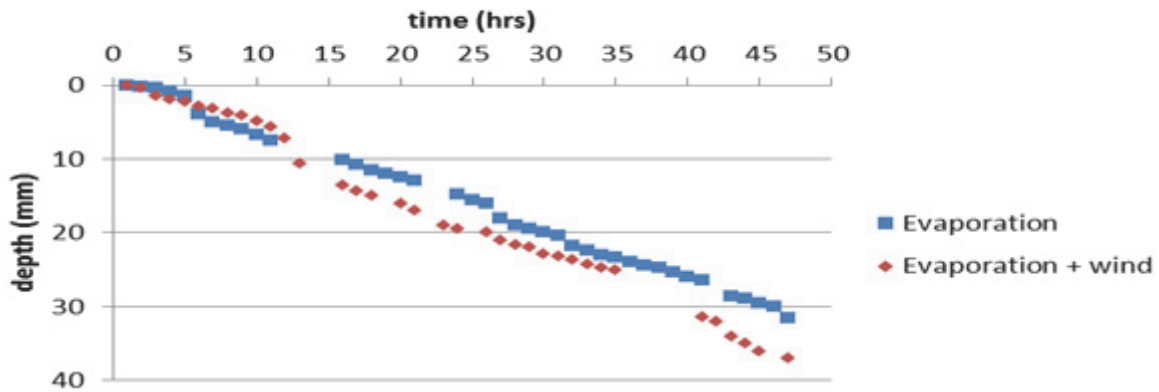


Figure 5.11: The evaporation rate is shown by the decrease in water level for the two experiments over the same time period.

The results obtained after the height between the IR bulbs and the water surface was increased to 200 mm (from 100 mm) (Figure 3.4) are presented in Figures 5.12 and 5.13.

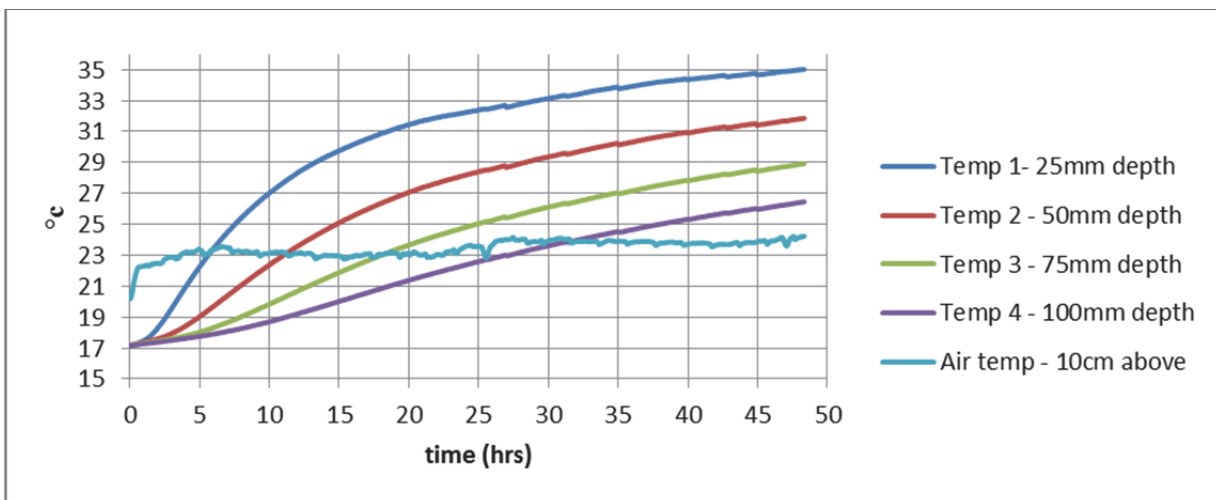


Figure 5.12: The temperature gradients after the height of the IR bulbs were increased from 100 mm to 200 mm from the water surface

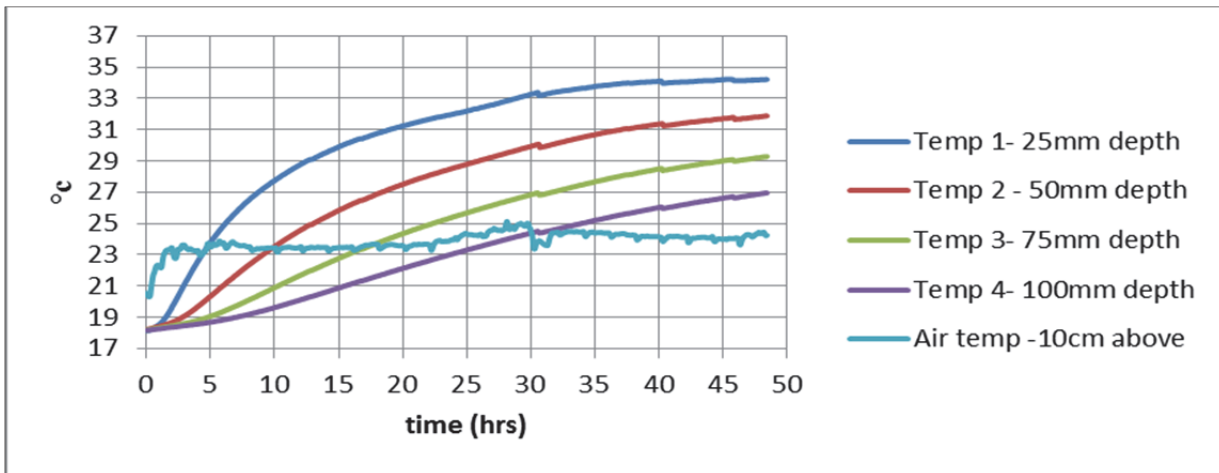


Figure 5.13: The temperature gradient after the increased distance of the heating source with the added wind factor.

The sensors in Figure 5.12, clearly showed temperature stratification within the container similar to the situation earlier when the energy source was situated closer to the water surface (Figure 5.6). The only difference being that the temperature did not rise to the same level as before. Sensor 1 (Temp1) recorded a temperature rise from 18.5°C to nearly 34°C after 48 hours in Figure 5.12. Sensor 2 showed a similar pattern but the peak temperature was lower, as expected. The energy from the light source was penetrating the water depth similar to Figure 5.6, but showed a delay in temperature increase. Both sensors 3 and 4 followed the same trend. The initial temperatures recorded by sensor 2, 3 and 4 after 48 hours were close to 32°C, 29°C, 26°C, respectively. Comparing the four curves in Figure 5.13, it is interesting to note that curve 1 (Temp1) reached a temperature of 27°C after about 8 hours while curves 2, 3 and 4 reached the same temperature only after 18 hr, 33 hr, and 48 hr respectively. Comparing Figure 5.12 with Figure 5.7, where the only difference in the experimental setup was the height adjustment of the energy source above the water surface, it was observed that curve 1 (Temp1) in Figure 5.7 reached a temperature of 28°C after 8 h while curves 2 (Temp 2), 3(Temp 3) and 4 (sensor 4) reached the same temperature after 18 h, 31 h and 48 h respectively. In both instances, the difference between surface water temperature and the temperature at 100 mm deep after 48 h had the same order, with 8°C in the first case and 7°C in the situation where the energy source was raised by 20 cm.

Similar to the previous results presented in Figure 5.7, the energy from the bulbs starts to dissipate with an increase in depth below the water surface. The last sensor (Temp 4) which was located at a depth of 100 mm had displayed the least difference in the temperature variations. The temperature sensor (Temp 4) followed identical patterns to the previous experiment without the wind contribution. A delay in the increase in temperature amounted to about 5 hours. Thereafter, a linear form of temperature increase started as result of an extended time delay of the energy reaching the last sensor. The air temperature remained relatively constant in relation to the temperature sensors in the container. The heating source (IR bulbs) had very little effect while the ambient temperature played a more significant role in the behaviour of (Air temp) in Figure 5.13.

Furthermore, Figure 5.14 displayed an identical pattern to the one in Figure 5.12. The maximum temperatures of the submerged sensors in the container were lower. However, the air temperature above the container showed minor variations.

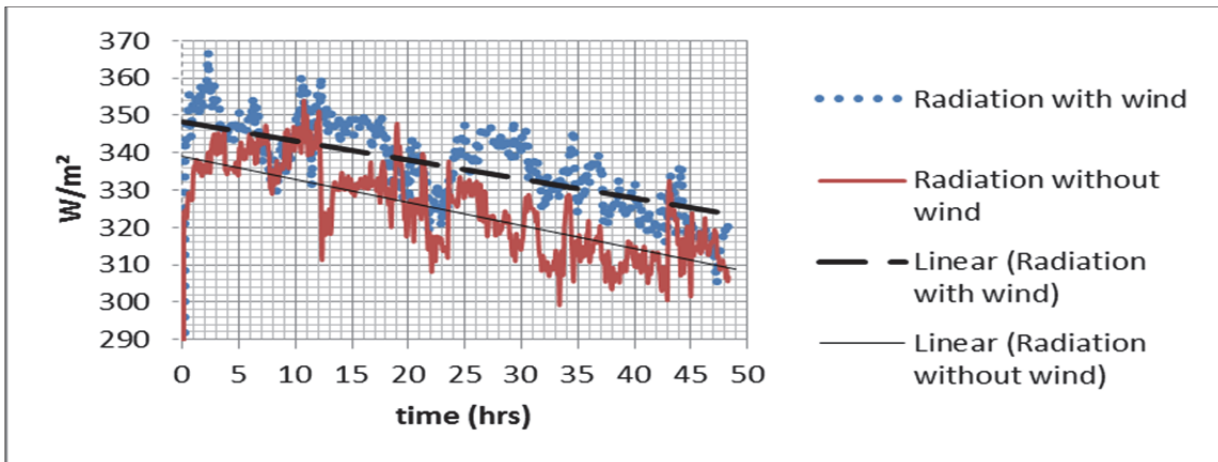


Figure 5.14: The energy recorded on the surface of the water during the experiments with and without wind. The height between the lights and the water was 200 mm

Figure 5.14 displays the radiation generated from the 2 IR bulbs (250 watts x2) and measured by a pyranometer in the same manner as in the previous experiments (Figure 5.12). The curves have indicated that the energy was reduced to about 100 Watts in comparison with the results of Figure 5.14. The linear decrease for both the curves in radiated energy are directly proportional to the surface level decrease of the water as the pyranometer was floating on the water surface. The smaller variations of the red curve in Figure 5.14 occurred due to the radiation flux oscillating in a wave pattern (Pal Arya, 1998). The red curve in Figure 5.14 showed a greater radiation decrease over the 48 hour period as a result of the wind influence on the experiment. A loss of nearly 40 Watts/m² was achieved at the end of the experiment.

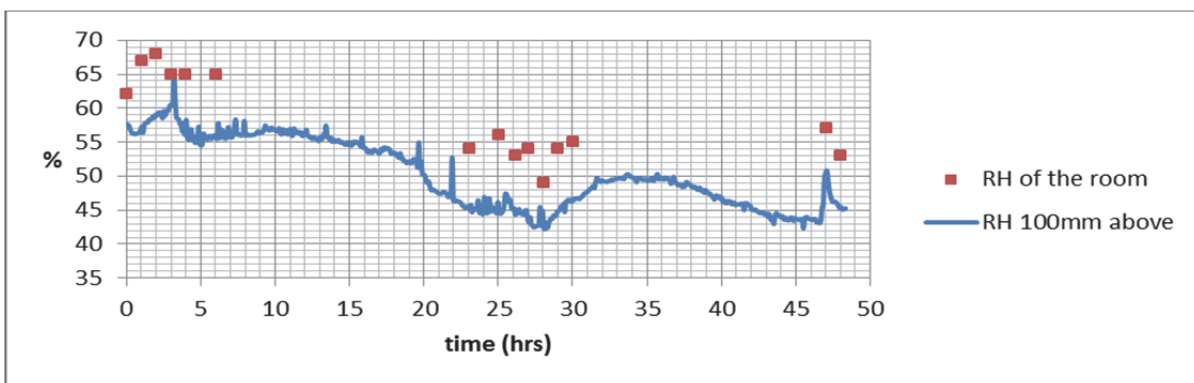


Figure 5.15: The relative humidity of the air above the water after the height of the energy source was increase to 200 mm.

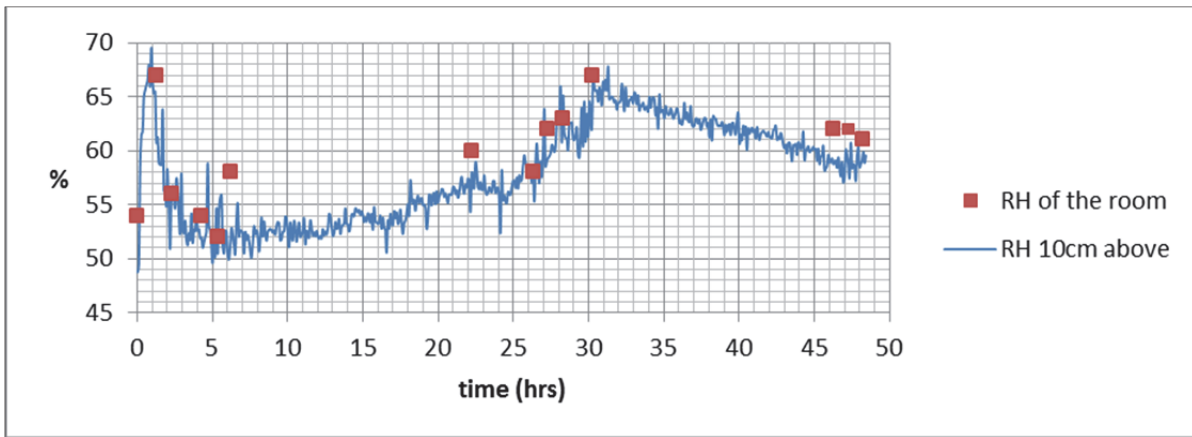


Figure 5.16: The relative humidity of the air above the water surface when the wind was included in the experiment.

The humidity of the room displayed in Figure 5.15 was not constant. The feed from the air-conditioning was set to maintain a humidity of close to 60%, but indicated some fluctuations during the experiment. Similar to the previous experiments, various factors had an effect on the humidity. The heat generated by the energy source above the water itself had an effect on the humidity of the room. The vapour released from the experiment contributed towards the humidity in the room, but air from the room was expelled through an extractor fan to achieve the 60% setting. The humidity in Figure 5.16 had no distinctive pattern. It did not correlate with the temperature or the radiation data. The humidity in Figure 5.15 had a range between 40% and 65%. The humidity was at the peak in the first 5 h while the lowest recordings occurred at 27 h and again at the 45 h mark respectively. From the graph in Figure 5.15 the humidity appeared to be constant between the 5 and 10 hours mark and then showed a steady decrease close to 40%. After 27 h, the humidity increased to 50% for about 5 h. After 36 h, the humidity increased again and then increased after 48 h. In this particular situation there was no actual link between the temperature of the water and the humidity measured above the container. The humidity above the water surface was mainly affected by the humidity of the room which was slightly higher at various intervals. This was reflected by the reading of the sensor above the water in the container. However, all variations have an impact on the water loss which was illustrated in Figure 5.17. With the addition of constant wind, it has caused a disruption of the air columns which can be illustrated by the smaller variation in the graph of Figure 5.17. The edge of the container may also play an important role. When the water level inside the container dropped below a certain level, the edge of the container may have blocked the main effects of the wind since the water surface was much lower than the container's side wall.

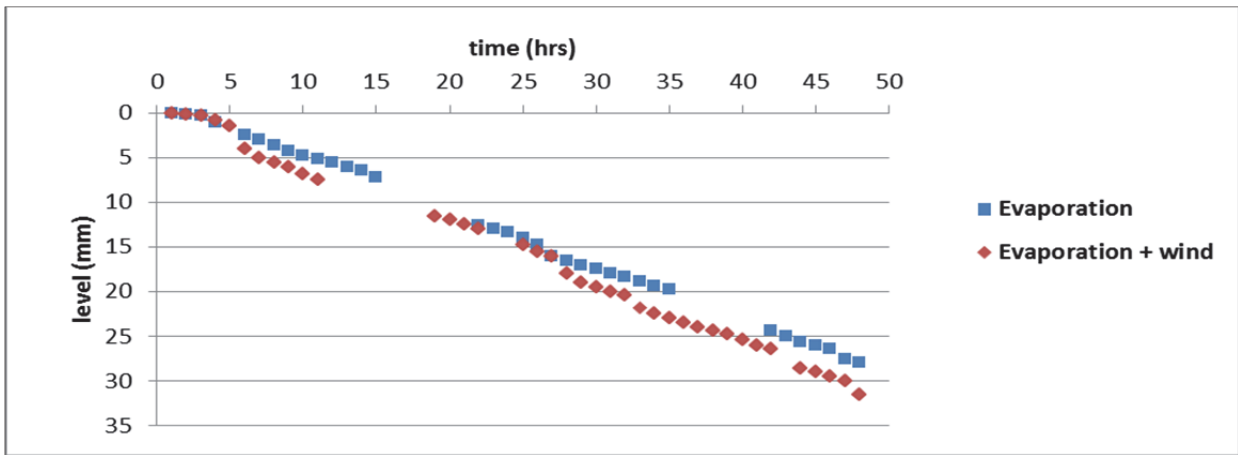


Figure 5.17: The evaporation as determined by the change in water level of two experiments (with or without wind) over the same period (200 mm distance)

The overall volume loss for both these experiments had a further reduction when the distance between the energy source and the water was increased to 200 mm. Based on empirical evidence the total amount of water loss had increased by 12% when wind was introduced (see Figure 5.17). The increase in evaporation rate was the result of turbulent air from the fan thereby removing the saturated air above the container. This happened despite the fact that the energy source was further away, something that was expected to lower the evaporation. It may be an indication of the effectiveness of the moving air, increasing the evaporation rates. The increased distance between the energy source and the water surface reduced the total volume of water loss in comparison to the experiment where the distance was 100 mm.

The experiments Figure 5.17 were conducted at different times, but ran for the same time duration. Similar water loss was recorded over the first 5 h for both the experiments (Figure 5.17). The temperature at 25 mm water depth was approximately 23°C. The temperature generated from the lamps had an effect on the saturated air above the water surface. This was evident when the humidity data was compared to the humidity of the room. In Figures 5.15 and 5.16, the humidity of the room was higher than the humidity above the water surface. During 6 and 10 h, the evaporation rates were similar which led to the data points of the two graphs being relatively parallel. During the period of 25 and 30 h, the two graphs nearly overlapped. The evaporation rate (illustrated by the red curve in Figure 5.17) decreased as a result of the increase in the humidity (Pal Arya, 2001). Humidity during this period was at its highest (see Figure 5.16). Furthermore, the evaporation rate of the experiment without wind assistance was constant and the humidity recorded above the container peaked at 50 %. This showed the impact of the humidity on the evaporation rate because the temperature for both the experiments had almost reached maximum. After 35 hours duration, the humidity steadily decreased (Figure 5.15 and 5.16). This however, kept the evaporation rates constant for both these experiments. The total water loss for the experiment without the wind factor was 7.8 litres. This figure amounts to a 12% lower rate than when the wind factor was added.

The results of the experiment carried out with reduction in radiation input (IR bulbs 250 Watts reduced to 125 Watts) (Figure 3.4) are shown in Figure 5.18.

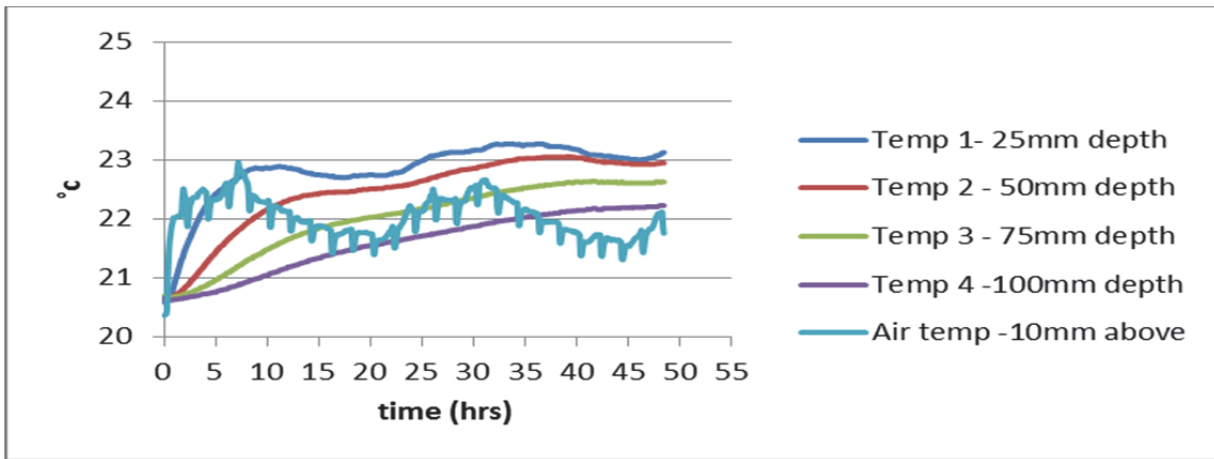


Figure 5.18: The temperature stratification in water during the reduction in radiation

With the reduction in the energy input along with the increase in height, the maximum temperatures for the various depths based on the previous experiment (Figure 5.6) were reduced by approximately 10°C (Figure 5.18). The range between the temperatures at different depths was much smaller than in the previous experiments. The surface temperature of the water was probably influenced by the ambient temperature. The changes in the ambient temperature clearly have an effect on the water temperature (Figure 5.18). The reduction in the energy from the IR bulbs caused the water surface temperature to be more dependent on the ambient temperature of the room. The lower part of the water in the container responded more slowly to these moderate changes.

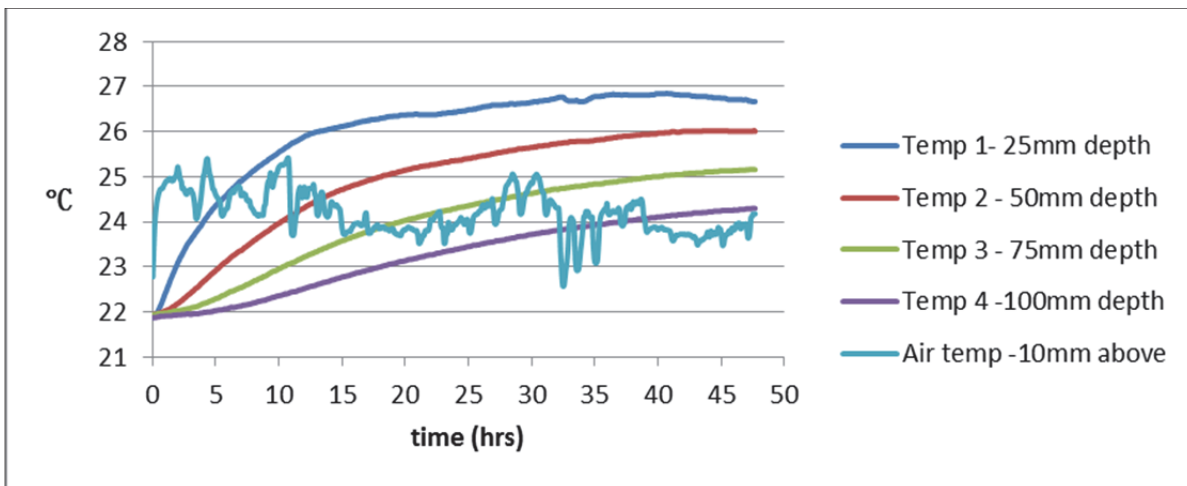


Figure 5.19: The temperature stratification during the experiment with reduced radiation.

The ambient temperature of the room on the air above the container had a range between 24°C and 25°C. In contrast to the previous experiments (Figure 5.6 and 5.12), the ambient (air temp) temperature fluctuated more vigorously (Air temp) in Figure 5.19. This fluctuation coincides with the temperature of the sensor at 25 mm depth in the water (Temp1 in Figure 5.18). The ambient temperature had a major effect on the energy input from the radiation source. The dissipation of the energy was reduced as the depth of the water increases. The highest temperature was significantly lower in relation to previous experiments in Figure 5.6 and 5.12.

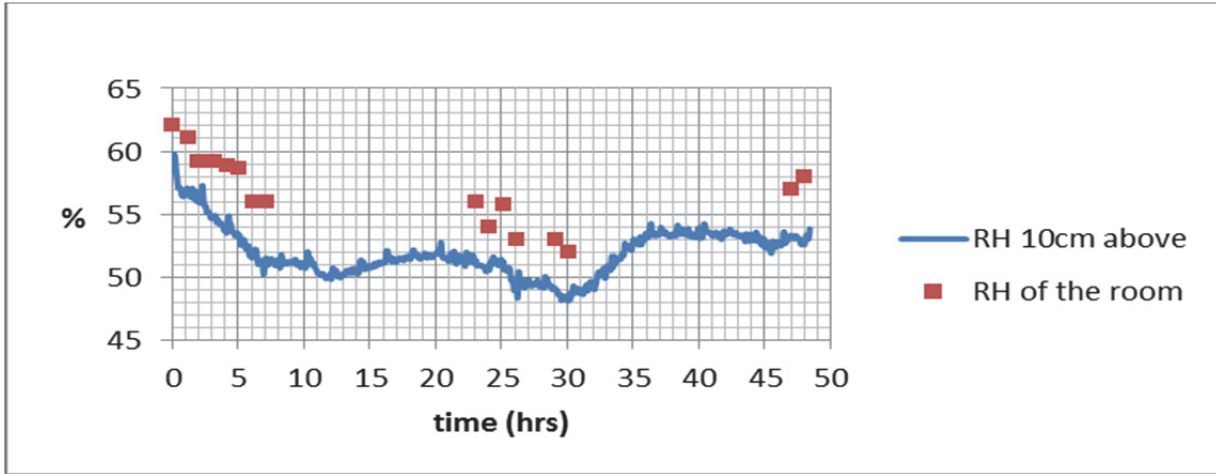


Figure 5.20: The relative humidity during the reduced radiation.

The humidity above the water surface of the container (Figure 5.20) had a range between 47 and 60%. The humidity of the room was higher than the humidity of the air above the container. This was the same effect the IR bulbs had on the humidity above the container as discussed earlier (Figure 5.15 and 5.16).

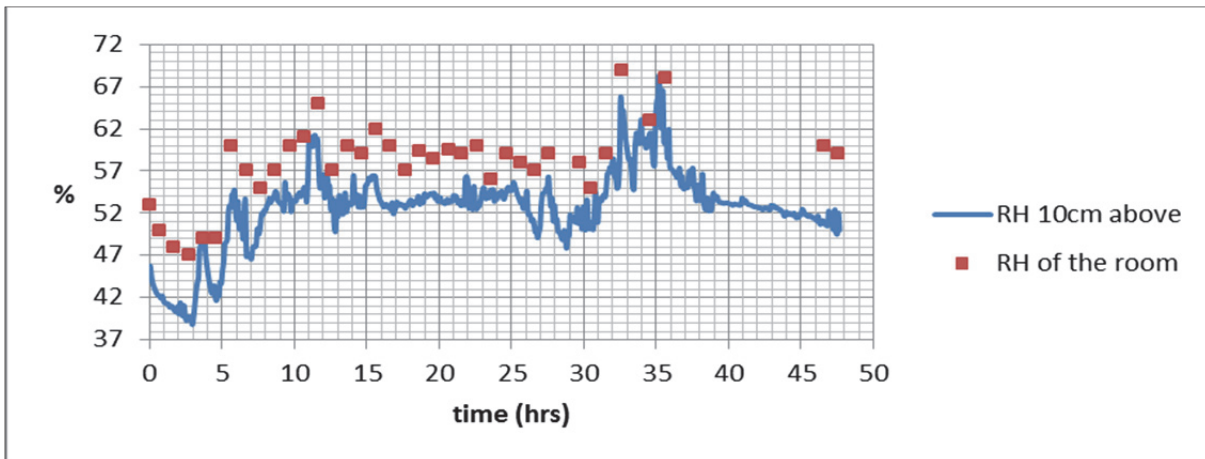


Figure 5.21: The relative humidity after the reduction in radiation input

The humidity starting point in Figure 5.21 was much lower than anticipated despite the increase in the temperature of the water and the room. The humidity sensor recorded a steady climb after 10 h. The reading was steady in the 50% range for another 15 h. The peak range between 32 to 36 hours of the experiment correlated with the temperature graph in Figure 5.19. It had a sudden reduction in the ambient temperature and surface temperature for the same period.

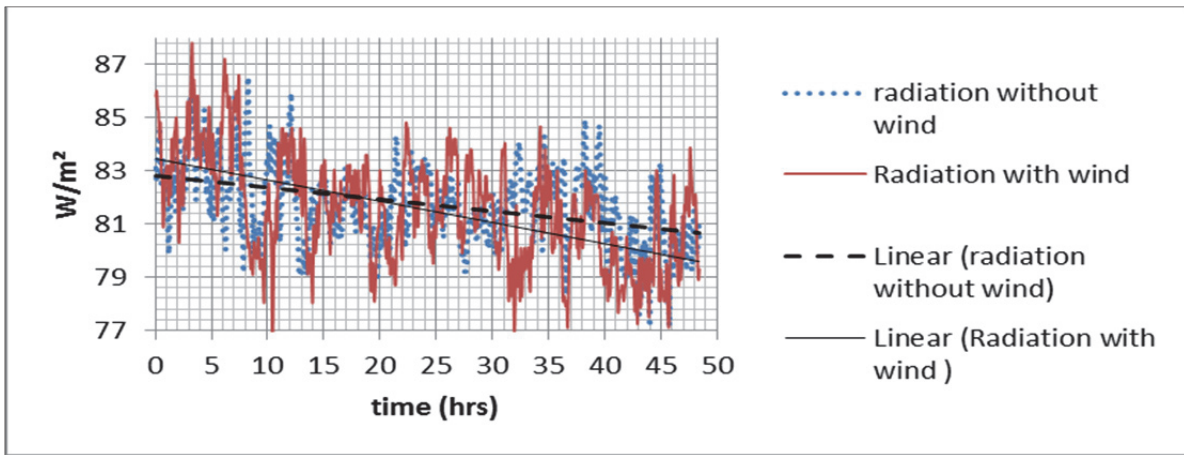


Figure 5.22: The radiation over a 48 hour period without wind when the radiation was reduced from 250 Watts to 175 Watts.

The radiation graph without the wind (Figure 5.22) showed a steady decline over the 48 hours of the experimental period. The graph had a linear representation which was illustrated by the trend line in Figure 5.22. This was linked to a steady decline in the water volume of the experiment. With a range of approximately 10 Watts in decline it was a direct result of the low volumes being evaporated as the radiation sensor was physically mounted on a floating system that fluctuated with the water level. A very similar pattern occurred for the experiment which was wind aided (radiation with wind). Furthermore, this was confirmed with the evaporation losses for both the experiments (Figure 5.23).

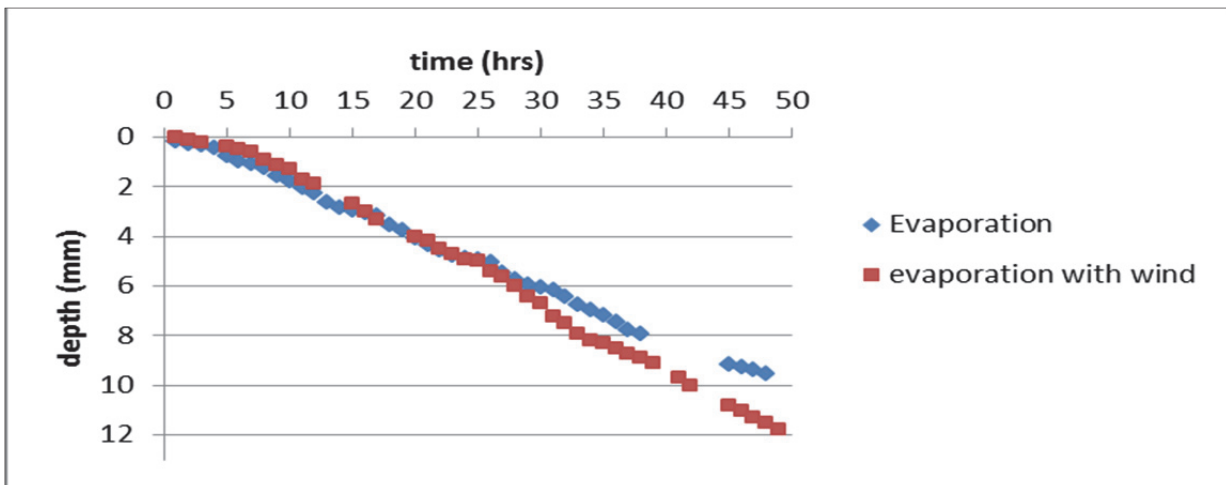


Figure 5.23: The experiments with and without the wind assistance with reduced radiation.

In Figure 5.23, both the curves showed reduction in water level decrease as a result of the input energy from the IR bulbs. The difference in evaporation rate between the two experiments cannot be clearly distinguished before 30 hours at which point there was a clear separation between the two trend lines. The inclusion of the wind was highly effective in this experiment when the radiation energy was previously at 250 Watts. The two curves in Figure 5.23 separated after about 25 hours as an indication that the evaporation rates changed. In the previous experiments (Figure 5.10), the radiation from the IR bulbs had a greater effect on the evaporation rate. In the experiment without the wind the total loss of the water volume was 2.7 litres. The

wind increased this volume by 18% as it played a greater role in the experiment. The reduction in the energy input reduced the volume by 67% compared to the initial experiment in Figure 5.14.

5.2.4.4 Discussion

The rate of evaporation can be quite complex to predict as it is caused by a number of variables. It was evident that the applied factors such as wind, humidity and temperature can each have a substantial impact upon the water being evaporated from the container. The air above a free standing water body has a direct effect on the evaporation rate along with the surface area, when subjected to moving air. The rate at which the saturated air is being replaced, governs the rate at which water is transformed to vapour. There is substantial evidence that the constant wind generated at 2 m/s increased the evaporation rate by more than 10% as shown in Table 5.1. The saturated pockets of air in the boundary layer above the water surface were being replaced at a higher frequency when the wind currents were applied. The humidity graphs illustrated more aggressive peaks when the wind element was added. The humidity in general was quite unpredictable under these experiments. With minor variations in the ambient temperature one can expect the humidity to fluctuate as well. There was a relationship between the ambient temperature and the peak temperatures of the experiments. The ambient temperature of the room was not constant and the operating temperature range was between 17-25°C. This affected the peak temperatures. The effective optimum temperature occurred after 5 hours for the first experiment as temperatures were raised and the evaporation process accelerated.

Table 5.1: Volume losses for all the experiments over a 48 hour period

Experiments over 48hrs	Radiation energy input (Watts)	Initial radiation at water surface (Watts)	Height from energy source (m)	Vol. loss estimated by evaporation (cm³)	Vol. loss with wind assistance (cm³)	Vol. Loss increase with wind assistance (%)
Maximum input	250Watts x2	450Watts/ m ²	100 mm	9045	10401	15%
Distance increased	250Watts x2	350Watts/ m ²	200 mm	7585	8722	12%
With reduction in energy input and distance increased	175Watts x2	88Watts/ m ²	400 mm	2985	3672	23%

The humidity of the room appeared to have no constant range. Although the supply range was set at 60%, the control of humidity had a working range of 35-75%. The temperature was indirectly proportional to the humidity. With the increase in temperature, the humidity decreased. The humidity of the room was slightly higher than the humidity near the container when the IR lights were switched on. The heat generated by the bulbs affected the reading of the humidity sensor where the humidity was lower in comparison to the room.

A reduction in the evaporation rate (Table 5.1) was observed in the case where the distance between the energy source and the water surface was increased. This reduced the intensity of the IR bulbs which also reduced the total volume of water being evaporated. The distance between the lights and the water potentially caused the variations but it was mainly affected by the temperature and the humidity of the room. During the experiments it was suspected that the vapour from the water being evaporated might affect the humidity of the room as the evaporated water becomes part of the room's moisture content. The wind had played an important part in these experiments while the temperature governed the degree of wind impact in terms of the effectiveness for most of the experiments.

The wind had a greater impact when the water temperatures were higher than the ambient temperatures in terms of the water volume loss from the container. The initial role of the wind was to remove the saturated air where it enhances the process of changing water to vapour. With the reduction in the radiation the wind had a greater impact when the energy input was reduced by changing the IR bulbs. The wind speed was probably not effective enough to be regarded as the sole contributor to increase the evaporation rate by a larger margin.

Finally the depth of stratification in temperatures illustrated the energy dissipation, which demonstrated the delay in energy transfer from the water surface to the deepest part of the water. The total distance between the first temperature sensor and the last sensor was 75 mm. The delay in the temperature was visible in Figure 5.8 when the surface temperature sensor (Temp 1) recorded a temperature of 21°C within 2.5 hours while (Temp 4) recorded the same temperature approximately 17.6 hours later. The humidity closer to the tank did not increase as expected during the experiment. In reality the evaporation of water raises the relative humidity above the water surface. From another perspective the humidity sensor could have been mounted closer to the water surface. Most of the experimental conditions applied have far exceeded the normal evaporation rate for what is physically possible in the real world. The experiment with the lower radiation input (Figure 5.23) was within range with a total 9.4 mm level drop (without wind) over a 48 hour period. Based on the annual evaporation data for the Witbank area this particular experiment was within range. In the real world, the variations with regard to the applied parameters might have a greater range. To improve the data simulation, day and night simulation of the water temperature would have provided a better estimate to express the evaporation rate as mm per day.

5.2.5 Effect of climatic parameters on water and NaCl solution

5.2.5.1 Temperature of the NaCl solution and H₂O at different depths

Figures 5.24 and 5.25 below show the temperatures of the NaCl solution or distilled water at different depths down the evaporation pans. This experiment was designed to give an insight into the possible change in the temperature of the solutions in the evaporation pan at different depths, and also to understand the difference in the internal temperature of water vs the NaCl solution compared to water over time.

The results of the evaporation experiments in Figures 5.24 and 5.25 showed that the temperature of the surface of the NaCl solution was about a degree higher (27 °C) after 20-40 hr than the distilled water (~26 °C). The temperature of the solutions was observed to decrease with an increase in the depth of the solutions but over time the deeper layers increased in temperature. These differences were attributed to the thermal heating capacity of the salt solution compared to the water as well as to the progressive transfer of heat to the deeper layers over time.

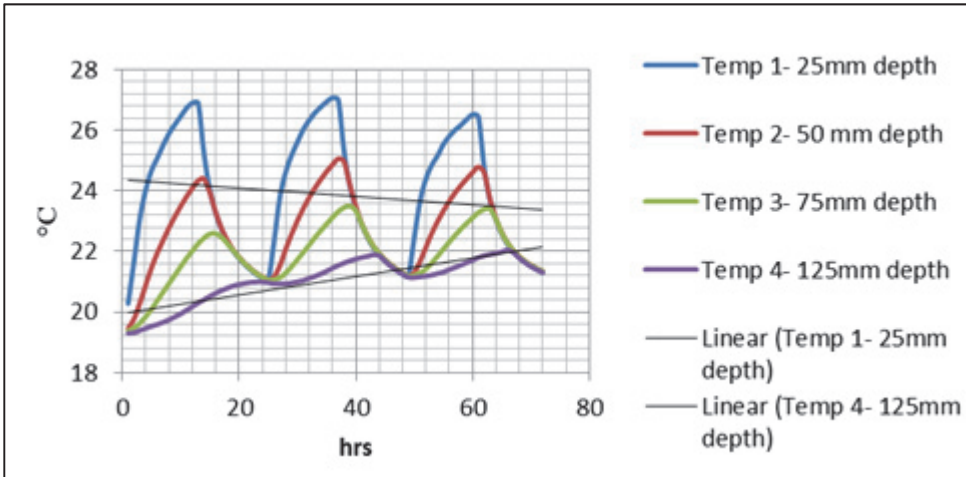


Figure 5.24: The temperature of the NaCl brine at various depths over time

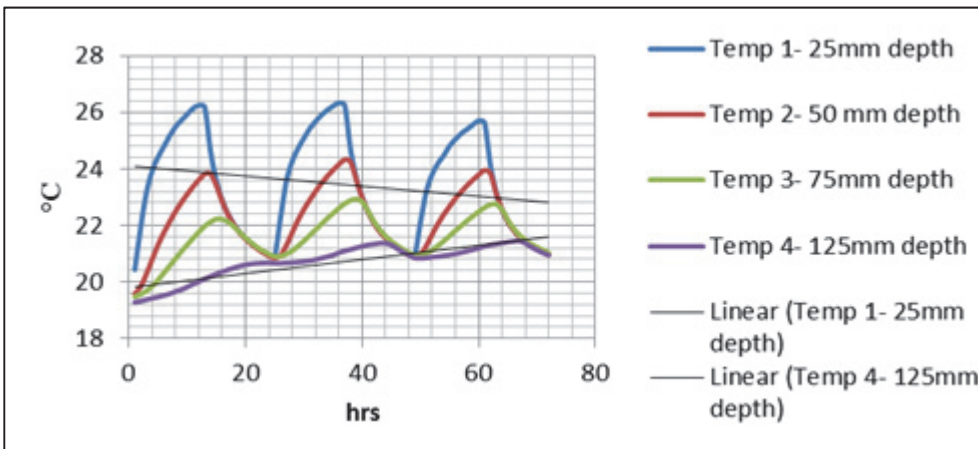


Figure 5.25: The temperature of the distilled water at various depths over time

The two containers had similar water depths when the experiment started. Both graphs have very similar patterns (Figures 5.24 and 5.25). The temperature at 25 mm within the NaCl solution was slightly higher than that of the water with similar depth. A similar trend was observed for the temperature of the NaCl and water at 50 and 75 mm depth, as the temperatures of the NaCl solution at these depths were higher than those of the distilled water. The temperature of the NaCl and the distilled water at 125 mm depth was almost the same. The difference in the temperature of the NaCl solution and the distilled water show that the solute in the NaCl solution could increase the temperature of the solution. This in turn could indicate that the solute in the solution could lead to an increased rate of evaporation of the solution. The NaCl in Figure 5.24 consistently had 0.5-1.0°C higher temperatures than the water as shown in Figure 5.25. Over the 72 hours of the experiment, the sensors close to the surface had shown a gradual decrease in the temperature, while the

lower sensors at 125 mm (Figures 5.24 and 5.25) showed a steady increase in the temperature. As the water and the NaCl solution evaporated during the experiment, the distance between the Infra-red (IR) lamps and the liquid surface increased. This subsequently relates to the temperature close to the surface of the water and the NaCl solution decreasing. With the sensors situated at the deepest part of the NaCl solution and the water containers, the temperature had a reverse effect in comparison to the sensors close to the surface. During the experiment the brine and the water temperatures of the deepest part had shown a gradual increase in temperature. This was the result of the efficient heat storage of the insulated containers along with the energy input during each cycle.

5.2.5.2 Humidity and surface temperature of the NaCl solution and H₂O

The humidity and the surface temperature for both the containers were recorded by humidity and temperature sensors, 10 cm above the containers. Note the differences in the temperature scale bars between Figures 5.26 and 5.27.

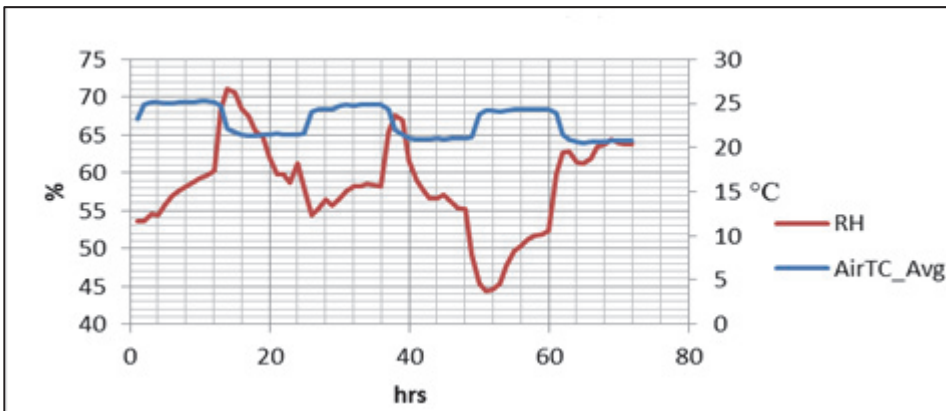


Figure 5.26: The relative humidity and air temperature fluctuations of the NaCl.

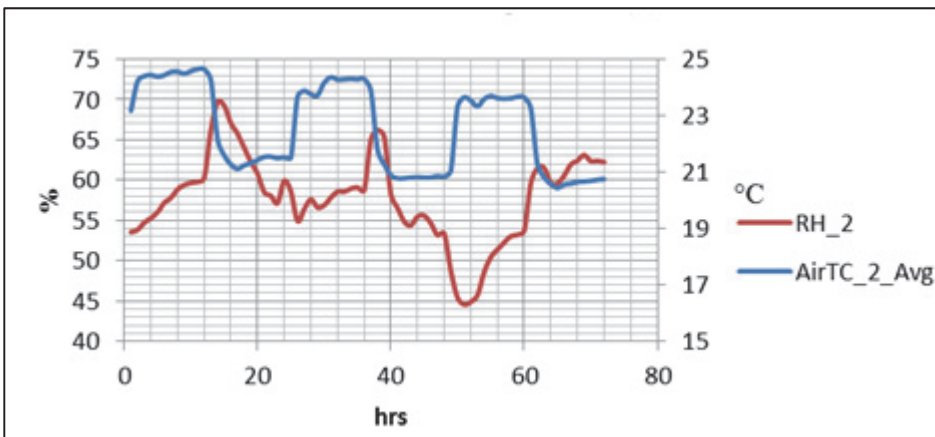


Figure 5.27: The relative humidity and air temperature variation of the distilled water container.

With each 12 hour cycle of the experiment, the temperature rose by 2°C and decreased again. On the whole an air temperature fluctuation ranging between 21.0 and 24.8°C was recorded 10 cm above the water container over the 72 h duration of the experiment with a decreasing trend. The humidity in both the graphs (Figures 5.26 and 5.27) did increase briefly by about 10% when the IR lamps were switched off after each

12 h daylight cycle, but even a fairly large decrease in relative humidity did not affect the temperature above the containers significantly.

5.2.5.3 Comparison of the evaporation rate of NaCl solution and distilled water

The evaporation rate of the NaCl solution compared to the distilled water was calculated by recording the volume lost during each experiment. A pressure transducer was placed at the bottom of each of the two containers to determine the evaporation rate. The distilled water and the NaCl had the same volume to start with, of 115 L, although the density of the brine was higher than the distilled water. This however equates to the brine volume appearing as a greater volume because of the greater pressure exerted on the pressure transducer.

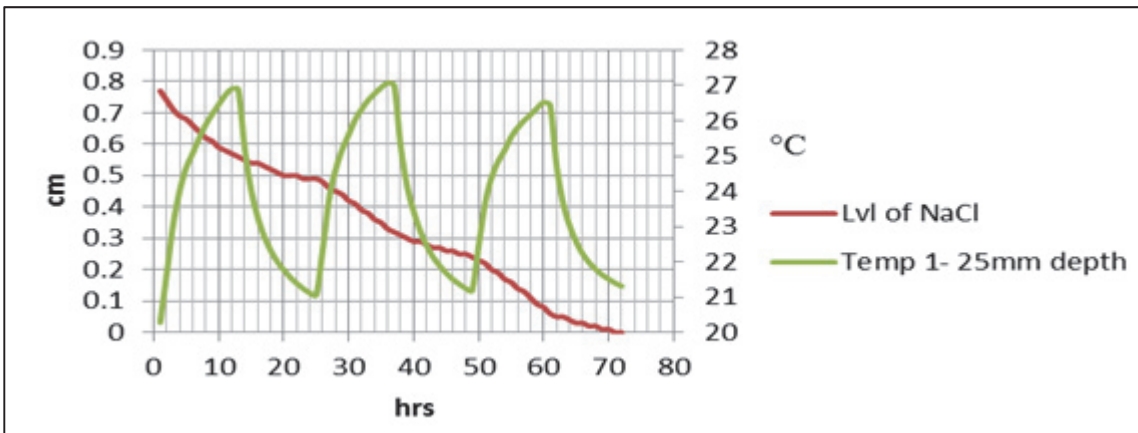


Figure 5.28: The variation in the surface temperature and the changes in the volume of the NaCl brine solution; Lvl = level

The temperature of the brine close to the surface (about 25 mm) and the rate of evaporation are shown as trend lines in Figure 5.28. During each 12 hour cycle the brine temperature rose by more than 4°C. This enhanced the evaporation rate. The total volume loss over the 72 hour period from the brine container was 1.875 litres.

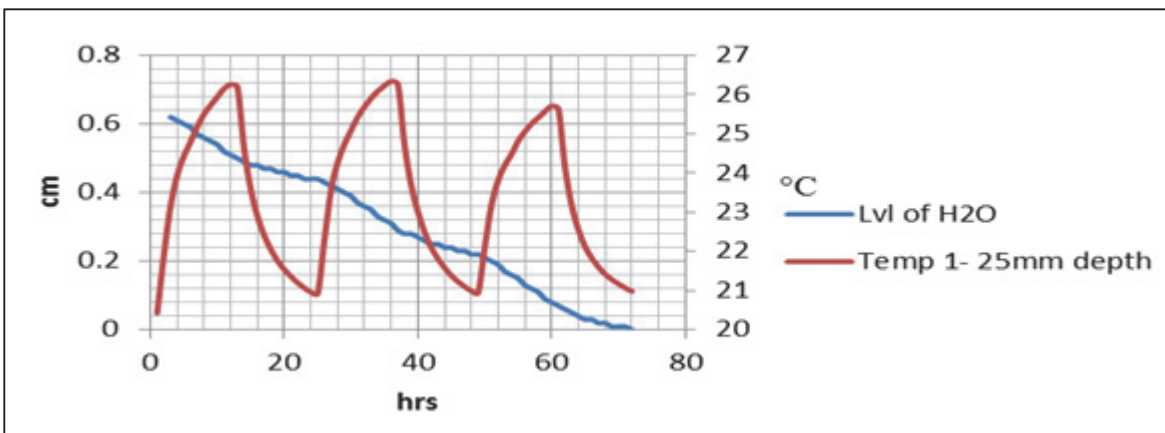


Figure 5.29: The variation in the surface temperature and the changes in the volume of the distilled water

The trends shown in Figure 5.29 resembled those of the brine container. The experiment had the same 12 hour cycle which resulted in the fluctuation of the evaporation rate. The total volume which evaporated from the distilled water container over the 72 h period was 1.6 litres, confirming that the evaporation over the brine solution (1.875 litres) was greater than that achieved over the water solution. The difference appears to be mainly due to the greater heat transfer into the brine solution over time.

Several further experiments were conducted as the previous experiments had some anomalies. To address these, the wiring of the pilot plant was rechecked for defects and rewired. Furthermore, the output energy from the IR lamps for both the systems was the same after testing. The evaporation rates for both containers were lower than previous experiments. The previous experiments had a greater volume loss for the same period without day and night simulation. With the exposure of the brine and water to the IR lamps with day and night simulation, the brine volume was reduced to half and resulted in less water being evaporated. The extractor fan which removes the saturated air from the room was switched off and could have played a major role in the lower evaporation rates. It was also expected that the distilled water would have a greater volume loss than that NaCl brine. The angle of the IR lamps was adjusted to synchronise the energy (in Watts) output for both containers.

5.2.5.4 *Effect of wind on the loss of water*

The experimental setup was modified to provide an airflow which is consistent with the same height above the water as well as NaCl brine surface. The wind was generated using a fan and funnelled through a heliflex pipe which was connected to a solid 40 mm PVC pipe. Evenly spaced holes were drilled into the PVC pipe (8 mm) to provide an even distribution of air flow over the water or brine surface. The wind was generated by an electric fan with a speed controller to simulate the wind speeds of an actual site (2 m/s). The wind was generated at a constant height above the water surface (approximately 15 mm). This ensured the wind effect was constant over the water and brine surface of the experiment even if the water or brine evaporates. A total of 3 cycles was completed where the two systems were subjected to 12 hours of day and 12 hours night by exposing the containers to IR-lamps in 12 hour cycles.

Figure 5.30 shows the level change of the systems. A total volume of 2.48 litres was evaporated for the water while 2.57 litres was lost in the case of the NaCl brine. This result provides some evidence that the density of the solution might affect the evaporation rate (Al Shammiri, 2002).

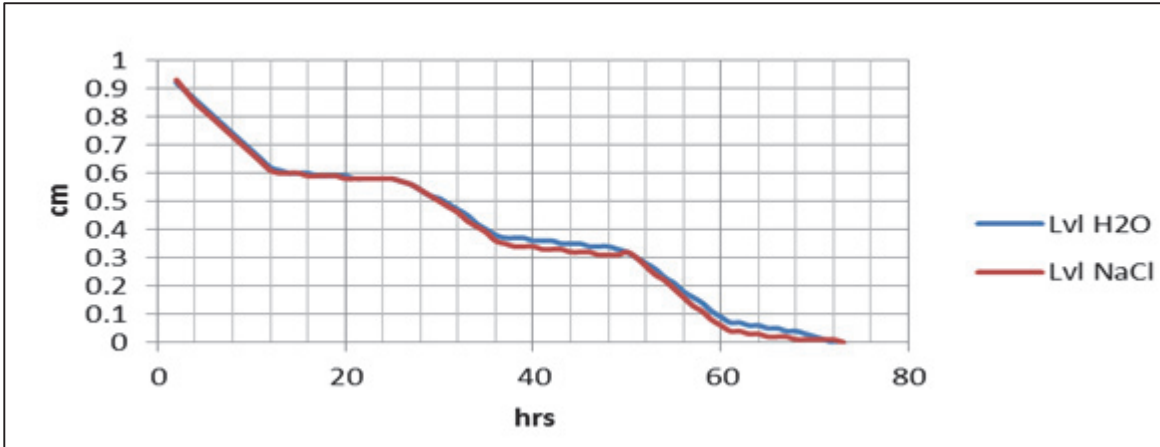


Figure 5.30: The change in the volume levels of both the distilled water and the NaCl over time under a windy condition.

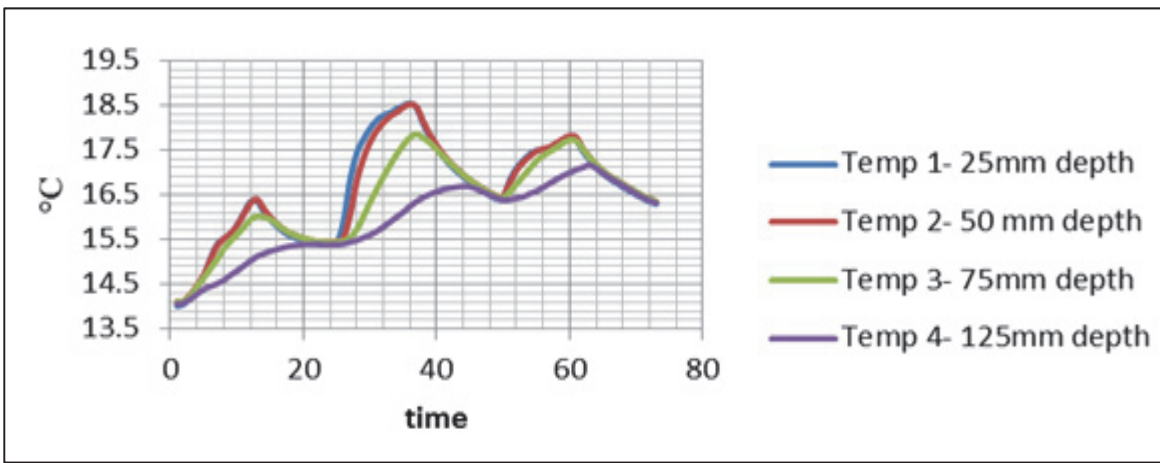


Figure 5.31: The temperatures at different depths of the NaCl brine with the wind blowing over the surface area at 2m/s.

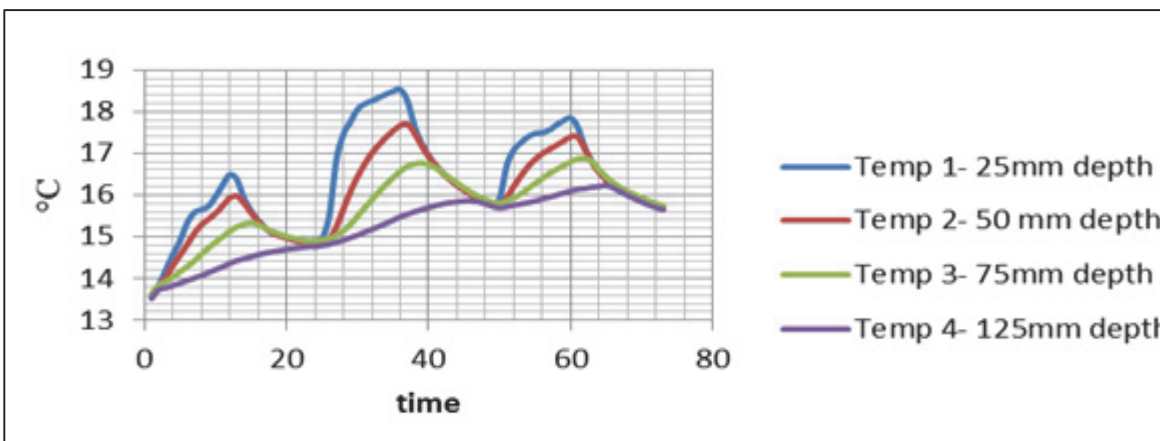


Figure 5.32: The temperatures at various depths of the water with the wind blowing over the surface area at 2 m/s.

The results of the systems shown in Figures 5.30 and 5.31 had greater variations in the temperature trends compared to the results shown in Figures 5.24 and 5.25. The temperature of both systems showed a decrease in the maximum temperatures. The system evidently took more than 30 hours to reach the

maximum surface temperature whereas without the wind factor both tanks had reached their maximum at the surface after 12 hours. Moreover the temperature of the surface layer was nearly 8°C lower overall with than without the wind factor. The differences were not so pronounced in the deeper layers but these layers were approximately 5°C cooler in the wind exposed tanks than in the case of the experiments done without the wind factor. Hence, a wind factor is expected to delay the evaporation rather than enhance the evaporation rate due to its effect upon the thermal transfer of heat into the pond. The decreases in the water levels are shown in Figures 5.33 and 5.34.

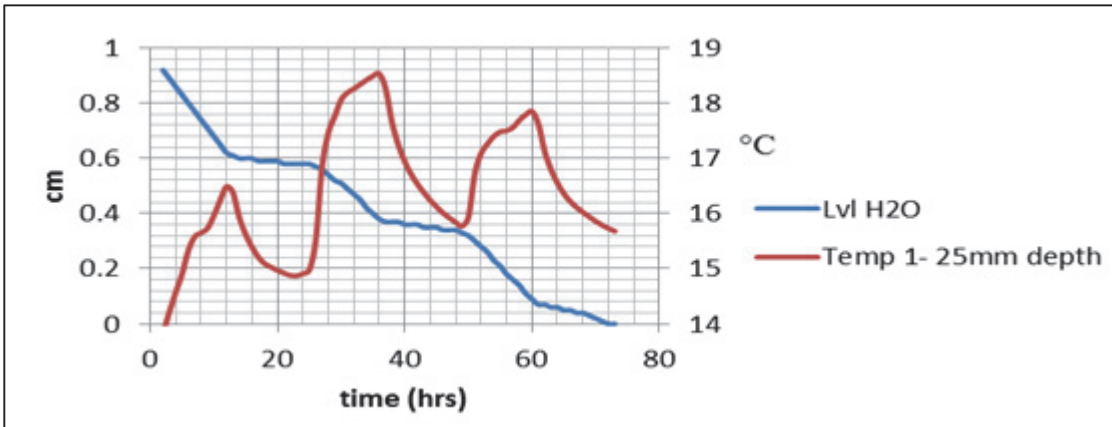


Figure 5.33: The evaporation of the water with the 2 m/s wind factor affecting changes in the surface temperature.

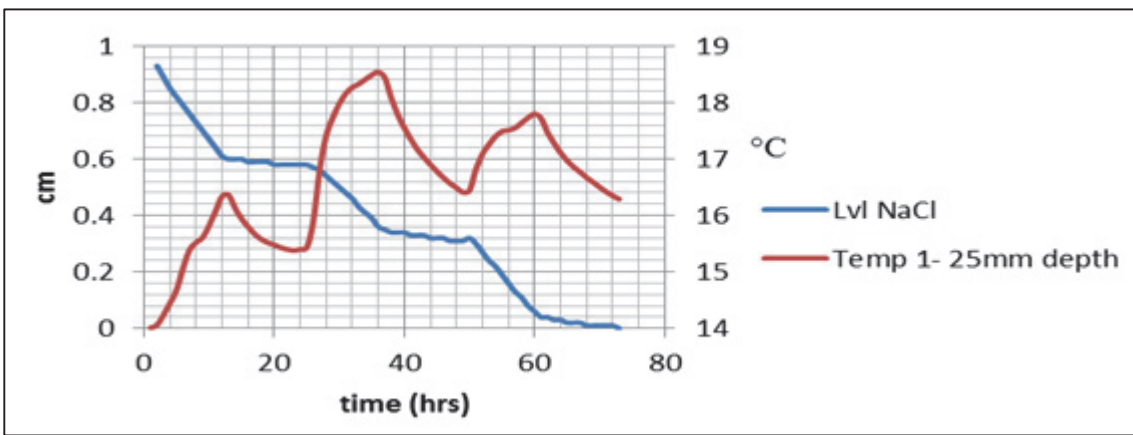


Figure 5.34: The evaporation of the NaCl brine with the 2 m/s wind factor affecting changes in the surface temperature.

The effect of the 12 h thermal cycle increase of the surface temperature was evident in both systems (Figures 5.33 and 5.34). The water container was observed to have a lower temperature after each 12 hour cycle than the NaCl solution under the same environmental conditions with the wind factor and overall the evaporation rate over the NaCl solution was again greater than that over the water filled container. Since the wind factor was similar in both cases, the difference is again ascribed to the capacity of the NaCl to absorb the radiative heat more effectively than water on its own despite the wind chill factor incorporated. However, the input energy from the IR lamps with the wind experiments was lower than the experiments without the wind. An average of 20 Watts in energy input was the difference between the experiments with and without wind.

5.3 EMPIRICAL AND THEORETICAL MODELLING OF INDUSTRIAL BRINE SYSTEMS

This section presents the empirical models developed to determine evaporation processes of industrial brines under controlled laboratory conditions

Modelling is regarded as a vital tool to expose geochemical processes, analyse laboratory experiments and use as a mechanism to predict unfolding events and monitoring plans for future. Geochemical modelling remains a tool to predict the chemical interaction of species in the brine solution. However, the calculation for brine solution requires a different approach from the conventional Penman method (Akridge, 2008). Oroud (1999 and 2000) developed an energy balance model for hyper-saline solutions like the Dead Sea, this model was more appropriate for this study as it incorporates the salinity aspect. The model was derived from the Penman equation.

5.3.1 Model description

$$E = \frac{\beta\Delta H}{\beta\Delta + \psi} + \psi f(u) \frac{\beta e_a^* - e_a}{\beta\Delta + \psi} \quad (20)$$

Where $\beta\Delta$ is referred as the change in the activity coefficient, H is the energy input, ψ is the psychrometric constant, $f(u)$ is the wind speed. e_a^* is the saturated air above the brine and e_a is the vapour pressure of the room.

Relationship with activity coefficient

$$\bar{V}E_i = RT \frac{\partial(\ln(\gamma_i))}{\partial P} \quad (21)$$

Calder and Neal

The conventional Penman (1948) and the Furguson (1952) equation (equation 22) was designed to calculate the evaporation over an open water surface. The equation incorporates the energy budget as well as the thermodynamics method of an environment to account for the loss of evaporation. The equation was tested on the hydrology of the Dead Sea as a case study. Penman (1948) and Furguson (1945) incorporated four meteorological variables in the initial equation to determine the evaporation loss, this include the wind speed, humidity, air temperature and net radiation (Calder, 1984).

$$E = \frac{\Delta}{\Delta + \gamma} Rn + \frac{\gamma}{\Delta + \gamma} f(u)(e_s - e) \quad (22)$$

The method was deemed insignificant to quantify the evaporation rate for saline lakes. The Penman method required an interactive approach and the Furguson a graphical solution to determine the evaporation rate of the saline lake (Calder, 1984; Bonython, 1965). According to Habeck (1955), the effect the temperature had

on the coefficient was rather trivial for seawater at 35% salinity. A temperature range between 10 and 35°C only produced a difference of less than 1% for seawater.

$$E = \frac{H + \rho C_p \frac{e_s(T_a) - e/a}{r}}{\lambda \left(\frac{de_s}{dT_a} + \frac{\gamma p}{a} \right)} \quad (23)$$

Pitzer

$$\frac{G^{ex}}{n_w RT} = f(u) + \sum_i \sum_j \lambda_{ij}(u) M_i M_j + \sum_i \sum_j \sum_k \delta_{ijk} M_i M_j M_k \quad (24)$$

Where G^{ex} is the free Gibbs energy that is available as per 1 kg of solution, M is the molality of the ions, $f(u)$ is the Debye-Hückel, λ is dependent on the ionic strength of the species. δ_{ijk} is referred to as the respective third vital coefficient while λ_{ij} is the second within the species (Sandler.S, 1989).

5.3.2 Activity Coefficient

The activity coefficient is referred to as a thermodynamic notion for liquid mixtures which is governed by temperature, pressure and composition (Sandler, 1989). The activity coefficient is related to what extent a system deviates from the actual system. The activity coefficient is regarded as a limit of an equation derived for an activity which is a factor with no units. It has been suggested that the activity coefficient plays a significant role in the temperature, radiation and evaporation of saline solutions which subsequently affects the boundary layer (Oroud, 1999).

5.3.3 Model selection

A large number of models exist and it is rather important to validate the appropriate model based on the assumptions when the model was developed (Crawford, 1999). The activity coefficient of the Emalaheni brine is a multi-component electrolyte solution which may not be easily determined. The Pitzer model is highly used and recommended to determine the activity of mixed brines (Krumgalz, 1997; Harvie, 1984). The ratio for combining different species in a multicomponent electrolyte is greater than isolated ions. Hence is more convenient to calculate as a collective for all the ions (Krumgalz, 1997). With the aid of database model Pitzer and PhreeqC, geochemical modelling software was used to determine the speciation of the Emalaheni brine. The solubility of the major ions played a significant role as the individual ions had different solubility characteristics. The major ions been investigated were Mg^{2+} , Na^+ , K^+ , Ca^+ , Cl^- , SO_4^{2-} , NO_3^- .

5.3.4 Brine analysis

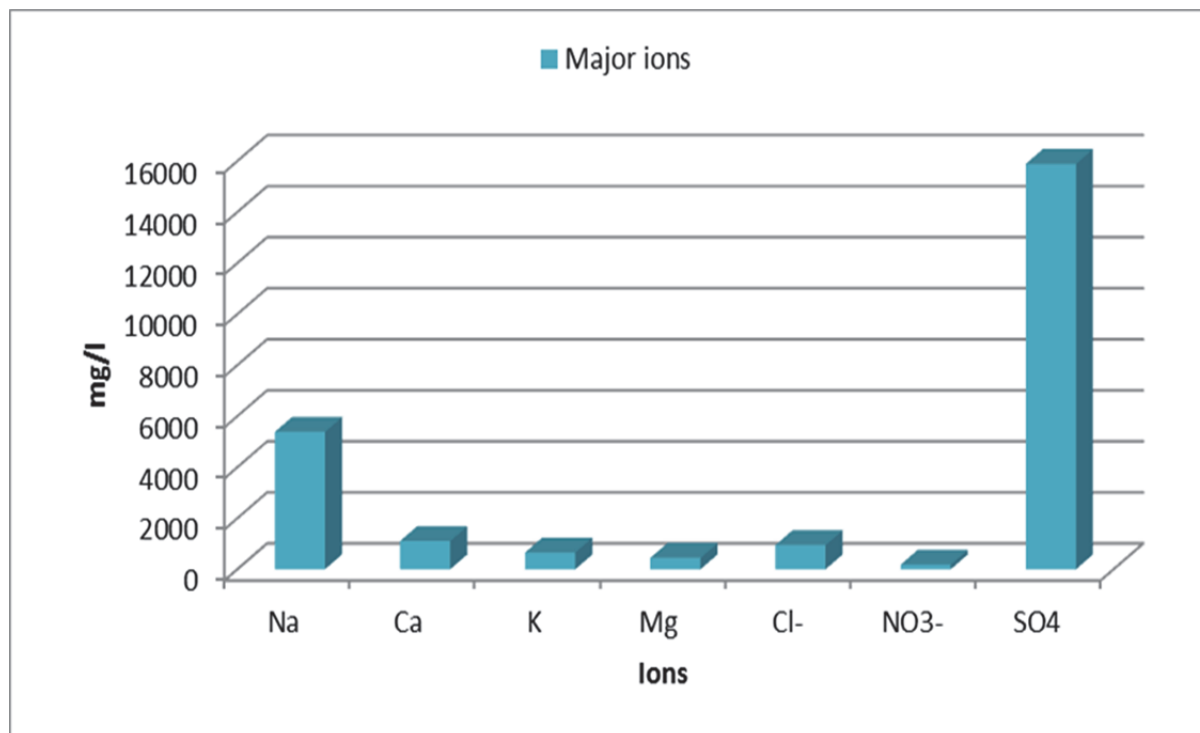


Figure 5.35: The major ions of the Emalaheni brine which was analysed in 2013 using an Inductive Coupled Plasma with a mass spectrometer.

The brine from Emalaheni was analysed and the results (Figure 5.35) showed that the concentrations of Na and SO_4 in the brine were high indicating that the brine is mainly Na_2SO_4 brine. The brine was closer to basic at a pH of 7.23. The initial pH of the water was predominantly acidic due to the generation of sulphuric acid as a result of oxidation of pyrite (Bell, 2001). However, the use of chemical such as a lime by the treatment plant raised the pH level (Du plessis, 2006). Apart from the pH of the brine, the chemical composition of the brine has a significant effect on the evaporation rate of the brine. It is important to develop a model to predict evaporation rates of brine considering the solute effects and the associated changes in the chemical composition when the water mole fraction decreases.

5.3.5 Emalahleni brine comparison

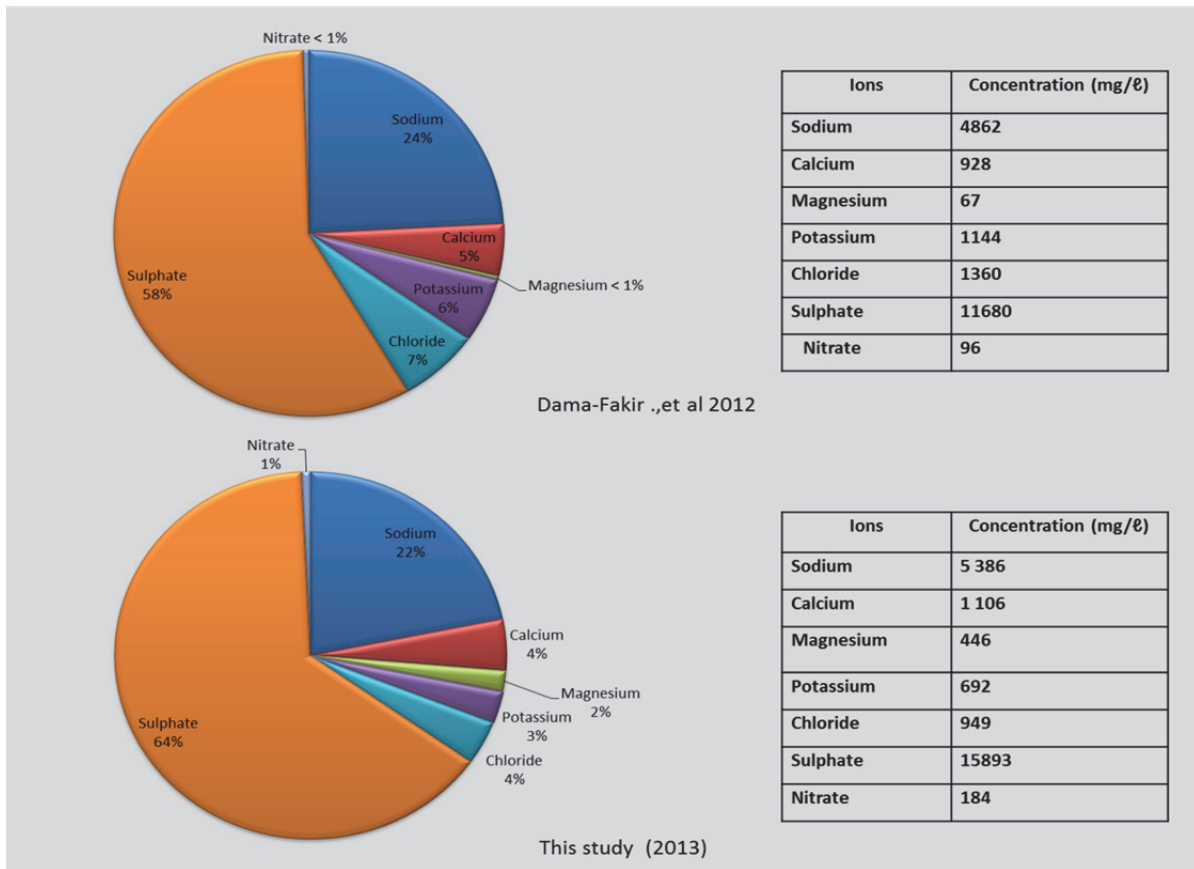


Figure 5.36: The analysis of Emalahleni brine based on the previous and the current study.

The analysis of the brine in both charts indicated that the Emalahleni brine is Na₂SO₄ brine. The comparison of the pie charts in Figure 5.36 shows that Emalahleni brine composition changed slightly over the last few years. The brine analysis by (Dama-Fakir, 2012) was presumably analysed in 2010 while the current study analysed the brine in 2013. In the current study, the brine composition showed a slight change, in particular an increase in sodium and a decrease in sulphate. Other notable change is the increase in the concentration of magnesium. The 6% sulphate increase and 2% decrease in sodium is likely to improve the evaporation rate, since calcium sulphate is suspected to be the first salt to precipitate out in the sequence of crystallization. A speciation analysis using PhreeqC suggested that the ionic strength of the (Dama-Fakir, 2012) brine is lower than that of the study done in 2013. This trivial change of the brine composition could have a greater impact over a longer period.

The analysis of brine using PhreeqC indicated a trivial change in certain parameters, in particular the ionic strength of the brine solutions. The previous study by Dama-Fakir was poised slightly towards a cation side while this study shown a balance towards the anion. This study has a marginal higher ionic strength than the brine solution from the Dama-Fakir study. The analysis of the brines suggested a small change in the composition and a very similar ionic strength which relates to a very similar evaporation rate under equivalent environmental conditions.

Table 5.2. The output file of the Emalahleni brine in PhreeqC

Parameter	This study	Dama-Fakir
pH	7.32	7
pe	4	4
Specific Conductance ($\mu\text{S}/\text{cm}, 25^\circ\text{C}$)	23656	21566
Density (g/cm^3)	1.01979	1.01506
Volume (L)	1.00604	1.00585
Activity of water	0.992	0.993
Ionic strength	4.19E-01	3.466e-01
Mass of water (kg)	1.00E+00	1.00E+00
Total carbon (mol/kg)	7.00E-03	7.50E+00
Total CO ₂ (mol/kg)	7.00E-03	7.50E+00
Temperature ($^\circ\text{C}$)	25	25
Electrical balance (eq)	-1.25E-02	3.05E+00
Percentage error 100*(Cat)	-2.2	0.62
Interactions	7	8
Total H	1.11E+02	1.110190e+
Total O	5.62E+01	5.602906e+

5.3.6 Model validation

In the following results (Figure 5.37) the change in Emalahleni brine levels over time under natural convection are compared with a control experiment.

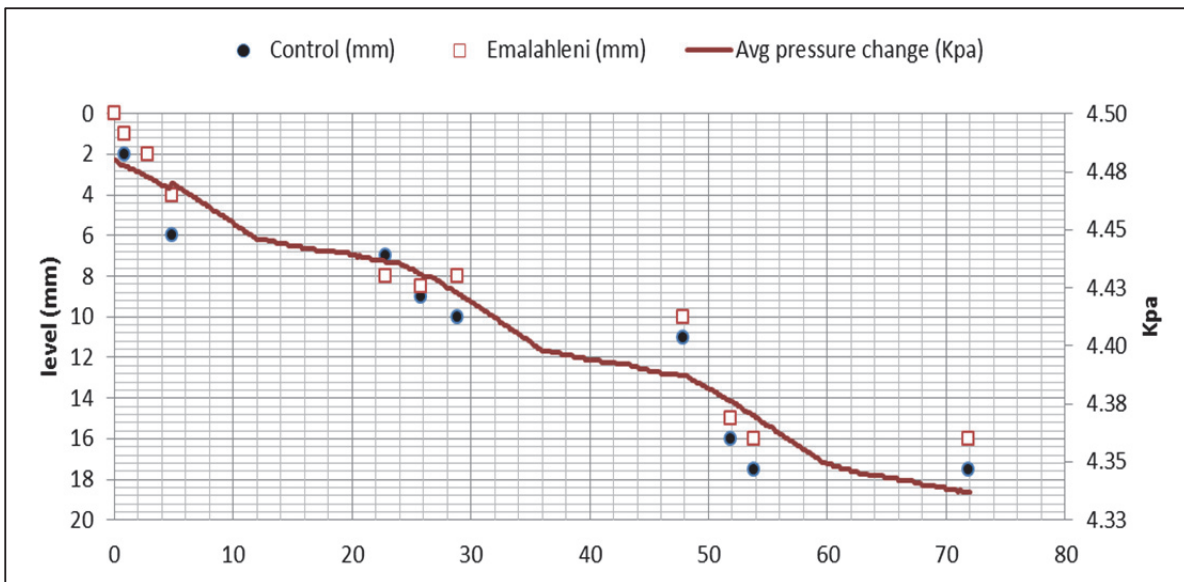


Figure 5.37: The change in brine levels over time of the Emalahleni brine under natural convection.

The overall graph (Figure 5.37) of the experiment appeared to be linear but under finer scrutiny subtle changes resonated with the energy input into the system. The pressure change suggests that the first 12

hours was relatively linear during the period when the Infrared lights were scheduled to be on. The first elapsed 5 hours, indicated that the control pond had exceeded the Emalahleni brine pond by 2 mm in water level changes. Over the experimental period of 72 hours, the difference between the water level of the control and the brine was less than 2 mm with the control experiment having the greater change.

The change in temperature at specific depths during the Emalahleni brine experiments under natural convection is shown in Figure 5.38.

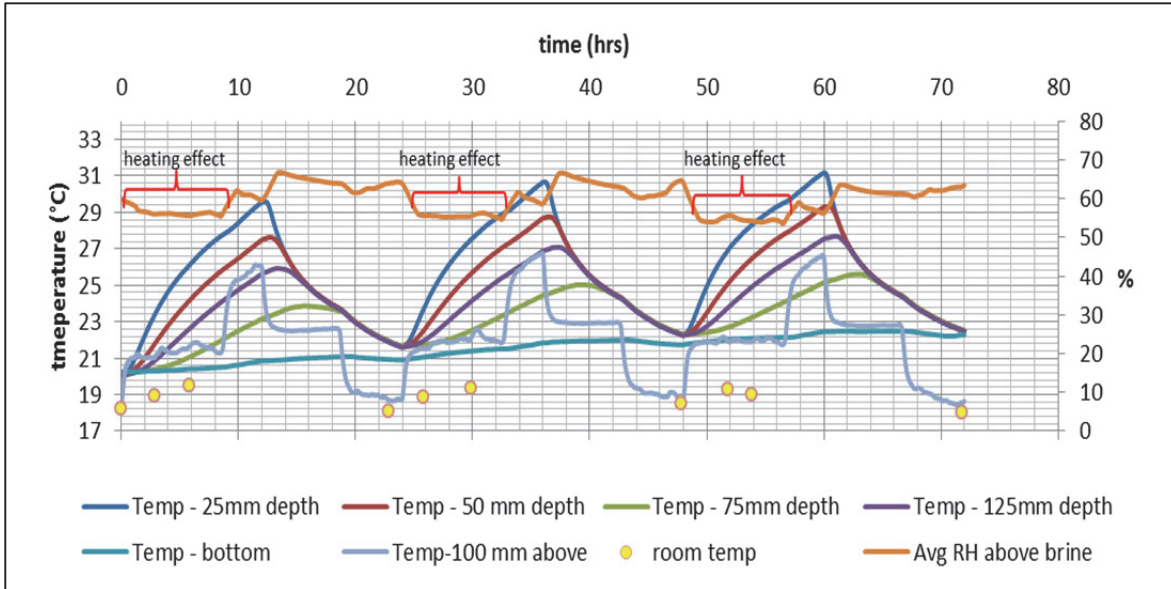


Figure 5.38: The change in temperature at specific depths during the Emalahleni brine experiments under natural convection.

The temperature stratification of the pilot plant (Figure 5.38) demonstrated the effect of the IR lamps on the system. As the energy penetrated the brine, it dissipated with depth. As shown in Figure 5.38, the bottom sensor recorded the lowest temperature while the sensor near the brine surface recorded the greater temperature. The initial impact on the humidity by the IR lamps as shown in the graph indicates the heating effect generated by the lamps. The humidity was being suppressed by nearly 5% due to the heating effect.

The level change of the Emalahleni brine under forced convection is shown in Figure 5.39 and Figure 5.40 shows the temperature stratification under forced convection.

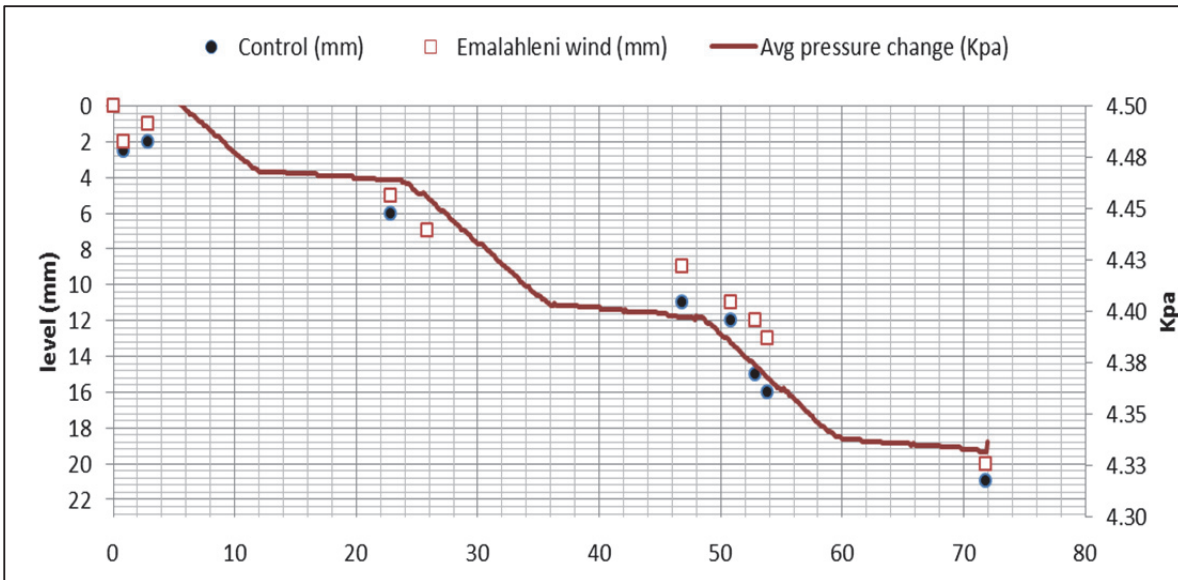


Figure 5.39: The level change of the Emalahleni brine under forced convection

A greater angle in the first 12 hour (Figure 5.39) indicates the influence of the wind on the system as a greater volume loss was achieved during the same period under natural convection. A similar volume loss occurred during the period when the lights were switched off. A very similar trend occurred at 36 and 60 hour period.

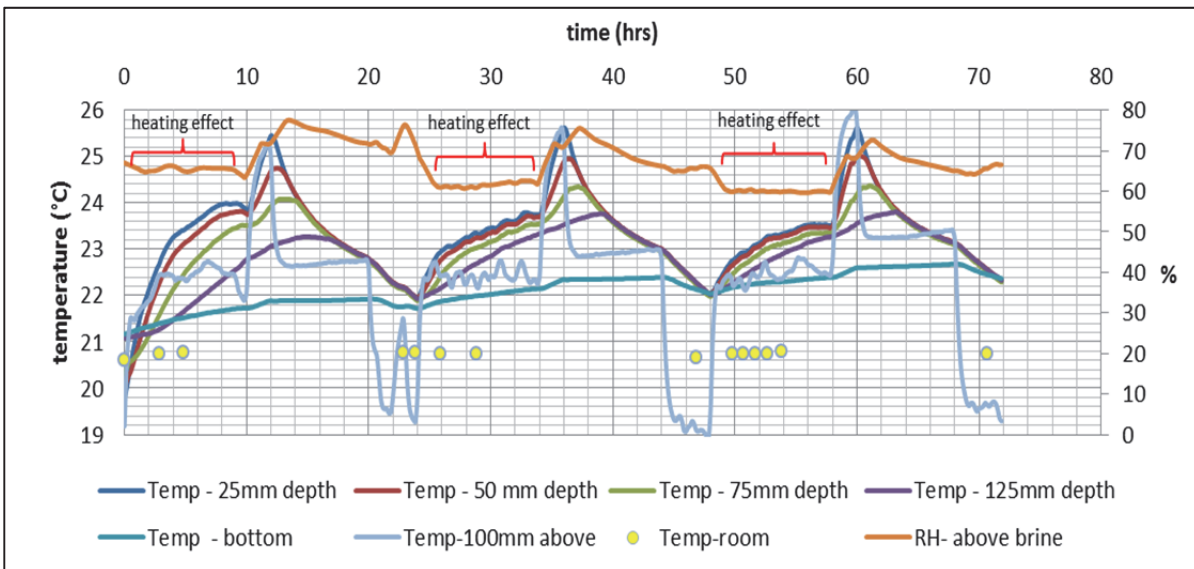


Figure 5.40: The graph indicates the temperature stratification of the Emalahleni brine during forced convection.

In contrast to the natural convection (Figure 5.38), the temperature stratification lines (Figure 5.40) appeared more compressed which indicates that the temperature stratification during forced convection was smaller in comparison with the natural convection temperature. The temperature near the surface of the brine was diffused to the deeper levels where other sensors were located. The peak temperatures of the brine were lower than the natural convection experiments as shown in Figure 5.38. The wind cooled the air above the container by connecting the air flow.

Table 5.3: Comparison of the actual measurements of the Emalahleni brine and the modelled brine evaporation for the same period.

	Emalahleni no wind	Oroud Model	Emalahleni with wind	Oroud wind model	Projected monthly (no wind)	Projected monthly (with wind)
Avg mm/day	5.33	5.33	6.5	6.003	159.90	180.10

As is shown in Table 5.3, the daily average evaporation of the Emalahleni brine under natural convection was 5.33 mm/day. The Oroud (1999; 2000) model suggests a very similar figure over the same period. Under the forced convection, the model was a bit lower than the actual recorded evaporation. The model also projects 11% increase in evaporation with wind being applied at 2 m/s every 12 hour cycle.

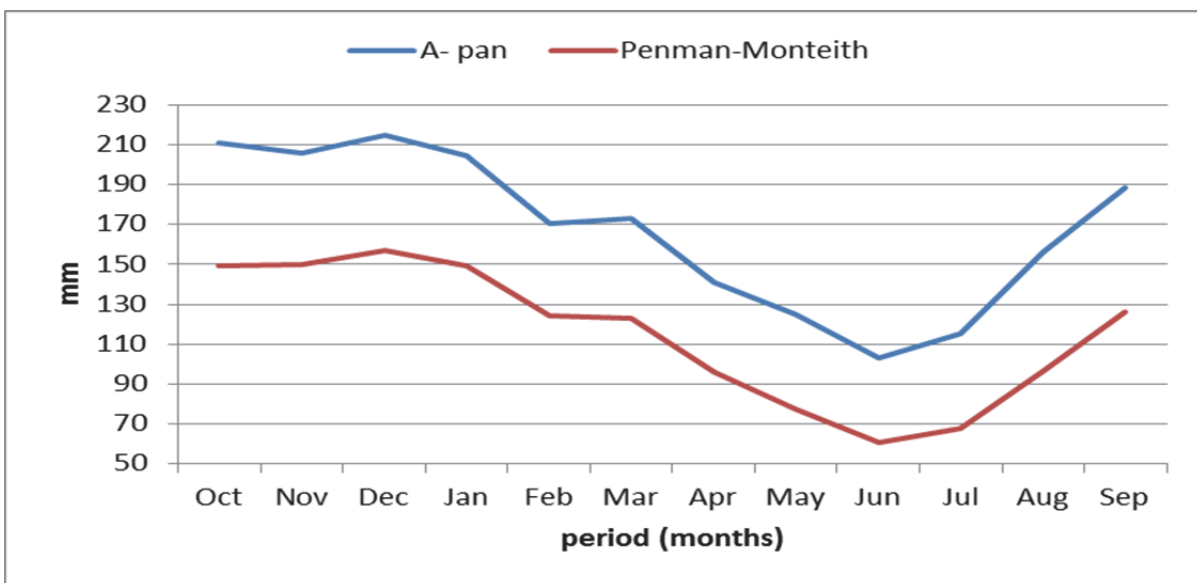


Figure 5.41: The mean monthly and annual A-pan equivalent potential evaporation annual evaporation of the relevant secondary catchment in the Olifants Catchment (Schulze et al., 1997).

In Table 5.3, the daily average of the Emalahleni brine under natural convection was 5.33 mm/day. The Oroud model suggested a very similar figure over the same period of time. Under the forced convection, the model was lower than the actual recorded evaporation. The experiments which incorporated the wind increased the evaporation rate to about 20%. The modelled data also projected an 11% increase in evaporation under forced convection applied at 2 m/s during the energy input. This data generated is in line with Figure 5.41 September forecast of the Olifants Catchment.

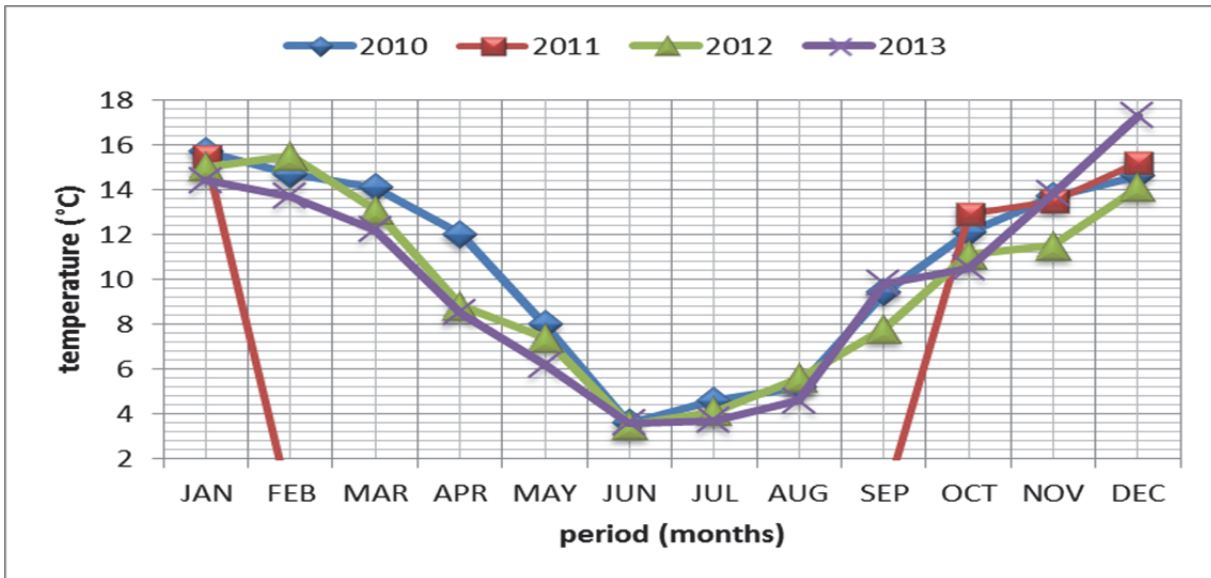


Figure 5.42. The average minimum temperatures of the relevant secondary catchment of the Olifants Catchment over the last four years (Courtesy of SAWS 2013)

The minimum temperatures of the secondary catchment in the Olifants Catchment ranged between 3 and 18°C over the last four years. The lowest temperatures occurred during the June and July period which signifies the winter period. The highest temperatures occurred in the January and December period where the temperatures exceed the 14°C mark. The higher temperatures contributed greatly to the evaporation rate.

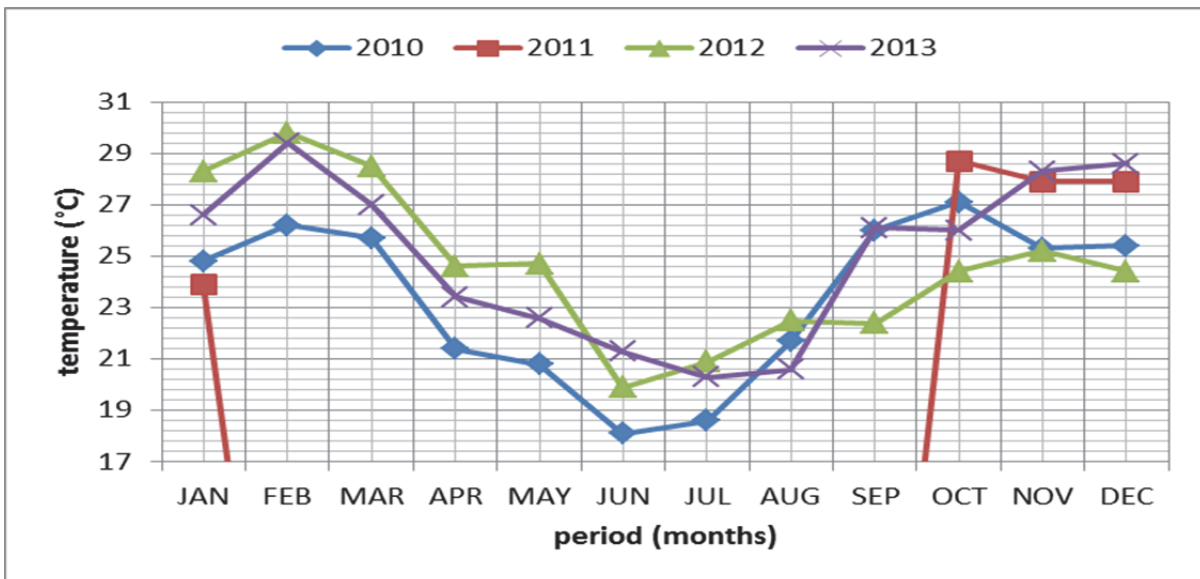


Figure 5.43. The monthly average maximum temperatures of Emalahleni area over the last four years (Courtesy of SAWS 2013)

The data from the South African Weather Service proposed that the average maximum temperatures of the Emalahleni area are portrayed as a moderate physical environment. In relation to Figure 5.43, the highest

temperatures occurred in the summer period with the highest rainfall in the same period as Figure 5.44 suggests. In relation to the laboratory experiments the maximum temperature was achieved.

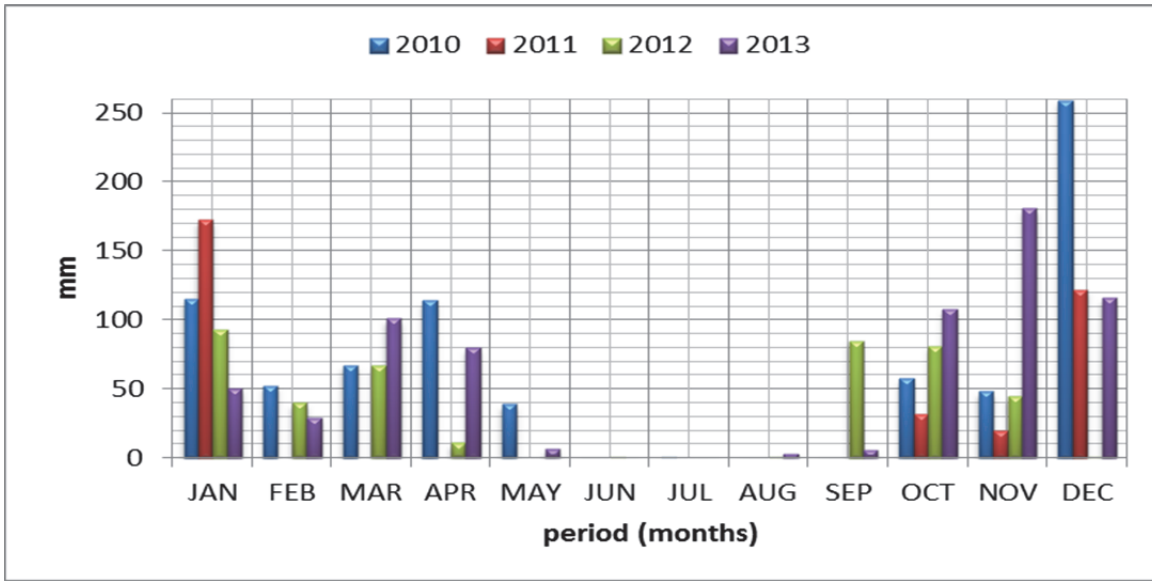


Figure 5.44. The monthly rainfall of the Emalahleni area over the last four years (Courtesy of the South African Weather Service, 2013)

The study area is situated in a summer rainfall region in particular the Highveld region (M.Van Veelen., 2011). The rainfall varies between 550 and 750 mm/annum in the Highveld and Eastern Lowveld (M.Van Veelen., 2011). In Figure 5.44 the highest rainfall occurred during the December and January period for the past four years.

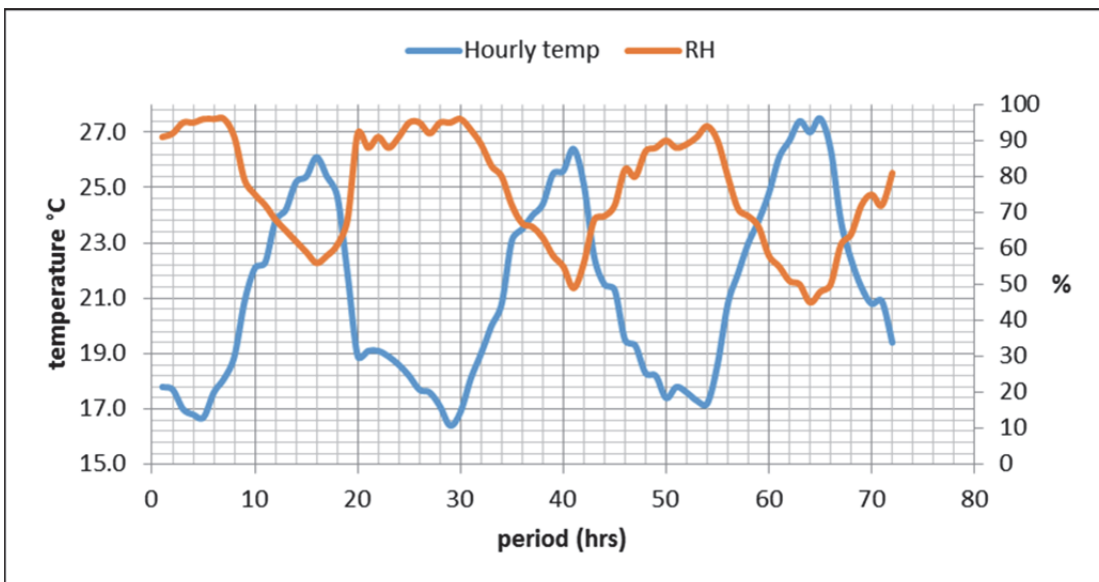


Figure 5.45. The temperature and the humidity of the Emalahleni area for 3 days (17 to 19 February 2009).

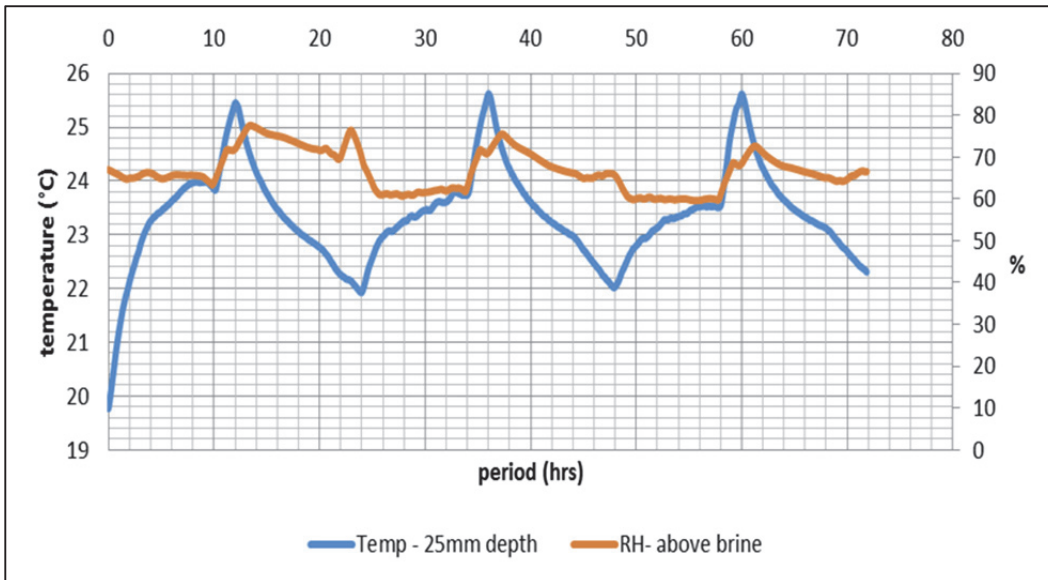


Figure 5.46. The temperature and humidity of the experimental results during the Emalahleni brine conducted in 2013.

The temperature and humidity of the lab experiments showed similar patterns to the real environmental conditions. However, the similarity between the mediums, the laboratory experiments was restricted to certain seasons of the eMalahleni area as the control of parameters was limited. The insulated containers from the laboratory experiments delayed the energy loss enough to be compared to a real environment. The data collected in the laboratory resonated well with real data although its changes were smoother and conformed.

5.3.7 Energy balance

The energy of the system was calculated for 12 hour per cycle according to the different temperature variation. The first segment of the energy was used to elevate the temperature and the second part to change the phase (Young, 1947). Evaporation is an endothermic process which requires energy to conduct the phase change. The dissipation of energy indicated that the surface level of the brine in the container absorbed a greater amount of energy than the substrata.

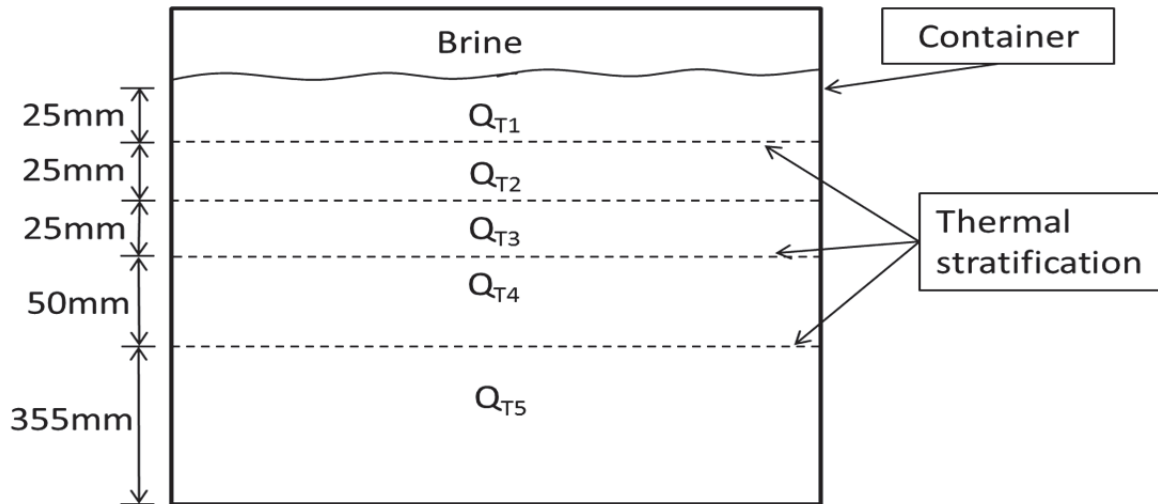


Figure 5.47. The thermal energy distribution during the Emalahleni brine experiment.

The thermal stratification level was calculated using the following equation (equation 25);

$$Q_{total} = mC\Delta t \quad (25)$$

T_1 =25mm from the surface

T_2 =50mm from the surface

T_3 =75mm from the surface

T_4 =125mm from the surface

T_5 = bottom of the container

Q_{T1} = 8.6%

Q_{T2} = 8.62%

Q_{T3} = 7.26%

Q_{T4} = 9.69%

Q_{T5} = 65.89%

$$\Delta U = Q + W \quad (26)$$

$\Delta \dot{U}$ = total energy

Q= temperature change

W= evaporation+ condensation

The total energy absorbed by the container was calculated for a 3 day cycle. The combination of evaporation, temperature change and condensation energy constituted towards the greater energy utilised of the experimental setup.

The wind input was calculated using the following equation (equation 27);

$$P = \frac{1}{2} \rho A v^3 \quad (27)$$

Where P= the power, ρ =the density of the air, A=the surface area exposed and v=the velocity of the wind force.

The wind energy was calculated for a 3 day cycle at 12 hour intervals. The wind energy was produced from the electric fan propagated through the ventilated air pipe. The distribution of energy showed that a greater amount of energy was absorbed by the lower section of the container as result of the temperature gradient and the larger volume. In addition, the upper section of the container reached a higher temperature but transferred a significant amount of energy to the lower section of the container. Approximately 27% of the energy from the system was absorbed by the surrounding area and expelled though the ventilation system. This loss of energy was a secondary effect in order to maintain the temperature of the experimental area during the experimental setup.

CHAPTER 6: ADSORPTION OF Ca^{2+} , Mg^{2+} , K^+ AND Na^+ ON PAN+ TiO_2 AND PAN+ZEOLITE NANOFIBRES

6.1 INTRODUCTION

This section presents and discusses the results of novel materials, namely PAN- TiO_2 and PAN-Zeolite nanofibres synthesised to adsorb cation components from brine in order to simplify brines and enhance brine evaporation. There are various methods that have been used to recycle and remove heavy metals from aqueous solutions. These methods include; electrochemical treatment, adsorption, membrane separation, ion exchange and chemical precipitation amongst others. (Miretzky et al., 2006; Shoushtari et al., 2006; Shi et al., 2004; Tahaei et al., 2008). Among all these, adsorption is one of the most common and simple methods. The adsorption of metals or ions can be achieved by employing polymer materials containing functional groups, for example, amidoxime, tetrazine, phosphoric, carboxyl and amino (Neghlani et al., 2011), to form strong complexes with metal ions through the coordination reaction. Adsorption of metals onto these materials is dependent solely on the functional groups present on the adsorbent surfaces. Zeolites and TiO_2 are often used in powder form for ion-exchange purposes but this form causes separation challenges of the particulates in water. This proof of concept study was performed to show the possibility to enhance removal of divalent cations from brine with composite nanofibres containing these known adsorbents/ionexchangers to overcome separation challenges.

Recently, the electrospinning technique, a simple and versatile method, has been widely applied to produce polymer based nanofibers. The electrospun nanofibers possess numerous interesting characteristics such as high porosity, small interfibrous pore size, and most importantly much larger specific surface in comparison to conventional fibres (Fenglin Huang et al., 2013). The high specific surface makes nanofibres better adsorbents (Ma et al., 2006), which have higher adsorption rates and capacities than other types of materials such as conventional fibres, foams and resins, etc. (Saeed et al., 2008). Thus, nanofibers, modified by introducing functional groups on their surface or by incorporating ionexchangers into the fibre could be applicable for the removal and recovery of cations and heavy metals from aqueous solutions. Therefore, the general objective of this section of the study is to develop an adsorption material to address the Ca^{2+} and Mg^{2+} ion contaminants in brine as these could affect the crystallization of NaCl during the eutectic freeze crystallization process in the treatment of brine and also, slow down the evaporation rate of brine from the evaporation pond.

6.2 CHARACTERIZATION OF PAN- TiO_2 AND PAN-ZEOLITE NANOFIBRES

Poly acrylonitrile (PAN) nanofibres prepared by electrospinning methods were loaded with titanium dioxide or zeolite Y. The structure of PAN, PAN+ TiO_2 and PAN+Zeolite nanofibers were analyzed using FTIR and SEM. The modified nanofibers were subsequently applied to adsorb calcium, potassium, magnesium and sodium ions from model salt solutions as set out in Chapter 3.

6.2.1 Fourier Transform Infrared Spectrometry (FTIR)

Figures 6.1, 6.2 and 6.3 show the FTIR spectra of the PAN, PAN+TiO₂ and PAN+Zeolite nanofiber mats respectively. The FTIR spectrum of PAN exhibited the characteristic bands of nitrile (2250 cm⁻¹), carbonyl (about 1725 cm⁻¹) and this indicates that PAN is a copolymer. The FTIR of the PAN doped with TiO₂ also exhibits the characteristics of PAN but with a major reduction in the magnitude of the peaks and an incorporation of the peak for TiO₂. The same applies to the incorporation of zeolite into the PAN structure, with a broad peak at around 1000 cm⁻¹ signifying that zeolite was incorporated into the fibre.

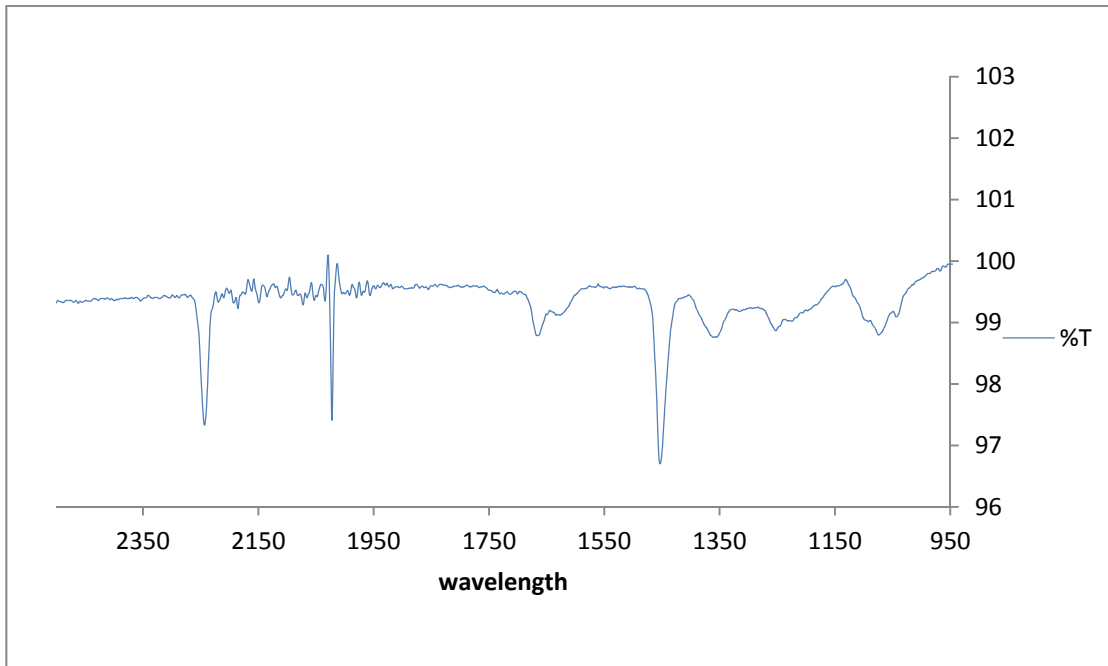


Figure 6.1: FT-IR Spectrum of PAN

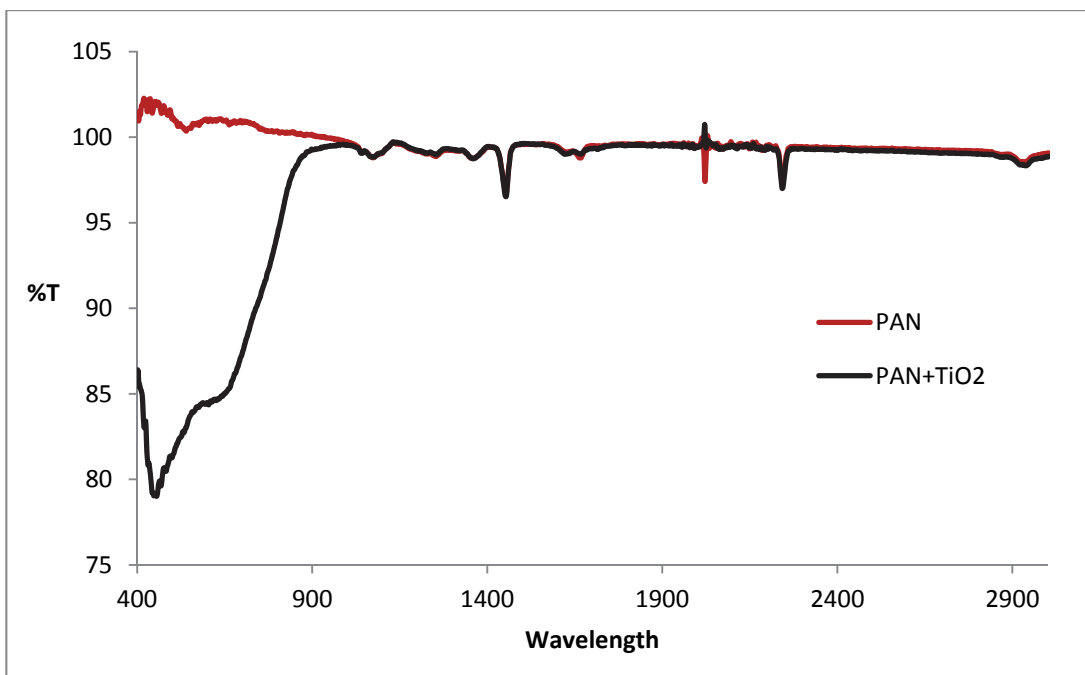


Figure 6.2: FT-IR Spectra of PAN and PAN+TiO₂

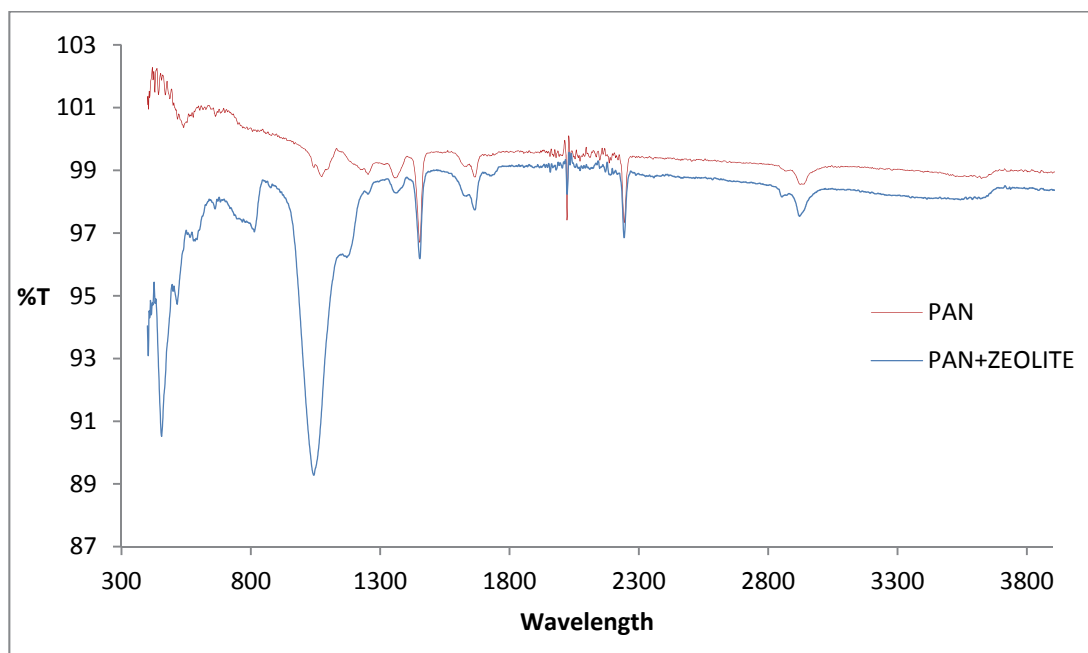


Figure 6.3: FT-IR Spectra of PAN and PAN+Zeolite Y

6.2.2 SEM images of raw PAN and PAN+TiO₂

The SEM images of raw PAN and PAN+TiO₂ are shown in Figures 6.4 and 6.5. The morphologies are similar to each other, hence incorporating the nanoparticulate powder TiO₂ did not disrupt the nanofibre morphology excessively. Figure 6.5 shows how the modified PAN nanofiber surface became somewhat roughened and undulating compared to the raw PAN nanofibres. The roughness can be attributed to the TiO₂ present in the structure, which was not evenly distributed on the PAN surfaces.

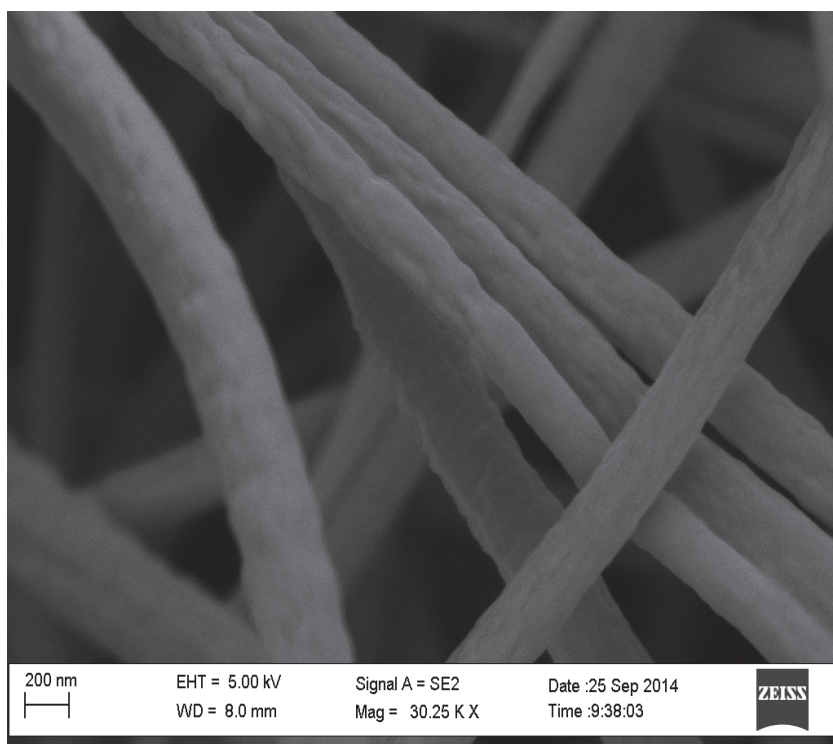


Figure 6.4: SEM image of PAN nanofibre

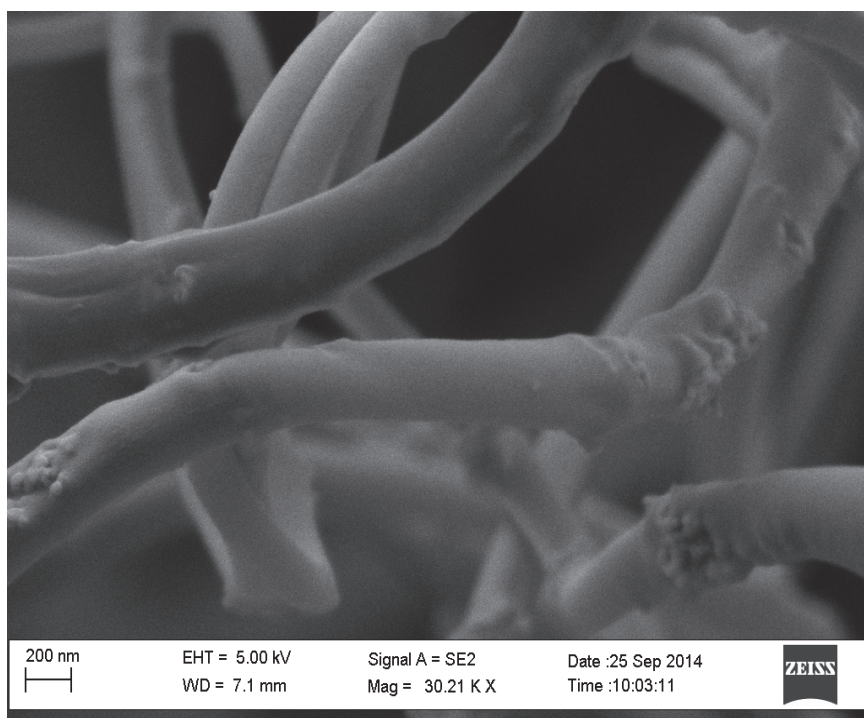


Figure 6.5: SEM image of PAN+TiO₂ nanofibre

6.3 EFFECT OF CONTACT TIME ON ADSORPTION OF METALS

Contact time is an important parameter because it is a factor that determines the adsorption kinetics of an adsorbate at a given concentration. The effect of contact time on calcium, magnesium, potassium and sodium metal ion uptake by PAN+TiO₂ and PAN+Zeolite nanofibers was investigated over 8 hours (Figures 6.6 and 6.7). The kinetic studies were carried out for different initial concentrations of 100, 200, 300, 400 and 500 mg/L for Ca²⁺, Mg²⁺, Na⁺ and K⁺ ions uptake on PAN+TiO₂ and PAN+Zeolite nanofibers at 298K.

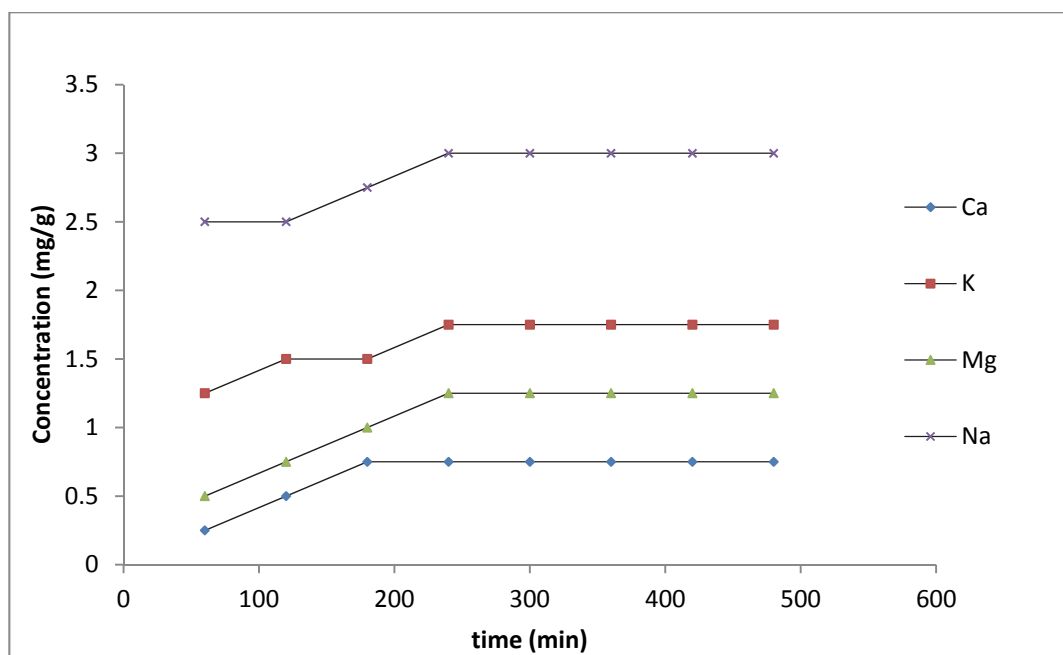


Figure 6.6: Effect of contact time on adsorption of metal ions on PAN+TiO₂ nanofibre

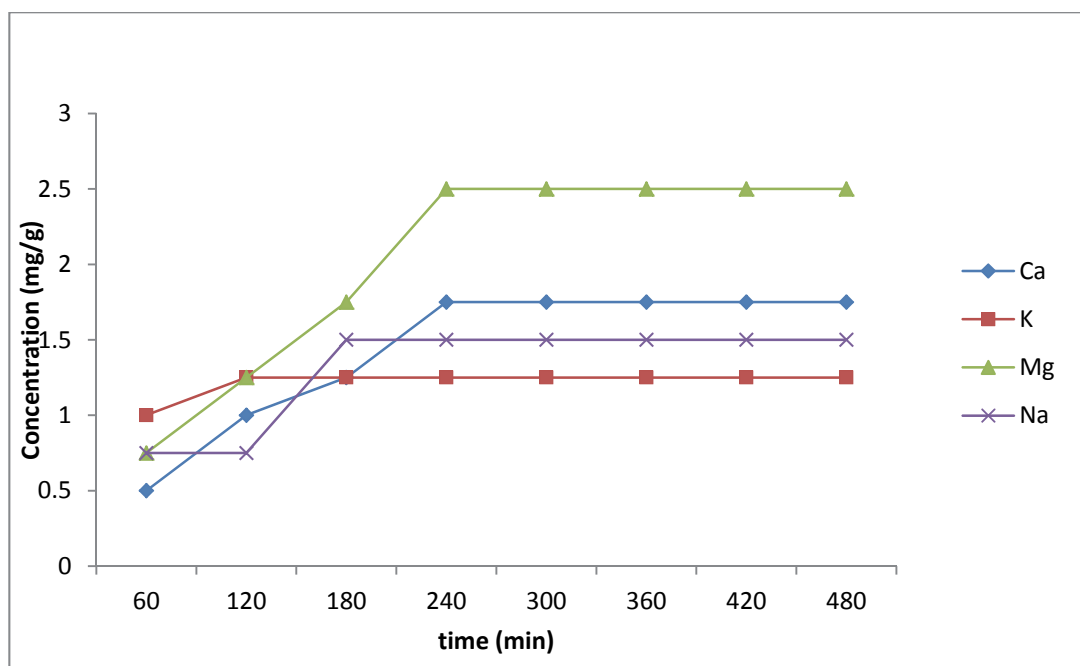


Figure 6.7: Effect of contact time on adsorption of metal ions on PAN+Zeolite nanofibre

6.3.1 Effect of contact time on adsorption of calcium Ca^{2+}

Figure 6.6 shows the amount of Ca^{2+} ions adsorbed on PAN+ TiO_2 nanofibre as a function of time at 298 K. It was observed that the uptake amount of Ca^{2+} ions on the PAN+ TiO_2 nanofibre increased rapidly from 0.25 mg/g to 0.75 mg/g with an increase in the contact time from 0 to 180 min. Thereafter, the concentration of Ca adsorbed did not increase with an increase in contact time. The initial rapid adsorption of Ca on the PAN+ TiO_2 nanofibre was attributed to the presence of many exchange sites, which resulted in a rapid increase in the concentration gradient between the adsorbate in solution and the adsorbent surface. At 240 min, the concentration of Ca adsorbed on the PAN+ TiO_2 nanofibre did not increase with an increase in the contact time due to the accumulation of calcium ions on the vacant sites, and ion-exchange capacity of the fibre being reached, leading to a decrease in gradient in the adsorption rate after 180 to 480 minute. The uptake of Ca^{2+} ions on the PAN+Zeolite nanofibre as shown in Figure 6.7 followed the same trend but with increase in the concentration of Ca adsorbed (1.75 mg/g) at 240 min. This is an indication that the adsorption capacity of PAN+Zeolite nanofiber for Ca was higher than that of PAN+ TiO_2 nanofibre.

6.3.2 Effect of contact time on adsorption of magnesium Mg^{2+}

Figure 6.6 shows the adsorption capacity of PAN+ TiO_2 nanofibre for Mg. It was observed that the Mg ions gradually adsorbed on the fibre from 0.5 to 1.25 mg/g with an increase in the contact time. The adsorption capacity was at equilibrium for Mg at 240 min. As shown in Figure 6.6, the trend was similar to that of calcium. Moreover, the uptake was greater than that of calcium. Meanwhile, Mg ions adsorption onto the PAN+Zeolite nanofibre was also favourable as a gradual increase in the concentration adsorbed was observed as the contact time increased. Similar to what was observed in the trend of Mg adsorbed on PAN+ TiO_2 nanofibre, the equilibrium was reached at 250 min for PAN+Zeolite nanofiber.

6.3.3 Effect of contact time on adsorption of potassium K^+

The effect of contact time on the adsorption of K^+ ion on PAN+TiO₂ and PAN+Zeolite was investigated at 298 K. Figures 6.6 and 6.7 showed the results of the adsorption of K on the nanofibers. As shown in the Figures 6.6, K^+ ions were gradually adsorbed by PAN+TiO₂, and reached equilibrium at 240 min. In Figure 6.7, it was observed that K^+ ions were also adsorbed gradually by PAN+Zeolite in a trend similar to that of PAN+TiO₂. Moreover, the concentration of K^+ ions adsorbed on PAN+TiO₂ nanofibre was significantly greater than PAN+Zeolite. This is an indication that the adsorption capacity of PAN+Zeolite nanofibre for K was less than that of PAN+TiO₂ nanofibre. The adsorption of K on PAN+TiO₂ nanofibre was at equilibrium at 240 min while its adsorption on PAN+Zeolite was at equilibrium at 120 min.

6.3.4 Effect of contact time on adsorption of sodium Na^+

The effect of contact time on the adsorption of Na^+ ion at different concentrations and temperatures on PAN+Zeolite and PAN+TiO₂ nanofibres are presented in Figures 6.6 and 6.7. In Figure 6.6, it was observed that Na^+ ions were gradually adsorbed by PAN+TiO₂ nanofibre and then reached equilibrium at nearly 250 minutes. The concentration of Na adsorbed by the TiO₂ nanofibres is significantly higher than the concentration adsorbed for other cations. In the case of PAN+Zeolite, Na adsorption increased gradually with increase in contact time and equilibrium was reached around 200 minutes, but a lower amount was adsorbed than in the case of the TiO₂ loaded nanofibres.

6.4 EFFECT OF CONCENTRATION ON ADSORPTION OF METALS

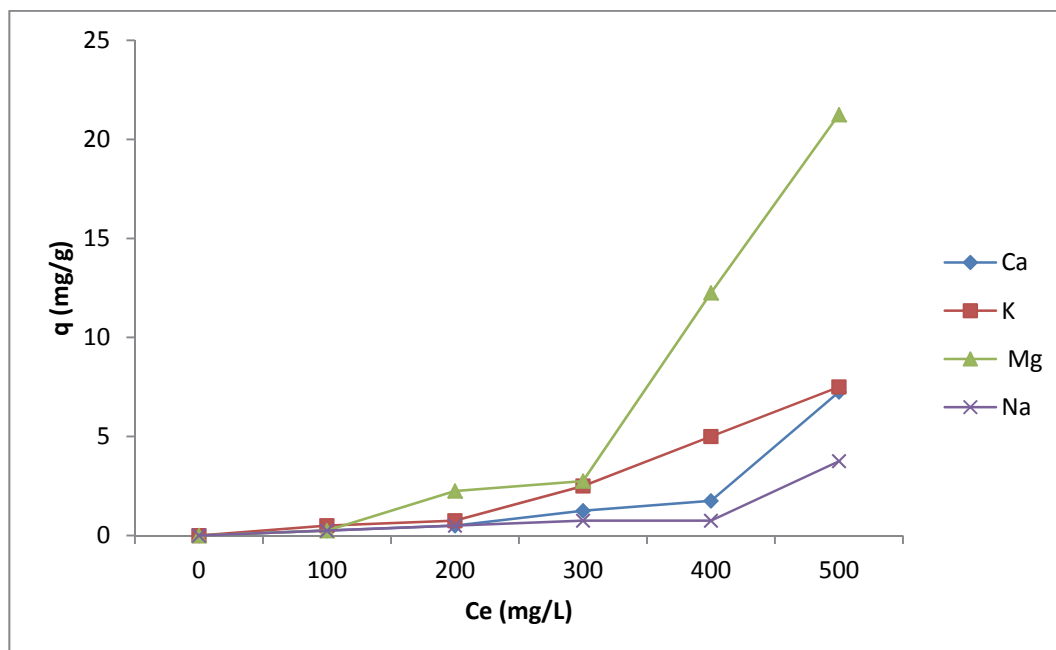


Figure 6.8: Effect of concentration on the adsorption capacity of PAN+TiO₂ nanofibre

Figure 6.8 shows that the quantity of metal ions adsorbed from the solution increased with an increase in the concentration of all metals ions, with magnesium having the highest quantity adsorbed on PAN+TiO₂. In

Figure 6.8, the situation is similar to that of the PAN+TiO₂ nanofibre, but the PAN+Zeolite showed an improved adsorption for all metal ions.

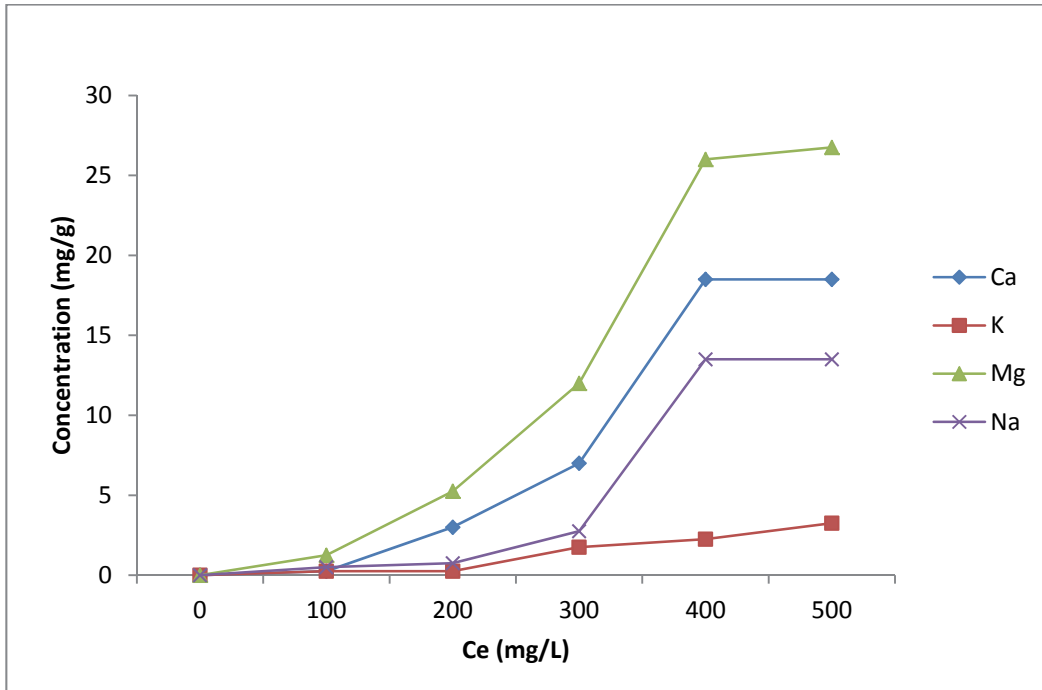


Figure 6.9: Effect of concentration on the adsorption capacity of PAN+Zeolite nanofiber

In both cases (Figures 6.8 and 6.9), divalent cation Mg was better adsorbed from the solution followed by Ca. The concentration adsorbed for other monovalent metals (Na and K) was lower. Consequently, the quantity of adsorption increased with increase in the concentration of metals in the solution.

6.5 DETERMINATION OF RATE PARAMETERS

The adsorption kinetics of Ca²⁺, Mg²⁺, K⁺ and Na⁺ ions were modelled by using the pseudo first order and pseudo second order equations. Lagergren's first order rate equation is one of the most widely used for the adsorption of solute from a solution.

6.5.1 Pseudo-first order

A kinetic model for sorption analysis is the pseudo first order rate expression of Lagergren in the form described in equations 28 and 29:

$$\frac{dq}{dt} = k_1(q_e - q) \quad (28)$$

$$\log(q_e - q) = \log q_e - \left(\frac{k}{2.303} \right) \times t \quad (29)$$

where q_e is the amount of metal ion (M^{n+}) sorbed at equilibrium (mg/g), q_t the amount of metal ion sorbed at time t (mg/g) and, k_1 the rate constant of pseudo-first order sorption (1/min). The value of k_1 can be obtained from the slope of the linear plot of $\log (q_e - q_t)$ vs. t .

6.5.2 Pseudo-second order

In a situation when the amount of metal ion sorbed at equilibrium (mg/g) obtained from the first order reaction is not the same as the one derived experimentally, the second order equation is applied in order to obtain k_2 (Ho and Mckay, 1998):

$$\frac{dq}{dt} = k_2(q_e - q)^2 \tag{30}$$

The integrated form of the equation (30) under the boundary conditions of $q = 0$ and $q_t = q_t$ at $t = t$ in the linear form (shown in Equation 31) makes it possible to obtain q_e and k_2 from the plots of t/q_t vs. t .

$$\frac{t}{q} = \frac{1}{k_2 q_e^2} + \frac{1}{q_e} t \tag{31}$$

Table 6.1: Rate constants for first and second order adsorption on PAN+TiO₂ and PAN+Zeolite.

ADSORBENT	Solution Conc 100mg/L	First Oder Rate Expression		Second Order Rate Expression	
		k_1 (min ⁻¹)	R^2	k_2 (min ⁻¹)	R^2
PAN+TiO ₂	Ca ²⁺	0.002303	0.4439	9.25×10^{-3}	0.9358
PAN+ZeoliteY		4.60×10^{-4}	0.0421	5.09×10^{-3}	0.9153
PAN+TiO ₂	Mg ²⁺	1.842×10^{-3}	0.3099	0.018	0.7599
PAN+ZeoliteY		9.21×10^{-4}	0.2494	4.6×10^{-3}	0.909
PAN+TiO ₂	K ⁺	3.2×10^{-3}	0.536	0.0327	0.9967
PAN+ZeoliteY		1.84×10^{-3}	0.333	0.131	0.9991
PAN+TiO ₂	Na ⁺	0.0253	0.4821	4.77×10^{-3}	0.1973
PAN+ZeoliteY		6.91×10^{-4}	0.5714	0.0103	0.9254

It was observed that the Lagergren model fits suitably at the early stage of the adsorption for both nanofibers, but at the later stage of the adsorption process, the results deviated from the theory. Therefore, the model represents the initial stage where adsorption takes place rapidly but cannot be applied for the whole adsorption process. Similarly, the first order equation did not apply well throughout the contact time in this adsorption process. But as it was observed in Table 6.1, the correlation coefficient of pseudo-second

order was superior to the pseudo first order reaction. This indicates that the adsorption process is not a first order reaction and therefore, pseudo second order fits best.

6.5.3 Adsorption equilibrium isotherm

The Langmuir and Freundlich model equations were applied to the adsorption isotherm study of the metal ion solution involving calcium, magnesium, potassium and sodium. In the Langmuir model, it was assumed that the uptake of metal ions occurred on a homogenous surface by monolayer adsorption without any interaction between the ions adsorbed. This model was expressed in the linearized form as shown equation 29 below:

$$\frac{1}{q} = \left[\left(\frac{1}{k_f q_m} \right) \left(\frac{1}{C_e} \right) \right] + \left[\frac{1}{q_m} \right] \quad (32)$$

where q is the amount adsorbed on the resin at equilibrium (mg/g), C_e is the equilibrium concentration of the adsorbate (mg/L), and k_f is the equilibrium constant related to the affinity of the binding sites for the metals or the Langmuir constant; q_m is the adsorbent capacity (maximum possible amount of metallic ion adsorbed per unit mass of adsorbent).

Langmuir theory suggests that adsorption takes place at specific homogenous sites within the adsorbent. It is then assumed that when a metal ion occupies a site, there cannot be any further adsorption taking place at that place. Whereas, in the Freundlich model, it is assumed that the uptake or adsorption of metal ions takes place on a heterogeneous surface through monolayer adsorption. Equation (33) describes the Freundlich model:

$$q = k_f (C_e)^{\frac{1}{n}} \quad (33)$$

$$\ln q_e = \left(\frac{1}{n} \right) \ln C_e + \ln k_f \quad (34)$$

Where q_e is the amount adsorbed (mg/g), C_e is the equilibrium concentration of the adsorbate (mg/L), K_f ((mg/g)*(mg/L)ⁿ) and n are the Freundlich constants related to adsorption capacity and adsorption intensity, respectively (Freundlich, 1926).

Plots obtained from the equation (31) which was the linearized form of Freundlich equation. In q_e versus $\ln C_e$ linear plots would give the value of $1/n$ as slope and k_f as an intercept. The value of k_f can be used as alternative measure of adsorption capacity, while $1/n$ determines the adsorption intensity.

Table 6.2: Plot of Freundlich Isotherms vs Langmuir Isotherms

Adsorbent	Solution Conc 100mg/L	Freundlich Isotherms			Langmuir Isotherms		
		n	k _f	R ²	q _m	k _L	R ²
PAN+TiO ₂	Ca ²⁺	1.259	0.4093	0.8127	0.316	2.901	0.8069
PAN+ZeoliteY		1.224	0.478	0.909	0.909	4.463	0.8562
PAN+TiO ₂	Mg ²⁺	1.263	0.469	0.8714	0.3104	3.729	0.7831
PAN+ZeoliteY		1.362	0.665	0.9289	0.909	4.463	0.887
PAN+TiO ₂	Na ⁺	2.899	2.076	0.1257	0.314	0.393	0.812
PAN+ZeoliteY		1.294	0.479	0.8535	0.49	3.906	0.8891

According to the results in Table 6.2, it was observed that calcium and magnesium adsorption on the nanofibers displayed a heterogeneous adsorption by fitting best to the Freundlich model, while the adsorption of sodium on the nanofibers fitted well to Langmuir model according to the results of their coefficient values.

6.5.4 Summary

The application of composite cation exchange material such as PAN+Zeolite Y and PAN+TiO₂ nanofibres is promising in the adsorption of major cations from model salt solutions. The application of these nanofibres is efficient considering the fact that the PAN nanofibre composite was able to adsorb alkali and alkaline earth metals from the solution with the inclusion of either TiO₂ or zeolite Y nanoparticulates. This implies that the added sorbent improves the performance of the nanofibres. Furthermore, the incorporation of inorganic materials such as titanium dioxide and zeolite onto the PAN contributed to the increase in the adsorption of metal ions from the solution. The PAN zeolite Y composite was found applicable to remove divalent cations from solutions, thus would aid in the simplification of brine streams. Calcium and magnesium adsorption on the nanofibers displayed a heterogeneous adsorption by fitting best to the Freundlich model, while the adsorption of sodium on the nanofibers fitted well to the Langmuir model.

CHAPTER 7: CONCLUSIONS & RECOMMENDATIONS

7.1 CONCLUSIONS

Reverse osmosis plants are increasingly being deployed to deal with waste waters from industry and mining in South Africa, and the brines produced by these plants constitute a residual challenge for waste disposal because the most economical way of dealing with them is to construct evaporation ponds. How much volume reduction can be achieved in these ponds depends on climate and may also be affected by the type and concentration of salts dissolved in the brine. It was the perceived need to assess the importance of these factors locally that prompted this study, which is a sequel to an earlier Water Research Commission project (Dama-Fakir et al., 2012) that attempted to address this objective but was insufficiently conclusive because field testing was hampered by the difficulty of controlling individual determinants of evaporation accurately for their relative importance to be assessed.

This report has summarised the issues relating to industrial brine generation and disposal in South Africa and has reviewed the literature on brines with particular emphasis on the water treatment processes that produce brines as a waste, the chemistry of brines and the factors which influence evaporation and determine brine evolution. The experimental focus has been on assessing the effect of salt concentration and composition on brine evaporation rate, and on developing a laboratory facility for testing the relative effect of different environmental parameters (wind speed, humidity, temperature, irradiance) on evaporation of water from brines of different composition.

The present study focused on the brine produced at the Emalahleni water treatment plant, and a section of this report summarises the different stages of brine development associated with the treatment process. Analysis of the stage 3 reject brine collected from the plant revealed that it is a Na-SO₄ type water although it does contain significant concentrations of other major ions, namely Ca, Mg, K and Cl. Seventy-one percent of the cation mole charge is accounted for by Na⁺, and the remainder by Ca²⁺ (15%) K⁺ (9%) and Mg²⁺ (4%). In the case of anion charge, SO₄²⁻ accounts for 88% and Cl⁻ (10%) and HCO₃⁻ (1%) for the remainder. The brine has a near-neutral pH.

It was this analysis that prompted the choice of salts for the small scale evaporation study designed to find out whether the type of salt has any effect on evaporation rate. The literature review indicated that it is salinity *per se* which has the most important effect on evaporation rate rather than the type of salt. This is because the effect of salt manifests itself primarily through control of vapour pressure which is a colligative property of solutions, implying that it depends on concentration rather than the nature of the dissolved species. Nevertheless there are situations in which the composition of the brine in its final stages can be expected to influence evaporation rate, simply because as the brine evolves through evaporative concentration, the less soluble species will precipitate leaving dissolved species which are typically the most hygroscopic or, as is the case with Ca and Mg chlorides for example, deliquescent. This phenomenon is well known in commercial salt production from sea water, where the residual bitterns, after fractional

crystallization of gypsum ($\text{CaSO}_4 \cdot 2\text{H}_2\text{O}$) and halite (NaCl), consist largely of MgCl_2 which cannot be evaporated to dryness even in the driest of earth climates.

The small scale evaporation experiments confirmed that an effect of salt type (single, binary and ternary solutions of Na_2SO_4 , NaCl , KCl , CaSO_4 , and MgSO_4 were studied) was sometimes discernible but not statistically significant, probably in part because while the effect of salt is generally to reduce evaporation the presence of salt also gives rise to greater heating of the solution by absorbing radiant energy. This latter effect seemed most discernible with CaSO_4 although establishing its magnitude was not possible because the concentration of this sparingly soluble salt could not match that (0.5M) of the other salts studied. There also seemed to be a solution heating effect leading to a higher evaporation rate (again not significant) in the case of those solutions dominated by divalent as opposed to monovalent cations, but again there could have been confounding by an anion effect since the Ca- and Mg-dominated solutions were also dominated by sulfate rather than chloride. In retrospect it might have been instructive to include chlorides of Ca and Mg in these experiments (or at least solutions containing higher concentrations of chloride relative to sulfate) so that the deliquescence of these salts (essentially terminating the evaporation) could have been observed during the last stage of brine evolution. Despite these uncertainties the overall effect of salts on evaporation rate was confirmed in both the small scale study as well as the subsequent pilot scale study to be essentially one of concentration, inhibiting evaporation as expected. The whole effect of salts on evaporation rate can probably best be viewed as a special case of the law of diminishing returns, according to which the rate at which water will separate from a salt solution declines in proportion to the amount of water which has already been evaporated. Comparison of the actual measurements of the Emalahleni brine and the modelled brine evaporation for the same period showed that the daily average of the Emalahleni brine under natural convection was 5.33 mm/day. The Oroud (1999; 2000) model suggests a very similar figure over the same period. Under the forced convection, the model was a bit lower than the actual recorded evaporation. The model also projects 11% increase with wind being applied at 2 m/s every 12 hour cycle. Based on the salinity experiments, all the synthetic salts exposed to various conditions had shown different volume loss. The results indicated that the greatest volume loss was obtained for the least soluble salt amongst the synthetic salts while the more highly soluble salts had the lowest volume loss.

Disassociation of ions will ultimately lead to a greater solubility of the brine. The activity coefficient increased which subsequently led to the lower evaporation rates as a result of the ion-ion bonds. Reducing the amount of salts with high dissociation prior to their disposal in the ponds will increase the evaporation rate by promoting precipitation and increase the endothermic ability of the ponds and serve as a secondary heating source.

The pilot scale study also involved making in duplicate a modified copy of the WAIV apparatus for brine evaporation which has been described in the literature, using infrared lamp-heated Perspex tanks 0.5 m square and 0.5 m deep fitted with accessories for generating wind and intensifying evaporation on a square mesh which can be used for testing novel materials that enhance evaporation by allowing the solution to spread by capillarity over a greater surface area. The novel high surface area materials developed, namely composite nanofibres comprised of PAN loaded with Zeolite Y nanoparticulates were shown to significantly

remove divalent cations from model brine solutions, allowing for brine simplification. The PAN TiO₂ nanofibres showed a high Na cation adsorption. These fibres in future could be applied for the WAIV system.

This study has been concluded successfully in terms of construction and testing to demonstrate a sensitive response of evaporation to parameters such as salt concentration, wind and irradiance, but forms part of a postgraduate research project which is still in progress and so substantive data will only be available later in the form of a dissertation.

In terms of taking this research further, perhaps the most interesting prospect based on what was learned from reviewing the literature is the potential for generating products of value from brine management that could help to offset costs of storage and disposal. In the case of the Emalaheni brine the dominant product would be sodium sulfate assuming it could be separated cleanly by fractional crystallization (assisted if necessary by sequestration of alkali earth cations using a conditioner such as sodium carbonate). Sodium sulphate has use as an additive in detergents although the demand for it is unlikely to be high. Gypsum has uses in agriculture but again the quantity of by-product gypsum generated from making phosphate fertilizers is large, although in some parts of South Africa stockpiles of waste gypsum have already been consumed due to agricultural demand. Potassium salts (either sulfate or chloride) will always fetch a high price because of the role of K as a major ingredient of fertilizers. Once all of these salts have been removed through crystallization, the residue of probably mainly Mg chloride (since although Ca is more abundant it will probably separate out as gypsum at an earlier stage of evaporation), which is usually referred to as bitterns, can have certain specialised uses as a desiccant, dust suppressant and fire retardant. Bitterns are also of value as a neutralising agent of caustic residues and can be reacted with sodium aluminate to form hydrotalcite, a layered double hydroxide (LDH) with a variety of uses.

7.2 RECOMMENDATIONS

It is recommended that the follow-on research could include:

- Scaling up of the composite nanofibre fabrics and studying their efficiency and durability under working conditions
- Larger scale WAIV experiments comparing the nanofibre composite fabrics developed in this study to enhance evaporation whilst simultaneously simplifying the brine stream by removal of divalent cations.
- Include chlorides of Ca and Mg in future experiments (or at least solutions containing higher concentrations of chloride relative to sulfate) so that the deliquescence of these salts (essentially terminating the evaporation) can be observed during the last stage of brine evolution
- Recovering of sodium sulfate by fractional crystallization (assisted if necessary by sequestration of alkali earth cations using a conditioner such as sodium carbonate).
- Establish the potential for generating products of value from brine management that could help to offset costs of storage and disposal
- Further investigation of the effect of temperature and salinity on absorption could be carried out to interpret the measured absorption values Cp. In addition to rectify the thermal stratification of a

traditional pond, a layer of coal cinder can be placed at the bottom of the pond to increase the temperature at the bottom of the pond and subsequently increase the evaporation rate.

REFERENCES

- Ahmed, M., Shayya, H., Hoey, D. and Al-Handaly, J. 2001. Brine disposal from reverse osmosis desalination plants in Oman and the United Arab Emirates, Department of Soil and Water Sciences, Department of Bioresource and Agricultural Engineering Sultan Qaboos University, Muscat, Sultanate of Oman, Department of Land and Water Conservation, New South Wales, Australia, pp 135-147.
- Ahmed, M., Shayya, W, H., Hoey, D., Mahendran, A., Morris, R. and Al-Handaly, J. 2000. "Use of evaporation ponds for brine disposal in desalination plants", *Desalination* 130, pp 155-168.
- Akridge, D., G. 2008. "Methods for calculating brine evaporation rates during salt production. *Journal of Archaeological Science* 335, pp 1453-1462.
- Alabdulaaly, A.I. and Khan, M. A. 1997. Trace metals in groundwater RO plants brine water, IDA World Congress on Desalination and Water Reuse, Vol. 15, pp. 573-596.
- Awerbuch, L. and Weeks, M. C. 1990. Disposal of concentrates from brackish water desalting plants by means of evaporation technology *Desalination*, Volume 78: pp 71-76.
- Brouwer, C. and Heibloem, M. 1986. *Irrigation water management: irrigation water needs*. FAO, Rome
- Brutsaert, W. 1982. *Evaporation into the Atmosphere*. 1st Edition, Netherlands: Kluwer Academic Publishers.
- Cabasso . I. 1987. *Membrane Encyclopedia Polymer Science Engineering*.
- Calder. I.R and Neal. C. 1984. "Evaporation from saline lakes: a combination equation approach." *Hydrological Sciences Journal* 29, pp. 89-97.
- Chia-Ren, C., Ming-Hsu, L., Yi-Ying, C. and Yi-Hsin, K. 2010. A wind tunnel experiment on the evaporation rate of Class A evaporation pan. *Journal of Hydrology* vol. (381): 221-224
- Coleman, M. 2000. Review and discussion of the evaporation rate of brines, Actis Environmental Services.
- Comrie, W. 2011. *Development of a Reconciliation Strategy for the Olifants River Water Supply System*. Department of Water affairs. aueron.
- Crawford. J. 1999. *Geochemical Modelling – A Review of Current Capabilities and Future Directions*. Division of Chemical Engineering, Royal Institute of Technology (KTH), Department of Chemical Engineering and Technology, Stockholm.
- Dama-Fakir, P. and Toerien, A. 2009. "Evaporation rate on brine produced during membrane treatment of mine water", Abstract of the international Mine Water Conference, Proceedings ISBN Number: 978-0-9802623-5-3, Produced by: Document Transformation Technologies cc, Pretoria, South Africa.

Dama-Fakir P., Wurster A. and Toerien A. 2012. Field testing to determine the evaporation rate of brine solutions formed during the membrane treatment of mine-water. Authors: 2012/04/01; Research Report No.1895/1/12

Department of Water Affairs and Forestry (DWAf), Water Quality Management. https://www.dwa.gov.za/Dir_WQM/wqmFrame.htm, Accessed in July 2015

Du Plessis, J., Burger, J., Swart, C. and Museev, N. 2006. A desalination Guide for South African Municipal Engineer, Pretoria: Water Research Commission.

Duan, Z., Martin .J.L., McAnally, W.H. and Stockstill .R.L. 2009. Combined Effects of Wind and Streamflow on Gas-Liquid Transfer Rate. *Journal of Environmental Engineering*

Einav, R., Harussi, K. and Perry, D. 2003. The footprint of the desalination processes on the environment. *Desalination* 152: pp 141-154.

El-Manharawy, S. and Hafez, A. 2003. A new chemical classification system of natural waters for desalination and other industrial uses, *Desalination*, 156(1-3), 163-180.

ESCWA, 1993. Water desalination: the experience of GCC countries. Regional Symposium on Water Use and Conservation, Report E/ESCWA/NR/1993/WG.1/WP.10. Amman, Jordan.

Fatoba, O.O. 2010. Chemical interactions and mobility of species in fly ash-brine co-disposal systems. PhD thesis. Bellville: University of the Western Cape. South Africa.

Finch, J. 2001. A comparison between measured and modeled open water. *Hydrological Processes*, 15, 2771-2778.

Fu, G., Charles, S. P. and Yu, J. 2009. A critical review of pan evaporation trends over the last 50 years, *Climate change* (2009) 97, pp 193-214.

Gilron, J., Folkman, Y., Savliev, R., Waisman, M. and Kedem, O. 2003. "WAIV – wind aided intensified evaporation for reduction of desalination brine volume." *Desalination* , no. 158, pp. 205-214.

Gitari, L. F., Petrik, L. F., Key, D., Etchebers, O. and Okujeni, O. 2005. Mineralogy and Trace Element Partitioning in Coal Fly Ash/Acid Mine Drainage Co-Disposal solid residue.

Glater, J. and Cohen, Y. 2003. "Brine disposal from land based membrane desalination plants: A critical assessment, Polymer and separation research laboratory, University of California, Los Angeles.

Greenlee, L.F.; Lawler, D.F.; Freeman, B.D.; Marrot, B. and Mouli, P. 2009. "Reverse osmosis desalination: water resources, and today's challenges", *Water Research* 43 (2009) pp 2317-2348

Harbeck, G.E, Jr. 1955. "The effect of salinity on evaporation." USGS Prof. Pap. A, no. 272 : 1-6.

Harbeck, G.E. 1962. In *A Practical Field Technique for Measuring Reservoir Evaporation Utilizing Mass-transfer Theory*. US Geological Survey, Washington D.C: US Government Printing Office, pp.101-105.

Hardie, L. and Eugster, H. 1970. The evolution of closed-basin brines. In *Fiftieth Anniversary Symposia, Mineralogy and Geochemistry of Non-Marine Evaporites*. Mineralogical Society of America Special Publication, pp273-290

Himawan, C., Vaessen, R.J.C., Kramer, H.J.M., Seckler, M.M. and Witkamp, G.J. 2003. Dynamic modelling and simulation of Eutectic Freeze Crystallization, *J. Cryst. Growth* 237-239 (2003), pp 2257-2263.

Hisatake, K., Tanaka S. and Aizawa, Y. 1993. Evaporation rate of water in a vessel. *Journal of applied physics* 73.11: 7395-7401.

Höpner, T and Windelberg, J. 1997. Elements of environmental impact studies on coastal desalination plants. *Desalination* 108: pp 11-18

Incropera F.P., Dewitt D.P., Bergman T.L. and Lavine A.S. 2006. "Fundamentals of heat and mass transfer", 6th edition John Wiley & Sons

Itier, B. B. 1996. Recent developments and present trends in evaporation research: a partial survey. In: *Evapotranspiration and Irrigation Scheduling. Proceedings of the International Conference*. ASAE.

Ji, X, L. 2001. Mean activity coefficients of NaCl in (sodium chloride + sodium bicarbonate + water) from T = (293.15 to 308.15) K. *J. Chem. Thermodynamics* (33), 1107-1119.

Khordagui, H., 1997. Environmental Aspects of Brine Reject from Desalination Industry in the ESCWA Region, ESCWA, Beirut, Lebanon.

Knox. J.W., Rodriguez-Diaz. J.A. and Hess. T.M. 2011. Estimating Evapotranspiration by Using Atmometers for Irrigation Scheduling in a Humid Environment. *Journal of Irrigation and Drainage Engineering*, 137(11), 685-691.

Koenig, L. 1958. *R&D Progress Report No 20*. Office of Saline Water, Washington D.C.

Kokya, B. A. and Kokya, T. A. 2006. Proposing a formula for the evaporation measurement from salt water resources. *Hydrological processes*, Volume 22, pp 2005-2012.

Krukowski, J. 2001. Opening the Black Box: Regulations and Recycling Drive Use of Membrane Technologies. *Pollution Engineering* 33:20-25.

Lattemann, S. and Hopner, T. 2008. Environmental impact and impact assessment of seawater desalination. Volume 220, pp 1-15

Leaney, F. and Christen, E. 2000. On-Farm and community-scale salt disposal basins on the riverine plain: Evaluating the leakage rate, disposal capacity and plume development. CRC for catchment hydrology.

Mabovu, B. 2011. Brine treatment using natural adsorbents, Unpublished Master's thesis. Department of chemistry, University of the Western Cape, Bellville, South Africa

Macedonio, F., Katzir, L., Geisma, N., Simone, S., Drioli, E. and Gilron, J. 2011. "Wind-Aided Intensified eVaporation (WAIV) and Membrane Crystallizer (MCR)." *Desalination*, no. 273, pp.127-135.

Mahi, P. 2001. "Developing Environmentally Acceptable Desalination Projects." *Desalination* 138: pp 167-172.

Mao, Y., S. 1999. Effect of chemical composition on saline water evaporation, Master's thesis, Department of agricultural and Biosystem engineering Macdonald campus, McGill University Ste. Anne de Bellevue, Quebec, Canada.

Maas, E.V. 1990. Crop Salt Tolerance. (Tanji, K.K, Ed.) *American Society of Civil Engineers*(New York), 262-303.

Marek, R.S. 2001. Analysis of the evaporation coefficient and the coefficient condensation of water. *International Journal of Heat and Mass Transfer*(44), 39-53.

McCartney, M., Yawson, D., Magagula, T., and Seshoka, J. 2004. Hydrology and Water Resource Development in the Olifants River Catchment. *Working Paper 76, International Water Management Institute (IWMI)*.

Mema, V. 2009. Impact of poorly maintained wastewater and sewage treatment plants: Lessons from South Africa. Council for Scientific and Industrial Research (CSIR).

Mickley, M, H. 1993. Membrane concentration disposal. *American Water Works Association Research Foundation*.

Mickley, M. 2006. Membrane Concentrate Disposal: Practices and Regulation, Second Edition. U.S. Department of the Interior, Bureau of Reclamation, Technical Service Center, Water Treatment Engineering and Research Group.

Mickley, M. 2004. Review of Concentrate Management Options. In Texas Water Development Board (2004). Volume 2: Biennial report on seawater desalination: Technical Papers, Case Studies, and Desalination Technology Resources. Austin, Texas. Retrieved June 4, 2011 from http://www.twdb.state.tx.us/innovativewater/desal/doc/The_Future_of_Desalination_in_Texas-Volume_2/documents/C9.pdf

Mickley, M., Himilton, R., Gallegos, L. and Truesdall, J. 1993. "Membrane concentration disposal", American water works association research foundation, Denver, Colorado.

Mohamed. A.M.O. 2005. Impact of land disposal of reject brine from desalination. *Desalination* 182(182), 411-433.

Mokhtar, G. and Naoyuki, F. 2012. Microfiltration, Nano-filtration and Reverse Osmosis for the Removal of Toxins (LPS Endotoxins) from Wastewater. *J Memb Sci Technol* 2:118. doi:10.4172/2155-9589.1000118

Monteith, J.L. and Unsworth, M.H. 2008. Principles of Environmental Physics. 3rd Edition London. Elsevier Inc.

Mooketsi, I.O., Ginster, M., Matjie, H.R. and Riedel, J.K. 2007. Leachate characteristics of ash residues from a laboratory-scale brine encapsulated simulation process. World of Coal Ash (WOCA), Covington, Kentucky, USA.

Morali, N. 2006. Investigation of zinc and lead removal from aqueous solution using clinoptilolite. Published Master's thesis in Environmental Engineering. Middle East: Middle East Technical University.

Muriithi G.N. 2009. CO₂ sequestration using brine impacted fly ash, Department of chemistry, University of the Western Cape, Bellville, South Africa.

Nathoo, J., Jivanji, R. and Lewis, A. E. 2010. Freezing your brines off: Eutectic freeze desalination for brine treatment, retrieved 16 October, 2010 from http://www.imwa.info/docs/imwa_2009/IMWA2009_Nathoo.pdf.

Nie, Z., Bu, L., Zhang, M. and Zhang, Y. 2009. Crystallization path of salt from brine in Zabuye salt lake, Tibet, during isothermal evaporation, Natural Resources and Environmental Issues, Vol.15 (2009), Art. 40.

O'Connor, D. J. 1983. Wind effects on gas-liquid transfer coefficients. J. Environ. Eng., 109 (3), 731-752.

Ong, C., G., Herbel, M., J., Dahlgren, R., A. and Tanji, K., K., 1997. Trace elements (Se, As, Mo, B) contamination of evaporation in hypersaline agricultural evaporation ponds, Environmental Science and Technology. Volume 31. , No 3, pp 831-837.

Oround. I., M. 1995. Effect of Salinity Upon Evaporation from Pans and Shallow Lakes Near the Dead Sea, Theoretical and Applied Climatology. 52, (1995), pp 321-240.

Ottes, S. and Oltes, S. 2004. Desalination techniques, EJEAFChem, 4(4), 2004, pp 963-966, ISSN 1579-4372.

Pal Arya, S. 1998. Introduction to Micrometeorology. 2nd Edition, Academic Press: London

Paneharatnam, S. 1972. Transient Behaviour of a Solar Pond and Prediction of Evaporation Rates, Department of Chemical Engineering, Stanford University, Stanford, Calif. 94305, Ind. Eng. Chem. Process Des. Develop., Vol. 11, No. 2.

Penman, H.L. 1948. "Natural evaporation from open water, bare soil and grass." Proc. Roy. Soc. Lond., no. 193, pp. 120-145.

Penman, H.L. 1955. "Evaporation from Lake Eyre. In: ,Lake Eyre, South Australia." The Great Flooding of 1949-50 (The Royal Geographical Society of Australasia, South Australia Branch), pp. 57-61.

Rayner, D.P. 2007. Wind Run Changes: The Dominant Factor Affecting Pan Evaporation Trends in Australia. Queensland Department of Natural Resources, Mines, and Water, Indooroopilly, Australia

Rohwer, C. 1931. "Evaporation from free water surface." Technical bulletin, no. 271.

Sabah, A., Abdula-Wahab Muhammed, A., and Al-Weshahi 2009. Brine management: Substituting chlorine with on-site produced sodium hypochlorite for environmentally improved desalination processes, *Water Resource Manage* 23: pp 2437-2454.

Saripalli, K.P., Sharma, M.M. and Bryant, S.L. 2000. Modelling injection well performance during deep-well injection of liquid wastes. *J Hydrology (Amst)* 227: pp 41-55.

Schultheis, B., Bach, J., Scherzberg, H. and Sondershausen, K-U. 2001. Reproduction of solar evaporation processes in an indoor pilot examination plant for an assessment of the usability of natural brines. K-UTEC Sondershausen. Germany. Retrieved June 4, 2011, from www.k-utec.com/download/solporteng.pdf

Schulze, R.E., Maharaj, M., Lynch, S.D., Howe, B.J. and Melvil-Thomson, B. 1997. South African atlas for agrohydrology and climatology. University of Natal, Pietermaritzburg.

Shadidzader-Bonn, N., Rafai, S., Bonn, D. and Wegdem, G. 2008. Salt crystallization during evaporation : Impact of interfacial properties. American Chemical Society

Skehan, S. and Kwiatkowski, P. J. 2000. Concentrate disposal via injection wells—permitting and design considerations. pp 19-22.

Sonqishe, T., Balfour, G., Iwouha, E. and Petrik, L. 2009. " Treatment of brines using commercial zeolites and zeolites synthesized from fly ash derivative". Proceedings of International Mine Water Conference, Pretoria, South Africa. p695-702.

Sonune, A. and Ghater, R. 2004. Development in waste water treatment methods, Water and inland management institute, *Desalination* 165: pp 55-63.

Squire, D. 2000. Reverse Osmosis Concentrate Disposal in the UK. *Desalination*, 132, pp47-54.

Tanaka, Y. and Ehara, R. 2003. Ion-exchange membrane electro-dialytic salt production using brine discharged from a reverse osmosis seawater desalination plant. *Journal of Membrane Science* 222, pp71-86.

Tanny, J. C. A. 2008. Evaporation from a small water reservoir: Direct measurements and estimates. *Journal of Hydrology*(351), 218-229.

Uyak V., Akdagli, M., Cakmakci, M., and Koyuncu I, 2014. Natural Organic Matter Removal and Fouling in a Low Pressure Hybrid Membrane Systems. *The Scientific World Journal*, Article ID 893203, 1-11 <http://dx.doi.org/10.1155/2014/893203>

Wählin, A.K., Johansson, A.M., Aas, E., G., Brostro, M.G., Weber, J.E.H. and Grue, J. 2010. Horizontal convection in water heated by infrared radiation and cooled by evaporation: scaling analysis and experimental results. *Tellus*, 62: 154-169

Water Corporation of Western Australia 2006. Environmental Literature Review and Position Paper for Perth Seawater Desalination Plant Two and Sydney Seawater Reverse Osmosis Plant.

Water Sewage & Effluent, 2006. Acid Mine Drainage – the BioSURE solution”, 26(3): 39-41.

World Health Organisation, 1988. Guidelines for Drinking Water Quality, Volume 3, Quality Control after the First Impression 1985, Geneva.

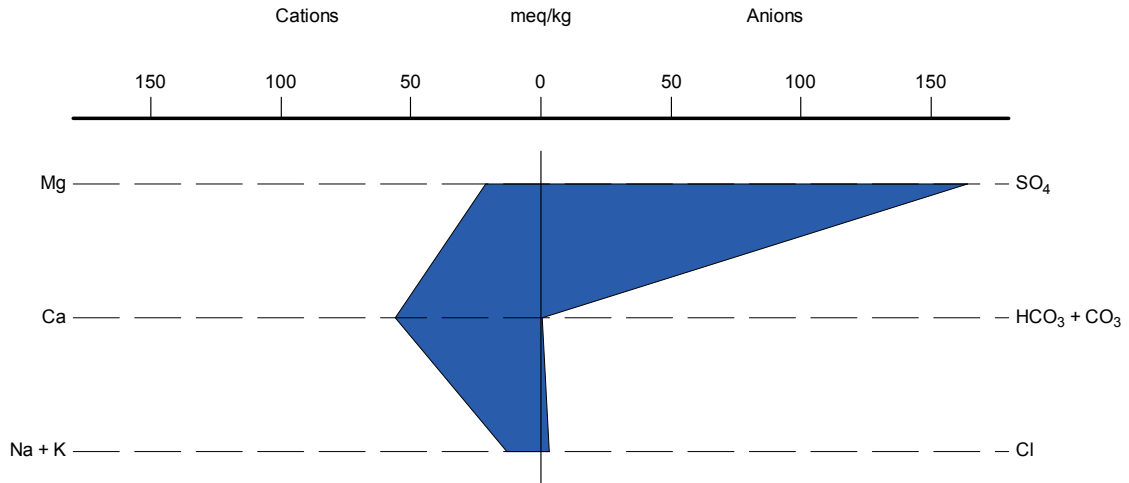
Xu. C. Y. 1997. Evaluation and generalization of 13 mass-transfer equations for determining free water evaporation. *Hydrological processes* (11), 311-323.

Younos, T. and Tulou, K. E. 2005. Overview of desalination technologies, Universities Council on water resources, Journal of contemporary water research and education, pp 3-10.

Zhu, .C. A. 2002. *Environmental Applications of Geochemical Modeling*. Cambridge: Cambridge University Press.

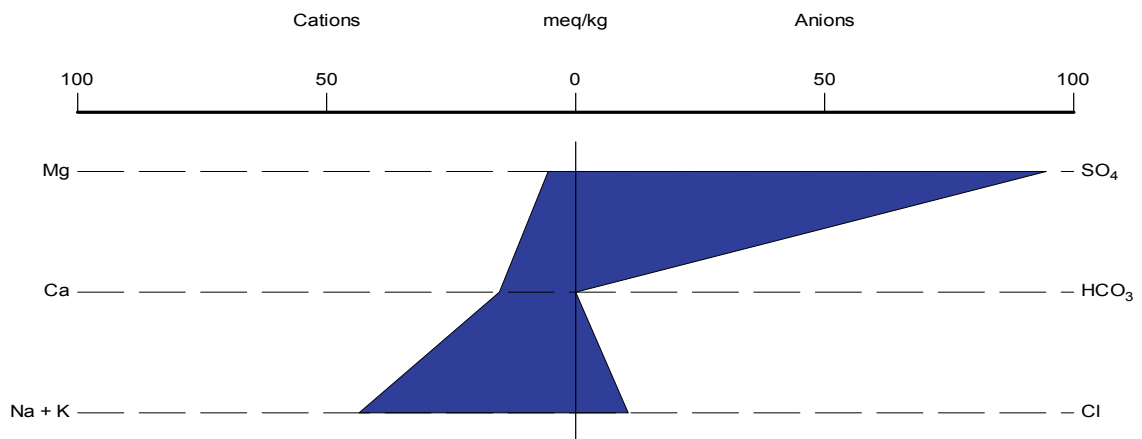
APPENDIX A

Stiff Diagram



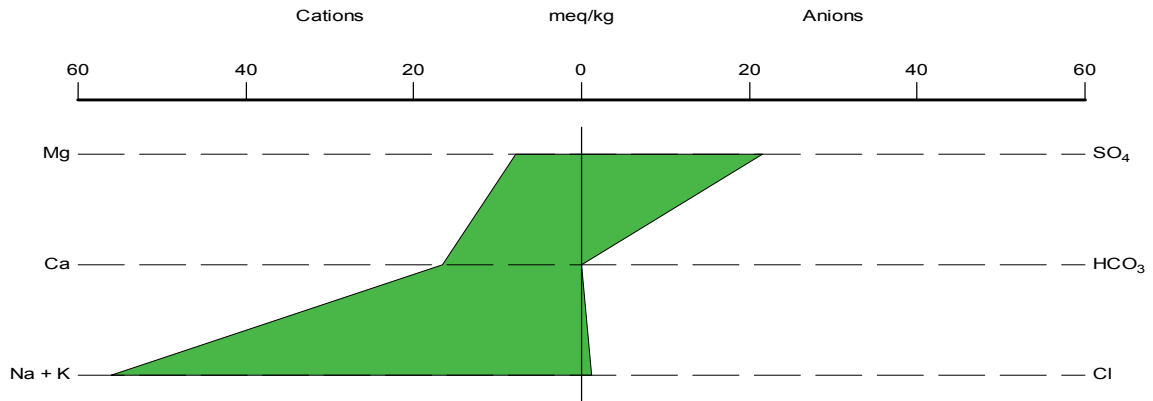
Stiff diagram showing the major ion chemistry of Emalahleni brine stage I

Stiff Diagram



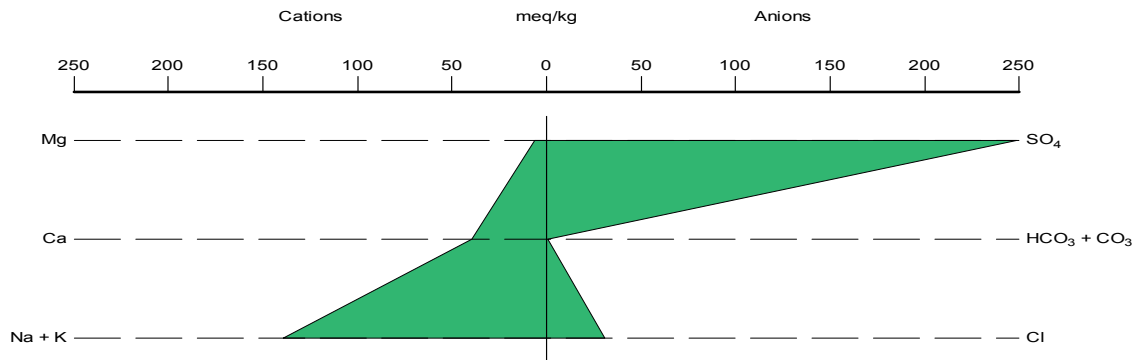
Stiff diagram showing the major ion chemistry of Emalahleni brine stage II

Stiff Diagram



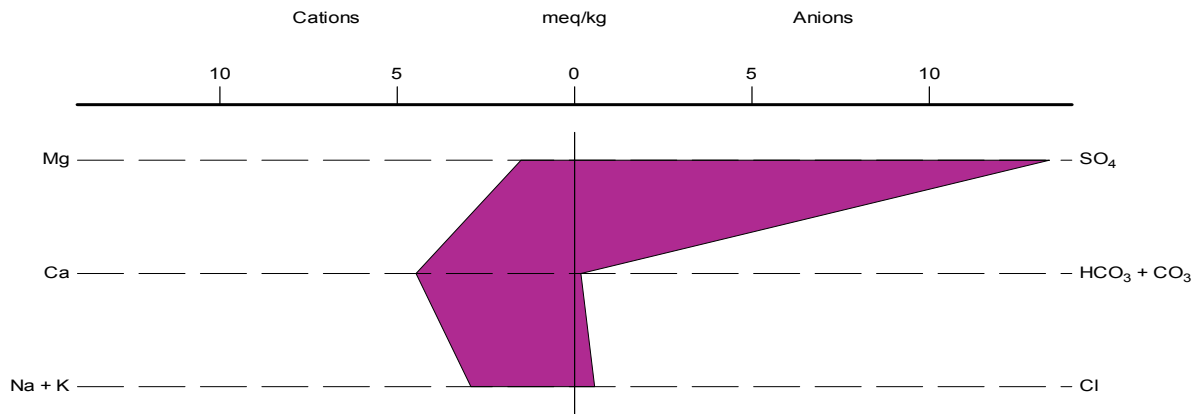
Stiff Diagram showing the major ion chemistry of Emalahleni brine stage II after crystallization

Stiff Diagram



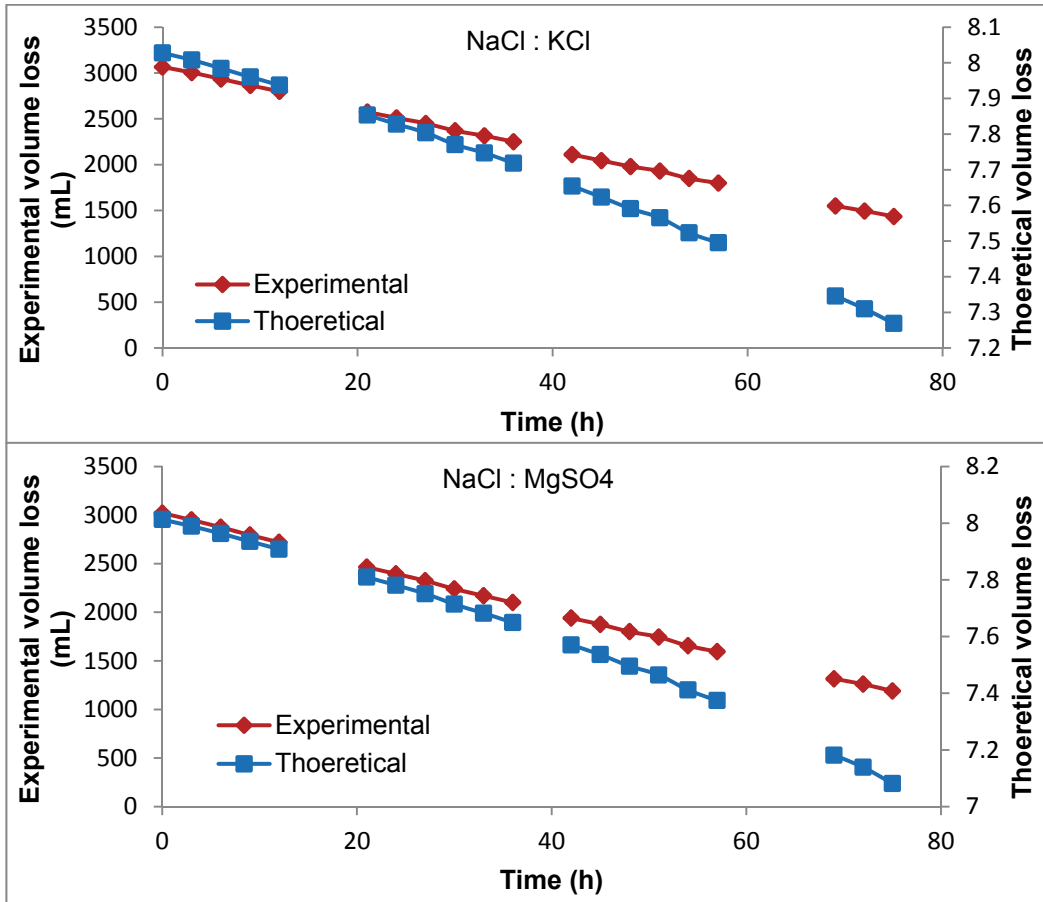
Stiff diagram showing the major ion chemistry of Emalahleni brine stage III

Stiff Diagram



Stiff Diagram showing the major ion chemistry of Emalahleni stage III permeate

A. Material balances



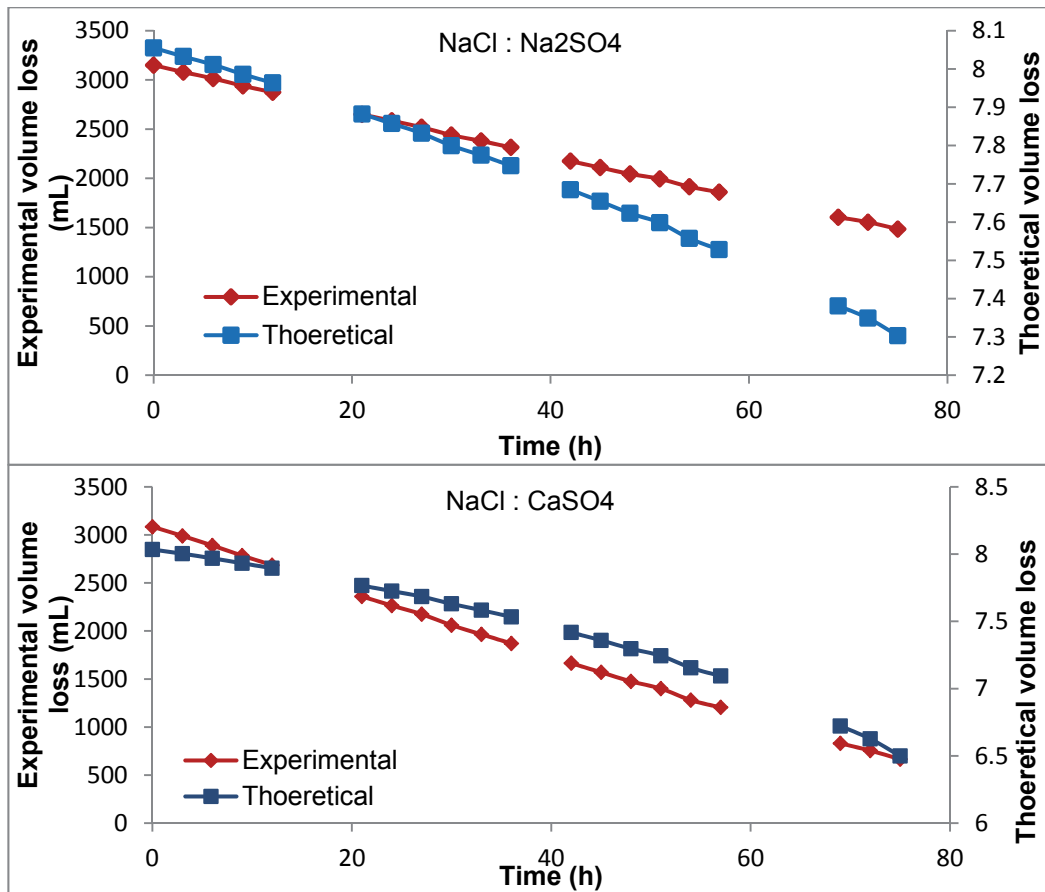


Figure A1: Experimental and theoretical volume loss for double salts

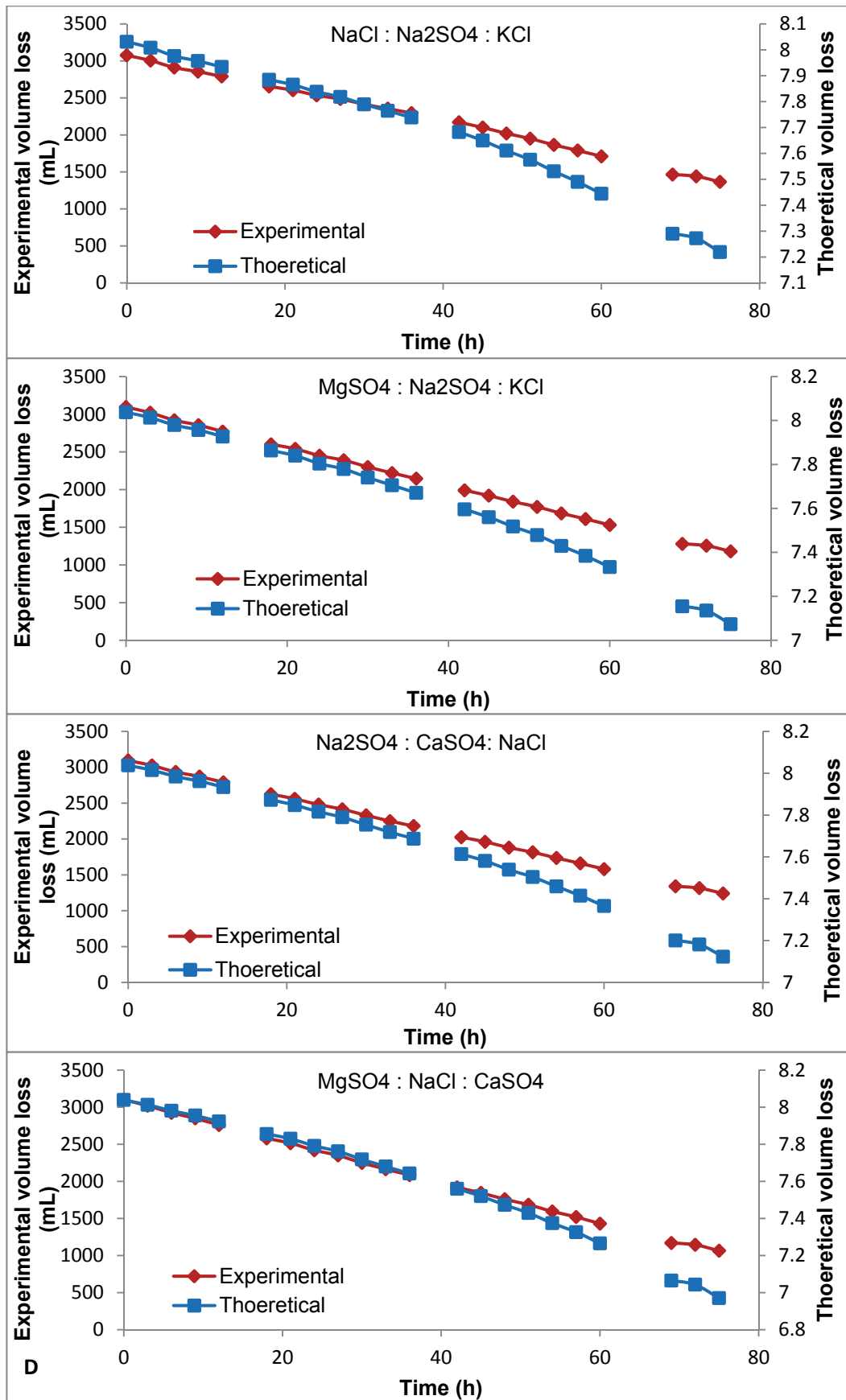
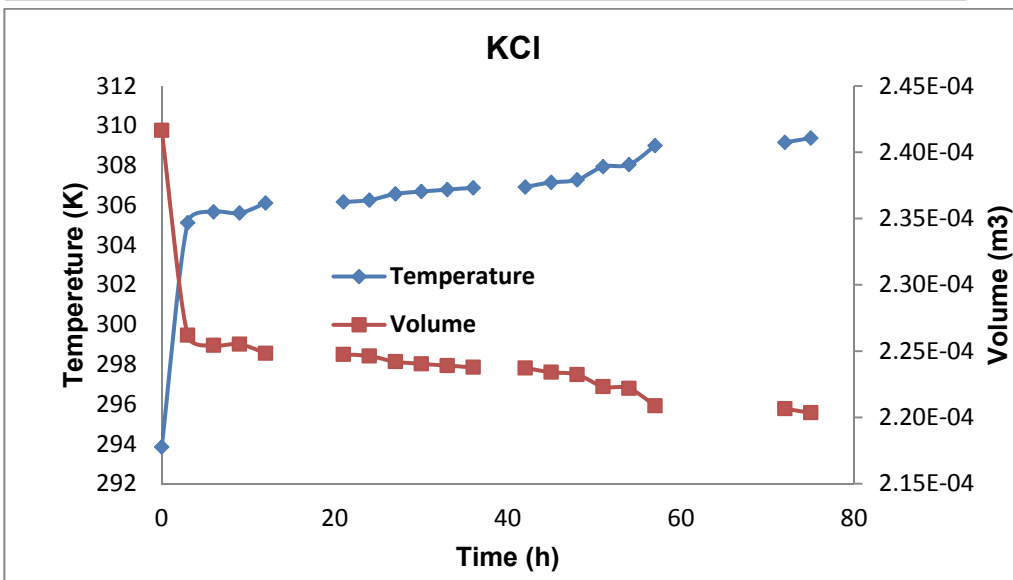
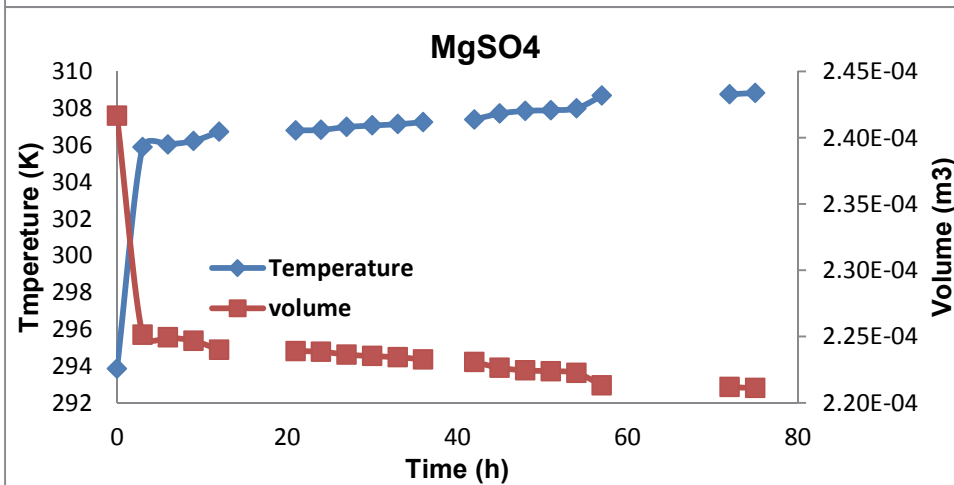
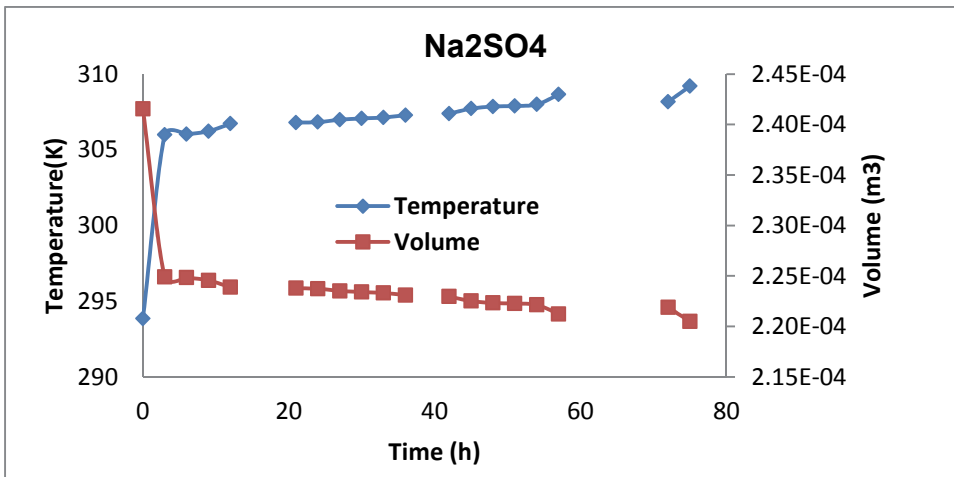


Figure A2: Experimental and theoretical volume loss for double salts

B. Energy balances



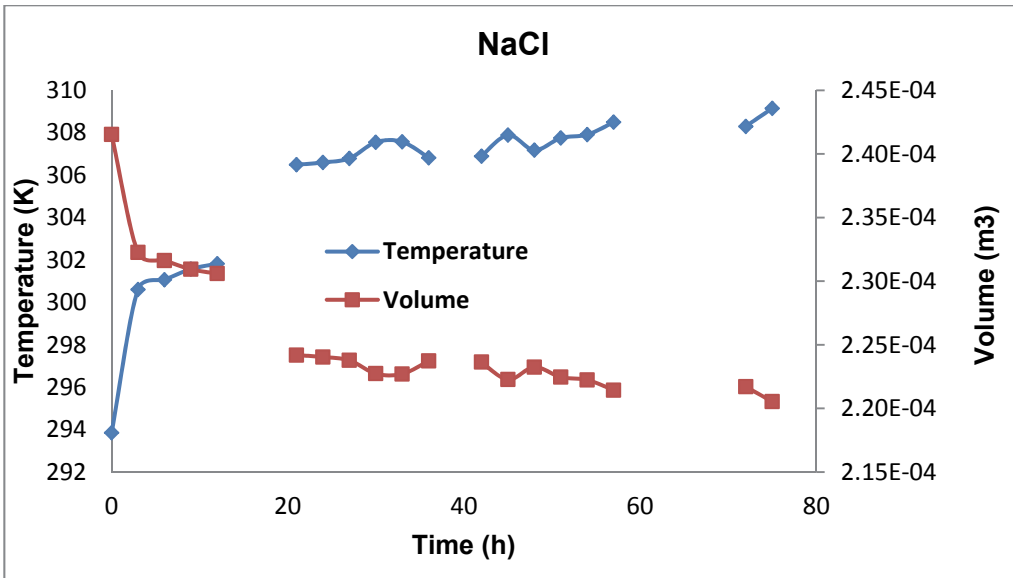
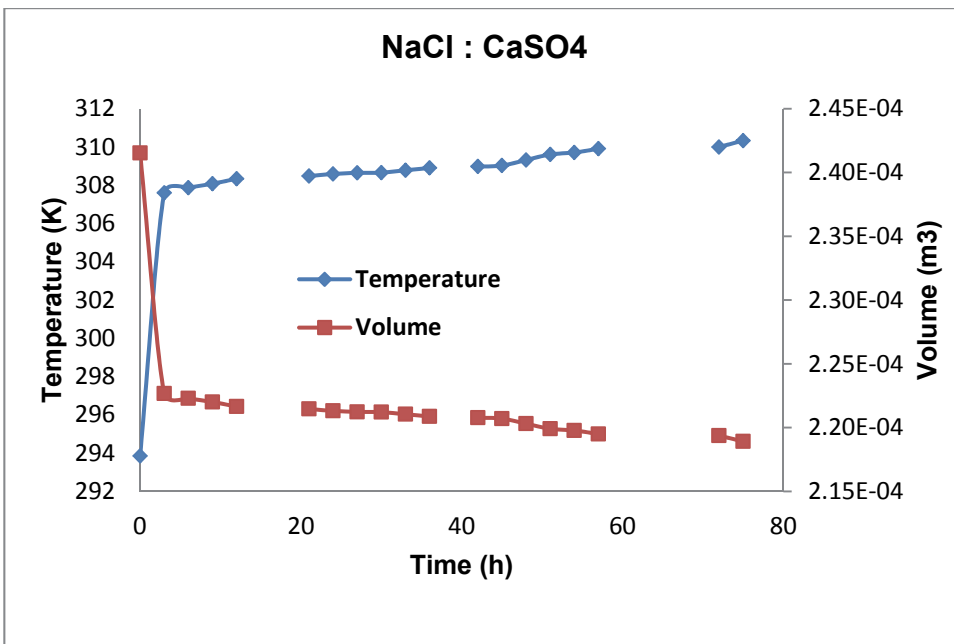


Figure A3: Experimental and theoretical volume of water for single salts (Na₂SO₄, MgSO₄, KCl, and NaCl)



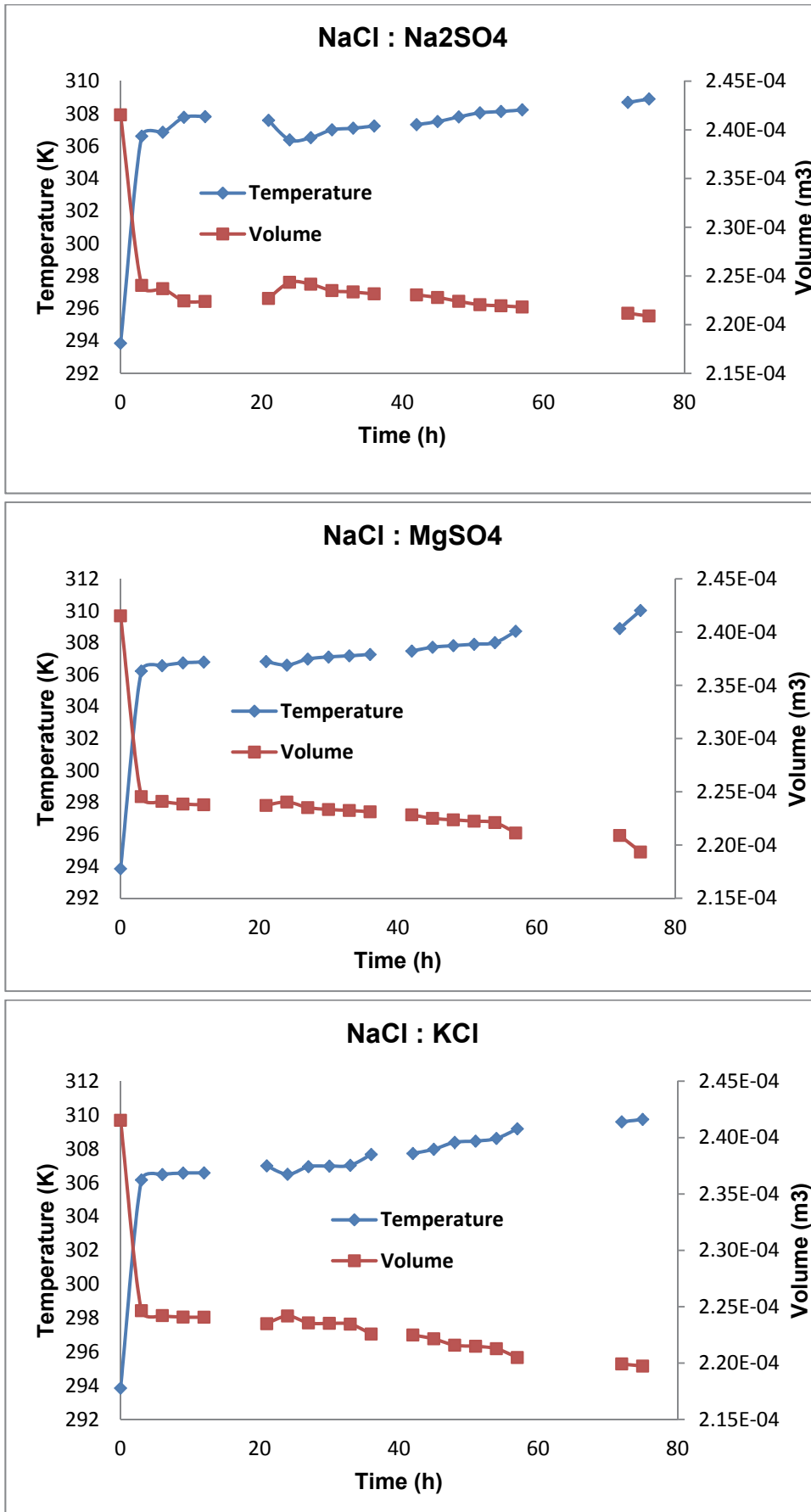
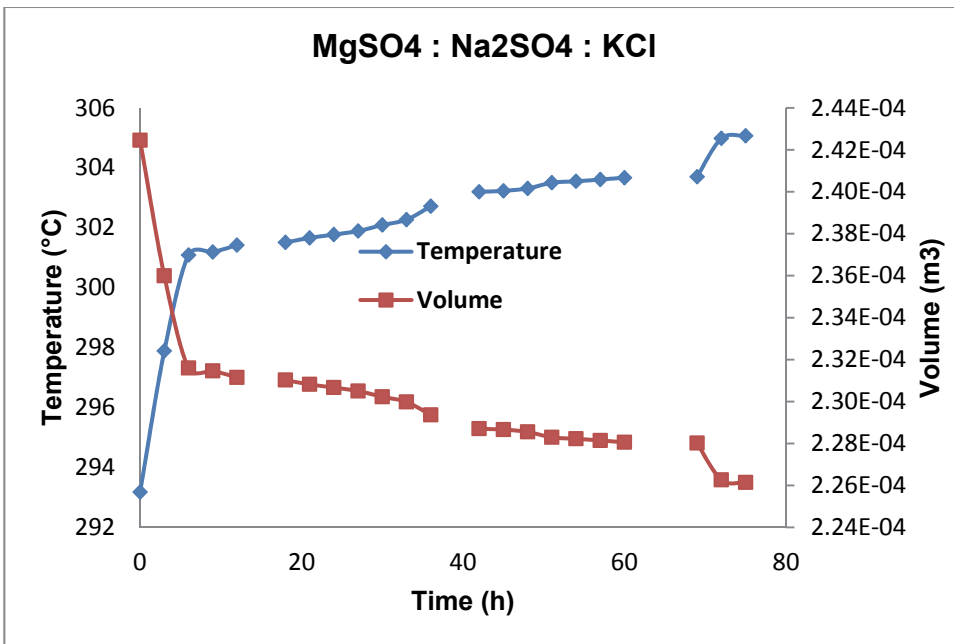
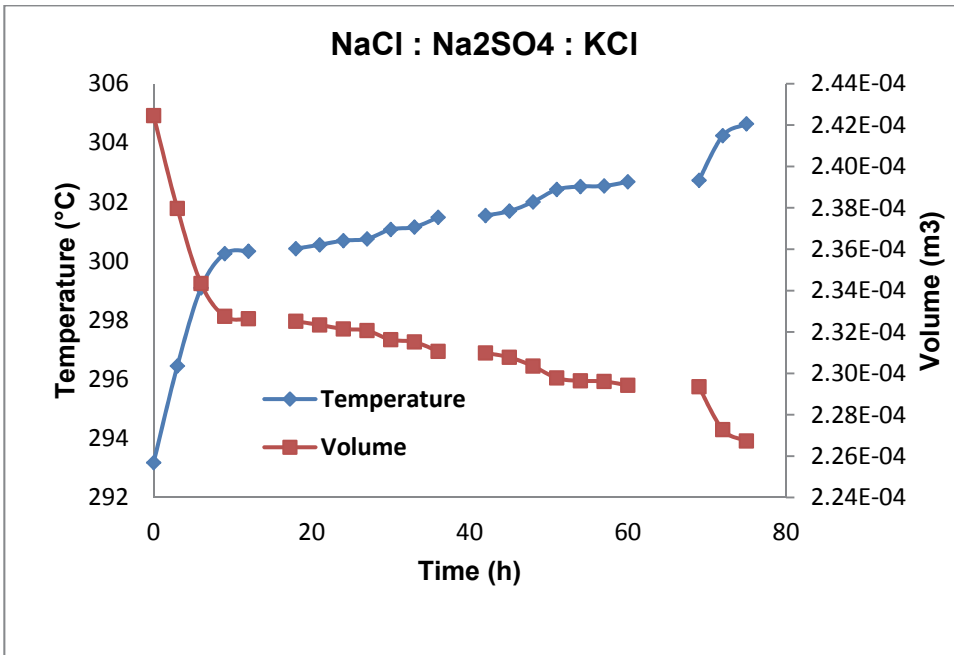


Figure A4: Experimental and theoretical volume loss of water for double salts (NaCl: CaSO₄, NaCl: Na₂SO₄, NaCl: MgSO₄ and NaCl: KCl)



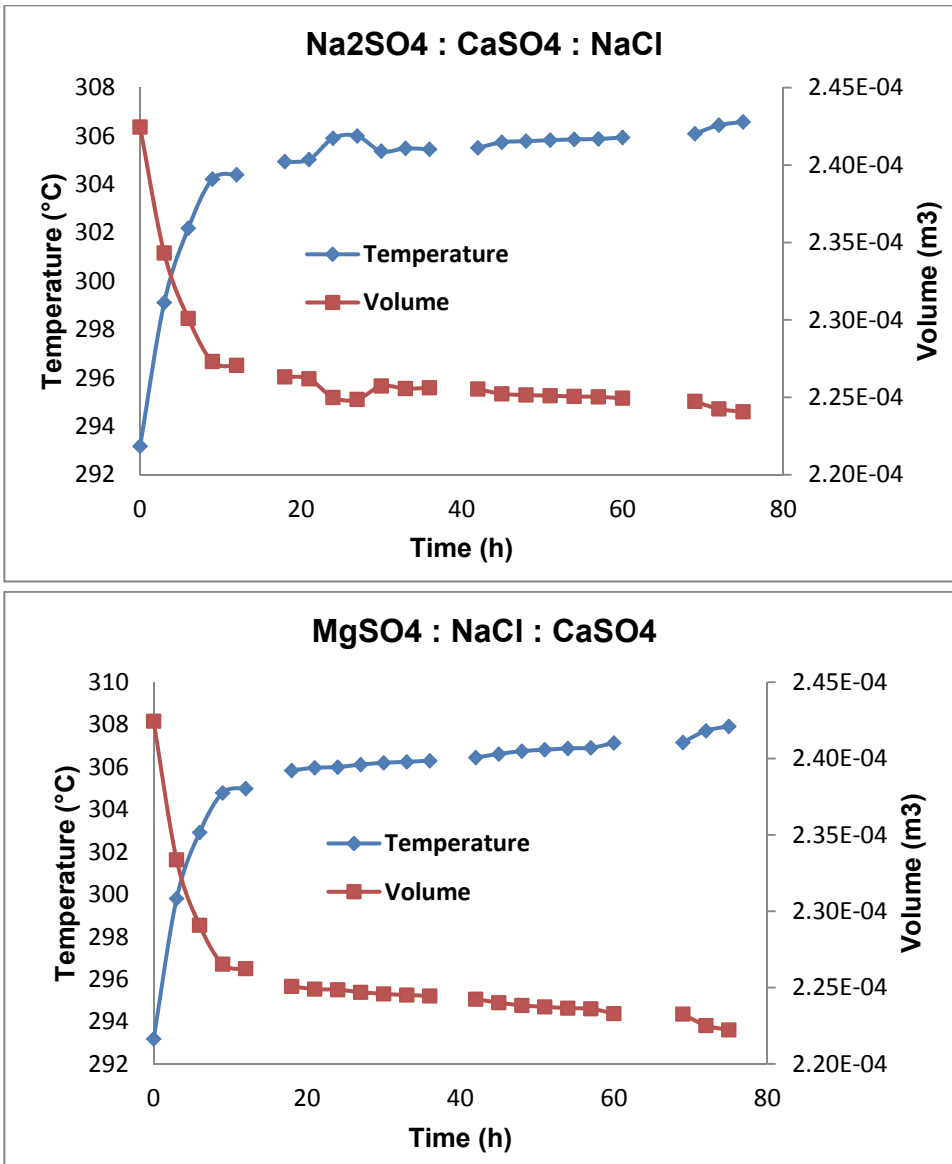


Figure A5: Experimental and Theoretical volume of water loss for triple salts (NaCl: Na₂SO₄: KCl, MgSO₄: Na₂SO₄: KCl, Na₂SO₄: CaSO₄: NaCl and MgSO₄: NaCl: CaSO₄)